OULU 2014
C 489

ACTA UNIVERSITATIS OULUENSIS

Jani Peräntie

ELECTRIC-FIELD-INDUCED DIELECTRIC AND CALORIC EFFECTS IN RELAXOR FERROELECTRICS

UNIVERSITY OF OULU GRADUATE SCHOOL;
UNIVERSITY OF OULU,
FACULTY OF INFORMATION TECHNOLOGY AND ELECTRICAL ENGINEERING,
DEPARTMENT OF ELECTRICAL ENGINEERING;
AALTO UNIVERSITY,
THE GRADUATE SCHOOL FOR ELECTRONICS, TELECOMMUNICATIONS AND AUTOMATION

ACTA UNIVERSITATIS OULUENSIS
C Technica 489

JANI PERÄNTIE

ELECTRIC-FIELD-INDUCED DIELECTRIC AND CALORIC EFFECTS IN RELAXOR FERROELECTRICS

Academic dissertation to be presented with the assent of the Doctoral Training Committee of Technology and Natural Sciences of the University of Oulu for public defence in OP-sali (Auditorium L10), Linnanmaa, on 23 May 2014, at 12 noon

UNIVERSITY OF OULU, OULU 2014

Acta Univ. Oul. C 489, 2014

Supervised by
Professor Heli Jantunen

Reviewed by
Professor Maarit Karppinen
Professor Jung-Hyuk Koh

Opponent
Professor Ahmad Safari

ISBN 978-952-62-0438-3 (Paperback)
ISBN 978-952-62-0440-6 (PDF)

ISSN 0355-3213 (Printed)
ISSN 1796-2226 (Online)

Cover Design
Raimo Ahonen

JUVENES PRINT
TAMPERE 2014

Peräntie, Jani, Electric-field-induced dielectric and caloric effects in relaxor ferroelectrics.
University of Oulu Graduate School; University of Oulu, Faculty of Information Technology and Electrical Engineering, Department of Electrical Engineering; Aalto University, The Graduate School for Electronics, Telecommunications and Automation
Acta Univ. Oul. C 489, 2014
University of Oulu, P.O. Box 8000, FI-90014 University of Oulu, Finland

Abstract

In this thesis, dielectric and thermal behaviours due to the application of an electric field were studied in relaxor ferroelectric $(1-x)Pb(Mg_{1/3}Nb_{2/3})O_3$-$xPbTiO_3$ (PMN-PT) and $(1-x)Pb(Zn_{1/3}Nb_{2/3})O_3$-$xPbTiO_3$ (PZN-PT) systems of great technological importance. Special attention was given to the behaviour of the electric-field-induced phase transitions and electrocaloric effect, which are closely related to the existing and potential applications. Reactive sintering or columbite methods were used to fabricate polycrystalline PMN-PT ceramics with various compositions (x=0-0.3). In addition, commercial PMN-PT single crystals with composition close to the morphotropic phase boundary region were used. A studied PZN-PT crystal composition was grown by solution gradient cooling technique. Materials were mainly studied by means of dielectric and direct temperature measurements.

The electrocaloric effect observed in a ceramic PMN-PT system was found to show distinct maximum values close to the thermal depolarization temperatures with low electric fields. The temperature range and magnitude of the electrocaloric effect was significantly expanded to high temperatures with increasing electric fields due to the contribution of polar nanoregions. The maximum electrocaloric temperature change was in the range of 0.77-1.55 °C under an electric field of 50 kV/cm. In addition, temperature change measurements on depoled PMN-0.13PT ceramics demonstrated that the electrocaloric effect is accompanied with an irreversible part below its depolarization temperature due to hysteresis loss and a possible phase transition type response related to the evolution of the macroscopic polarization.

An electric field application to the <001> and <011> directions in PMN-PT crystals was found to cause distinct anomalies in the dielectric and temperature change responses. These anomalies were attributed to the complex polarization rotation routes and different phase stability regions in the electric-field-temperature phase diagrams of PMN-PT. Furthermore, measurements on PMN-PT crystals provided the first direct indications of a temporarily reversed electrocaloric effect with an increasing electric field. In addition, the measured electrocaloric trends in PZN-PT crystal were reproduced by a simple lattice model and mean-field approximation around the transition temperature. This demonstrated that the electrocaloric effect is driven mainly by the dipolar entropy lowering.

Keywords: dielectrics, electric-field-induced effects, electrocaloric effect, ferroelectrics, phase transition, PMN-PT, polarization, PZN-PT, relaxor

Peräntie, Jani, Sähköisesti indusoidut dielektriset ja kaloriset ilmiöt ferrosähköisissä relaksoreissa.

Oulun yliopiston tutkijakoulu; Oulun yliopisto, Tieto- ja sähkötekniikan tiedekunta, Sähkötekniikan osasto; Aalto yliopisto, Elektroniikan, tietoliikennetekniikan, ja automaation valtakunnallinen tutkijakoulu

Acta Univ. Oul. C 489, 2014

Oulun yliopisto, PL 8000, 90014 Oulun yliopisto

Tiivistelmä

Tässä työssä tutkittiin dielektristen ominaisuuksien ja lämpötilan käyttäytymistä teknologisesti merkittävissä (1−x)Pb($Mg_{1/3}Nb_{2/3}$)O_3-x$PbTiO_3$ (PMN-PT) ja (1−x)Pb($Zn_{1/3}Nb_{2/3}$)O_3-x$PbTiO_3$ (PZN-PT) ferrosähköisissä relaksorimateriaaleissa sähkökentän vaikutuksen alaisena. Tutkimuksen erityishuomion kohteena olivat sähköisesti indusoidut faasimuutokset sekä sähkökalorinen ilmiö, jotka liittyvät läheisesti nykyisiin sekä tulevaisuuden sovellutuksiin. Monikiteisiä PMN-PT keraamikoostumuksia (x=0−0,3) valmistettiin sekä reaktiivisella sintrauksella että kolumbiittimenetelmällä. Lisäksi tutkimuksessa käytettiin kaupallisia PMN-PT erilliskiteitä, joiden koostumus on lähellä morfotrooppista faasirajaa. Työssä käytetty PZN-PT erilliskide kasvatettiin jäähdyttämällä korkean lämpötilan liuoksesta. Materiaaleja tutkittiin pääosin lämpötilan ja dielektristen ominaisuuksien mittauksilla.

Kun PMN-PT keraamisysteemiin kohdistettiin alhainen sähkökenttä, sähkökalorisen ilmiön selkeä maksimiarvo havaittiin lähellä materiaalin termistä depolarisaatiolämpötilaa. Suuremmilla sähkökentän arvoilla sähkökalorinen ilmiö voimistui ja sen lämpötila-alue laajeni korkeampiin lämpötiloihin polaaristen nanoalueiden kytkeytymisen vuoksi. Sähkökalorisen lämpötilamuutoksen maksimi vaihteli välillä 0,77-1,55 °C sähkökentän arvolla 50 kV/cm. Lisäksi lämpötilamittaukset depoolatulle PMN-0,13PT koostumukselle osoittivat, että sähkökalorisen ilmiön ohella materiaalissa esiintyy makroskooppisen polarisaation muodostumiseen liittyvä palautumaton lämpöenergia depolarisaatiolämpötilaa pienemmissä lämpötiloissa hystereesihäviön ja mahdollisen faasimuutoksen vaikutuksesta.

PMN-PT erilliskiteiden dielektrisyys- ja lämpötilavasteessa havaittiin selkeitä muutoksia sähkökentän vaikuttaessa <001> ja <011> kidesuuntiin. Nämä muutokset ovat selitettävissä PMN-PT:n polarisaation kompleksisten rotaatiosuuntien ja erityyppisten sähkökenttä-lämpötila -faasidiagrammien stabiilisuusalueiden avulla. PMN-PT kiteiden mittauksissa havaittiin myös ensimmäinen suora osoitus väliaikaisesti käänteisestä sähkökalorisesta ilmiöstä sähkökentän kasvaessa. Lisäksi mitatut PZN-PT erilliskiteen sähkökaloriset ominaisuudet transitiolämpötilan läheisyydessä pystyttiin pääpiirteittäin mallintamaan käyttämällä yksinkertaista hilamallia ja keskimääräisen kentän approksimaatiota. Mallinnuksen mukaan sähkökalorinen ilmiö aiheutuu pääasiassa sähköisesti indusoidusta dipolientropian alenemisesta.

Asiasanat: dielektri, faasimuutos, ferrosähköinen, PMN-PT, polarisaatio, PZN-PT, relaksori, sähkökalorinen ilmiö

Acknowledgements

This work was mainly carried out in the Microelectronics and Materials Physics Laboratories at the University of Oulu. Part of the work was performed during a research visit to the Department of Chemistry and the 4D LABS of Simon Fraser University, Burnaby, Canada.

The main financial support of this work came from the Graduate School in Electronics, Telecommunication and Automation (GETA). In addition, personal grants and scholarships from the Nokia Foundation, the Jenny and Antti Wihuri Foundation, the Ulla Tuominen Foundation, the Tauno Tönning Foundation, the Seppo Säynäjäkangas Science Foundation, the Kaute Foundation, the Finnish Cultural Foundation, and the Riitta and Jorma J. Takanen Foundation are greatfully acknowledged.

I would like to express my sincere gratitude to my supervisor Professor Heli Jantunen who provided me all the necessities for pursuing this work in the first place. In particular, her encouragement, belief, and support were guiding me along the way. I wish also to thank Dr. Juha Hagberg who lured me into this research topic, enabled all the complicated measurements, and gave me support in all aspects throughout this work. I want to acknowledge Professor Zuo-Guang Ye who gave me an opportunity to visit his lab in Burnaby and to learn some basics of relaxors and crystal growth.

I wish to thank the personnel of Microelectronics and Materials Physics Laboratories for some nice conversations and debates over various issues. Special thanks go to Dr. Antti Uusimäki for helping me with publication writing and to the Center for Microscopy and Nanotechnology for technical assistance in the experimental work. In addition, I would like to thank Professor Ye's group members for providing me with help and friendship.

I would like to thank Professor Maarit Karppinen and Associate Professor Jung-Hyuk Koh for reviewing my thesis work, and Professor Arthur Hill for revising the language of the manuscript.

On a personal level, I praise all my friends for being there. Above all, I express my deepest gratitude to my parents, sister's family, and Maiju for their patience, encouragement, and support. Thank you all!

Oulu, September 2013 Jani Peräntie

List of abbreviations and symbols

ABO_3	General formula for the oxide perovskite structure
C	Capacitance
C_{ph}	Lattice heat capacity per unit volume
$C_{p,E}$	Heat capacity per unit volume at constant pressure and electric field
c_p	Specific heat capacity (per unit mass) at constant pressure
D	Electric displacement
d_{33}	Longitudinal piezoelectric coefficient (response in the direction of the stimulus)
E	Electric field/energy
E_C	Coercive electric field
E_c	Configurational energy
E_{CP}	Electric field at the critical point
E_{th}	Threshold electric field
f	Frequency
f_c	Helmholtz free energy
G	Gibbs free energy
ΔH	Enthalpy change
J	Current density
k	Boltzmann constant
m	Mirror plane/Mass
M_A, M_B, M_C	Monoclinic phase (A-, B-, and C-type)
O	Orthorhombic phase
P	Dielectric polarization
P_r	Remanent polarization
P_s	Spontaneous polarization
P_{sat}	Saturation polarization
Q	Heat energy/Partition function
R	Rhombohedral phase
S	Entropy
S_c	Entropy of cold reservoir
S_{dip}	Dipolar entropy
S_h	Entropy of hot reservoir
S_{ph}	Lattice entropy
ΔS	Entropy change

T	Temperature/Tetragonal phase
T_B	Burns temperature
T_C	Curie point
T_c	Temperature of cold reservoir
T_{CP}	Temperature at the critical point
T_{dp}, T_d	Depolarization temperature
T_f	Freezing temperature
T_h	Temperature of hot reservoir
T_m	Temperature of maximum permittivity
T_{R-T}	Temperature of phase transition between (pseudo)rhombohedral and tetragonal phases
T_t	Order-disorder phase transition temperature
T*	Onset temperature of permanent polar regions in relaxors
ΔT	Temperature change
ΔT_{sat}	Saturated electrocaloric temperature change
t	Tolerance factor
tan δ	Dielectric loss tangent
V	Volume
x	Strain/fraction of moles or ions
X	Stress
z	Average coordination number
β	Monoclinic angle
ε	Real part of permittivity
ε_r, ε'	Real part of relative permittivity
Θ	Curie constant
μ	Dipole moment
Ω	Number of orientational states
COR	Chemically/compositionally ordered (nano)region
DSC	Differential scanning calorimetry
EC	Electrocaloric
ECE	Electrocaloric effect
FE	Ferroelectric
HRD	High-resolution diffraction
IR	Infrared
MPB	Morphotropic phase boundary
PLM	Polarizing light microscopy
PLZT	$Pb_{1-x}La_x(Zr_yTi_{1-y})_{1-x/4}O_3$, La-modified Lead zirconate titanate

PMN	$Pb(Mg_{1/3}Nb_{2/3})O_3$, Lead magnesium niobate
PMN-PT	$Pb(Mg_{1/3}Nb_{2/3})_{1-x}Ti_xO_3$, Lead magnesium niobate-lead titanate
PMT	$Pb(Mg_{1/3}Ta_{2/3})O_3$, Lead magnesium tantalate
PNR	Polar nanoregion
PSN	$Pb(Sc_{1/2}Nb_{1/2})O_3$, Lead scandium niobate
PSN-PT	$Pb(Sc_{1/2}Nb_{1/2})_{1-x}Ti_xO_3$, Lead scandium niobate-lead titanate
PST	$Pb(Sc_{1/2}Ta_{1/2})O_3$, Lead scandium tantalate
PT	$PbTiO_3$, Lead titanate
PVDF	Polyvinylidene fluoride
P(VDF-TrFE)	Poly(vinylidene fluoride-trifluoroethylene)
P(VDF-TrFE-CFE)	Poly(vinylidene fluoride-trifluoroethylene-chlorofluoroethylene)
PZN	$Pb(Zn_{1/3}Nb_{2/3})O_3$, Lead zinc niobate
PZN-PT	$Pb(Zn_{1/3}Nb_{2/3})_{1-x}Ti_xO_3$, Lead zinc niobate-lead titanate
PZT	$PbZr_xTi_{1-x}O_3$, Lead zirconate titanate
SRBRF	Spherical random bond-random field model
XRD	X-ray diffraction

List of original papers

This doctoral thesis is based on the following papers, which are cited in the text by their corresponding Roman numerals.

I Peräntie J, Hagberg J, Uusimäki A & Jantunen H (2008) Temperature characteristics and development of field-induced phase transition in relaxor ferroelectric $Pb(Mg_{1/3}Nb_{2/3})_{0.87}Ti_{0.13}O_3$ ceramics. Applied Physics Letters 93(13): 132905.

II Peräntie J, Hagberg J, Uusimäki A & Jantunen H (2009) Field-induced thermal response and irreversible phase transition enthalpy change in $Pb(Mg_{1/3}Nb_{2/3})O_3$–$PbTiO_3$. Applied Physics Letters 94(10): 102903.

III Peräntie J, Hagberg J, Uusimäki A & Jantunen H (2010) Electric-field-induced dielectric and temperature changes in a <011>-oriented $Pb(Mg_{1/3}Nb_{2/3})O_3$–$PbTiO_3$ single crystal. Physical Review B 82(13): 134119.

IV Peräntie J, Hagberg J, Uusimäki A, Tian J & Han P (2012) Characteristics of electric-field-induced polarization rotation in <001>-poled $Pb(Mg_{1/3}Nb_{2/3})O_3$–$PbTiO_3$ single crystals close to the morphotropic phase boundary. Journal of Applied Physics 112(3): 034117.

V Valant M, Dunne LJ, Axelsson A-K, Alford NM, Manos G, Peräntie J, Hagberg J, Jantunen H & Dabkowski A (2010) Electrocaloric effect in a ferroelectric $Pb(Zn_{1/3}Nb_{2/3})O_3$-$PbTiO_3$ single crystal. Physical Review B 81(21): 214110.

VI Peräntie J, Tailor H, Hagberg J, Jantunen H & Ye Z-G (2013) Electrocaloric properties in relaxor ferroelectric $(1-x)Pb(Mg_{1/3}Nb_{2/3})O_3$-$xPbTiO_3$ system. Journal of Applied Physics 114(17): 174105.

Papers I and II are devoted to investigations of the dielectric and thermal response to isothermally applied electric fields in PMN-13PT ceramics. Special attention is paid to the development of the response below the thermal depolarization temperature. Measurements demonstrate that an irreversible response is found at low temperatures in addition to the hysteresis and electrocaloric responses. Results are discussed in terms of electric-field-induced phase transition and development of macroscopic polarization.

Papers III and IV focus on studies of electric-field-induced dielectric and thermal characteristics in PMN-PT single crystals close to the morphotropic phase boundary region. Observed changes in dielectric and thermal response are discussed in the framework of the electrocaloric effect and various electric-field-induced phase transitions.

Paper V describes the electrocaloric effect and its measurement in PZN-PT single crystal. A theoretical description based on the mean-field theory is used to describe the temperature and electric field dependence of the observed electrocaloric temperature change.

Paper VI describes the characteristics and behaviour of the electrocaloric effect in a polycrystalline PMN-PT material system. Electrocaloric temperature change was directly measured as a function of electric field, temperature and composition. The results are discussed by considering the relaxor nature of the system and compared with recent theoretical descriptions of the electrocaloric effect in relaxor ferroelectrics.

The Thesis author has performed all the experimental measurements in papers I–VI and material preparation in Papers I, II and VI. The main ideas and writing work in Papers I–IV and VI were developed and performed by the Thesis author with the kind help of the co-authors. In Paper V, the Thesis author performed all the electrical measurements, while the ideas and the theoretical description were developed by the main authors of that Paper.

Contents

1 Introduction

This introductory chapter gives some basic information on the phenomena and materials studied in this work. Ferroelectricity and its requirements in general are briefly discussed especially from the perovskite structure viewpoint. Additionally, another closely connected phenomenon of relaxor ferroelectricity and some collective applications are introduced to open up the general background for this research work. Finally, the main objectives of the Thesis are presented and the outline of the work is given.

1.1 Ferroelectricity and perovskite structure

A ferroelectric (FE) material is a dielectric material that has two or more orientational states (directions of spontaneous dielectric polarization) in the absence of any electric field over some temperature range, and the orientation (spontaneous polarization) can be switched between these states by an external electric field. (Lines & Glass 1977)

The very origin of ferroelectricity, i.e. switchable spontaneous polarization, is directly exploited in only a few applications (e.g. in ferroelectric memories). However, some derivative characteristics of the polarization, such as permittivity and piezoelectric response, show high values and make ferroelectrics useful in diverse applications (Tagantsev *et al.* 2010). In fact, ferroelectric materials can be considered as smart materials since they show many advantageous indirect or coupled effects, where different types of outputs, such as electric charge/current, strain, temperature, light, can be produced by various types of inputs, such as electric field, stress, heat, and light (Uchino 2000). The Heckmann diagram in Figure 1 presents some of these effects combining thermal, electrical, and mechanical properties of a crystal (Nye 1980). Thick arrows joining the outer corner ‘forces’ to the inner corner ‘results’ of these forces represent the three principal effects. The coupled effects are presented by thinner arrows joining the points in different corners. Especially, the coupled electromechanical and electrothermal effects, such as piezoelectricity and pyroelectricity, are known to be strong in ferroelectric materials (Newnham 2005, Lang 2005).

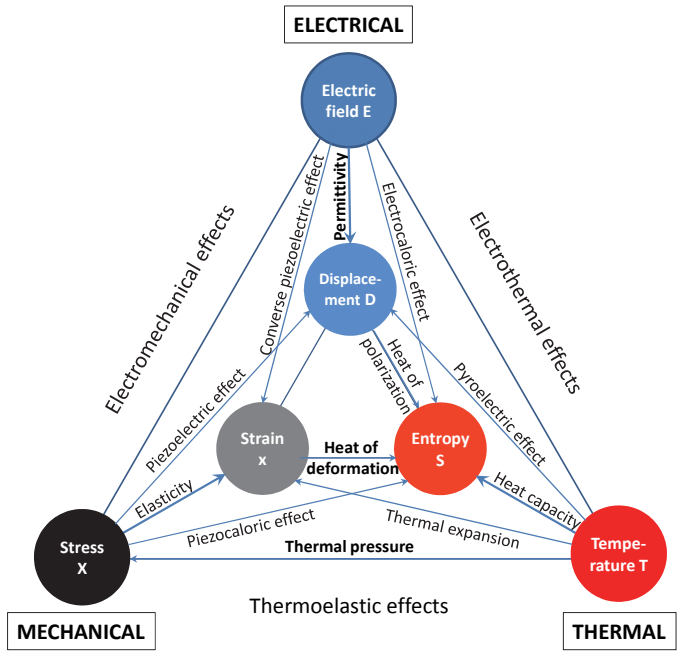

Fig. 1. The Heckmann diagram relating thermal, electrical, and mechanical properties of a crystal. Figure recreated according to Nye (1980).

The presence and magnitude of ferroelectricity is most critically dependent on a material's crystal structure and its symmetry, as well as on the chemical nature and interaction of the constituent elements. First of all, the occurrence of spontaneous polarization necessarily requires a crystal structure without a centre of symmetry, i.e. without inversion symmetry (Nye 1980). Out of 32 possible crystallographic point groups of crystals, 11 point groups contain an inversion centre as one symmetry element. The presence of the inversion symmetry leads to a situation where centres of positive and negative charge coincide, cancelling each other, and spontaneous polarization is not able to form. Furthermore, the remaining 21 point groups without the centre of symmetry are also required to belong to a point group with a unique polar axis, which requires a line of points unchanged by all symmetry operations of that point group, in order to show spontaneous polarization. Totally there are 10 point groups belonging to six different crystal systems that have this unique polar axis. The occurrence of spontaneous polarization over some temperature range classifies material as pyroelectric. If the polarization can be reversed by an electric field, the material is

further classified as ferroelectric. (Lines & Glass 1977) The aforementioned symmetry-based classification shows that all ferroelectric materials are necessarily pyroelectric and piezoelectric, which means that they exhibit spontaneous polarization that can be changed with temperature and also with mechanical stress. The first requirement of noncentrosymmetry already places a major restriction for the occurrence of ferroelectricity. A wide survey of 283 000 different inorganic and organic compounds reveals that only around 22% of all studied compound structures do not have a centre of symmetry, and in more detail, only 12% belong to a polar point group with a spontaneous polarization (Newnham 2005). Again, only some small proportion of spontaneously polarized materials show a switchable polarization as a sign of ferroelectricity. However, ferroelectricity is still met in a variety of materials ranging from polymers and liquid crystals to complex oxides and even some biological materials. For example, one of the latest findings shows that ferroelectricity is present in the aortic walls, and it may play a key role in explaining some basic phenomena related to blood vessels (Liu *et al.* 2012).

In general, the polar ferroelectric phase takes place below a specific temperature called the Curie point, where a structural phase transition from a high-temperature nonferroelectric (or paraelectric) phase to a low-temperature ferroelectric phase occurs (Damjanovic 1998). A simultaneously forming spontaneous polarization is arranged into small regions of uniform polarization, i.e. ferroelectric domains, which are oriented in a specific complex pattern and are separated by domain walls. If neighbouring domains have 180° difference in their polarization directions (antiparallel), these domains and the wall between them are purely ferroelectric in nature. Adjacent domains with non-180° difference in polarization directions necessarily have different orientations of spontaneous strain as well, which also makes them separate ferroelastic domains. A formation of domains and their arrangement into complex domain patterns occurs even in a single-crystalline ferroelectric material in order to minimize the electrostatic and elastic energies. (Damjanovic 1998) Basically the polarization directions in different domains and permissible ferroelectric and ferroelastic domain walls are imposed by the symmetry of the ferroelectric and paraelectric phases (Aizu 1966, Fousek & Janovec 1969, Erhart 2004). Figure 2(a) shows a schematic presentation of a possible domain structure in a polycrystalline ferroelectric material.

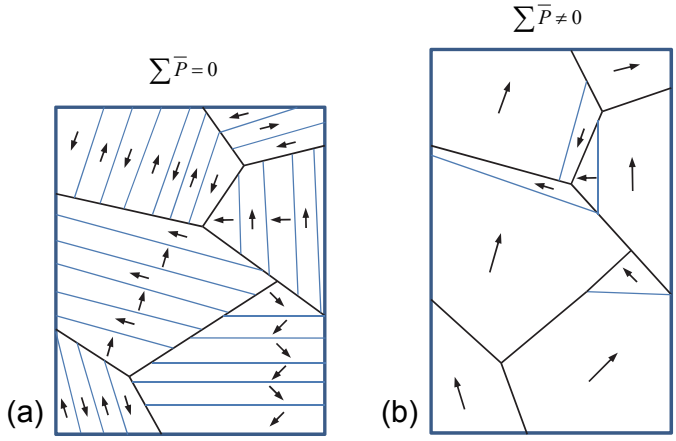

Fig. 2. Simplified presentation of a possible domain structure in (a) unpoled and (b) poled ferroelectric ceramics with 180° and 90° domain walls. The overall sum of local polarizations *P* becomes non-zero in the poled structure while its dimensions change.

Due to the large number of domains with different random polarization orientations, a bulk ferroelectric material tends to be macroscopically non-polar (Figure 2(a)). When an electric field is applied to the non-polar ferroelectric sample, macroscopic polarization (P) first starts to increase linearly with increasing electric field as shown in Figure 3. With a strong enough electric field, domains with unfavourable orientation will reorient towards the electric field direction and macroscopic polarization increases nonlinearly. After the reorientation of domains, polarization regains its linear behaviour as a function of field. Extrapolation of the linear behaviour at higher fields to the interception with the polarization axis gives the value for the spontaneous polarization (P_S). In reality, true spontaneous polarization can only be reached in single-crystalline materials when all the domains are aligned. For this reason, it is sometimes more appropriate to describe P_S as the saturated polarization. (Damjanovic 1998). With decreasing electric field, some domains start to switch back towards their original position but the majority remain aligned closer to the field direction even in the absence of the electric field. This means that there is a macroscopic remanent polarization (P_r), which remains in the sample (Figure 2(b)). A reverse electric field is then needed in order to bring the polarization back to zero, and this field is called the coercive electric field (E_C). Furthermore, a continuing increase of the reverse electric field (i.e. $E > E_C$) leads to the switching of polarization which takes place by the nucleation and growth of new and existing antiparallel domains.

This cycling of the electric field leading to polarization switching is the essential property of ferroelectrics, and it gives rise to the formation of the ferroelectric hysteresis loop shown in Figure 3. Basically, its presence provides an experimental confirmation for the switchable polarization and underlying ferroelectric nature. However, some materials may easily show *P*-*E* characteristics similar to true ferroelectrics (e.g. Jaffe *et al.* 1971, Scott 2008, Yan *et al.* 2011) and additional evidence is therefore required for the confirmation of the ferroelectric nature.

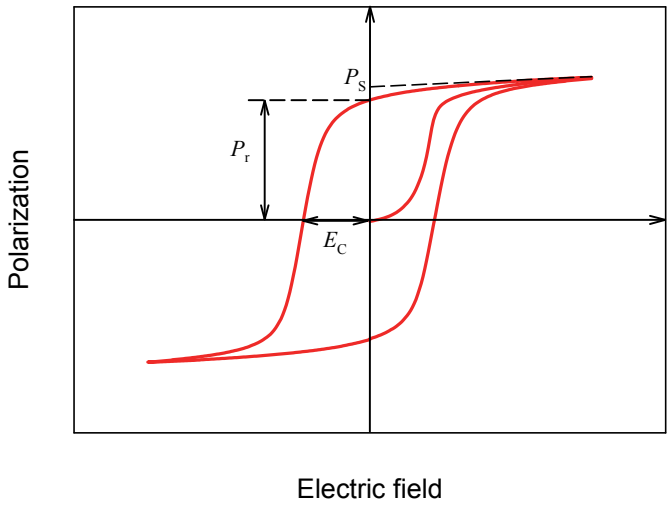

Fig. 3. Typical polarization vs. electric field hysteresis loop for ferroelectric materials. P_S, P_r, and E_C refer to the spontaneous/saturated polarization, the remanent polarization, and the coercive electric field, respectively.

A large proportion of the most significant inorganic ferroelectric materials, such as the well-known $BaTiO_3$ and $PbZr_{1-x}Ti_xO_3$ (and the materials studied in this Thesis), are oxides with a perovskite ABO_3 structure as shown in Figure 4. The perovskite structure family is very versatile and is adopted by a wide range of useful materials with different electrical, magnetic, optical and mechanical properties (Bhalla 2000). A simple ABO_3 structure in cubic form can be considered to be based on a close-packed cubic arrangement of oxygens (red spheres in Figure 4), where large A-site cations (blue spheres) replace some of the 12 coordinated O^{2-} ions, and small B-site cations (green spheres) occupy the octahedral sites surrounded by six O^{2-} ions. This forms an arrangement of

octahedral BO_6 units linked by the corners, and remaining interstices are filled with A-site cations (Moulson & Herbert 2003), as in Figure 4(b).

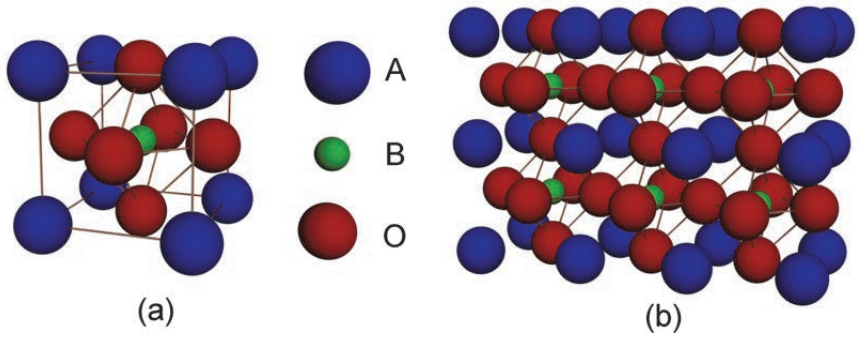

Fig. 4. A cubic ABO_3-type perovskite structure: (a) B-type unit cell, and (b) part of the network of corner-shared BO_6 octahedrons with A-site interstitials.

The sum of A- and B-site cation valences must naturally compensate for the negative charge posed by three oxygen ions, which basically allows a number of different combinations to be formed. However, the size and bonding of the constituent ions are far more critical and limiting factors for the stability of the perovskite structure (Shrout & Halliyal 1987). A simple geometrical view shows that the perovskite structure fitting can be described by the tolerance factor t which depends on the effective ionic radiis of the twelve coordinated A-site ion, six coordinated B-site ion, and six coordinated oxygen ion, respectively (Goldschmidt 1926). The perovskite stability is maximized with $0.8 < t < 1.05$, where $t = 1.00$ corresponds to an ideal fit in a cubic cell (Zhang *et al.* 2008). Small allowed departures from the ideal tolerance factor tend to favour either distortions with B-site off-centring and ferroelectricity (mainly for $t > 1$) or octahedral tilting (for $t < 1$) (Itoh & Taniguchi 2008). Another critical factor for perovskite stability is the amount of ionic bonding, which is proportional to the electronegativity difference between anions and cations. The higher the averaged difference in the electronegativity, the larger the fraction of ionic bonding and the greater the perovskite stability. (Shrout & Halliyal 1987)

The ferroelectric distortions in perovskites are mainly based on displacive-type transitions, where small displacements of cations in relation to anions take place and create noncentrosymmetric structures with a net dipole moment per unit

volume (Lines & Glass 1977, Cohen 1992). The spontaneous polarization is favoured in the perovskite crystal due to its higher Lorentz factor (internal field constant) in comparison to some other crystal structures (Slater 1950, Uchino 2000). The ferroelectric ABO_3 perovskite structures contain corner-linked octahedral networks with d^0 transition metal B-ions (e.g. Ti^{4+}, Nb^{5+}), which are ferroelectrically more active and octahedrally coordinated with respect to the accompanying oxygen ions as shown in Figure 4(a). Chemically these atoms have different types of atomic orbitals which are close in energy, and a hybrid bonding is typical due to the large number of preferred coordination geometries. The hybrid bonding between B-site cations and oxygens is essential for ferroelectricity because it softens the repulsive forces so that the bonding energy of the BO_6 complex can be lowered. This lowering distorts the octahedron which leads to a lower symmetry structures and the formation of molecular dipole moments. (Cohen 1992, Newnham 1998). The A-site of the ferroelectric perovskite structure is filled with other cations (e.g. Ba^{2+}, Pb^{2+}, K^{+}, Bi^{3+}) to preserve charge neutrality. Depending on the chemical identity of the A-site cation, it can also enhance the polar distortions and ferroelectricity of the perovskite structure. In fact, in multiferroic ferroelectric-ferromagnetic compounds the A-site cation is suggested to play the active role in the erection of the spontaneous dipole moment (Hill 2000). Especially, a stereochemically active lone-pair of electrons present in the Pb^{2+} ion is expected to enhance ferroelectric distortions in Pb-based perovskites (Newnham 1998, Davies *et al.* 2008).

At high temperatures, most FE perovskites have a cubic structure, which is centrosymmetric and paraelectric (shows polarization under an applied electric field). This high-temperature cubic prototype of ABO_3 perovskite has a point group of $m\bar{3}m$, which allows for six different lower symmetry polar species belonging to the tetragonal, orthorhombic, trigonal, monoclinic or triclinic crystal systems (Aizu 1966). The corresponding perovskite tetragonal, orthorhombic, and rhombohedral ferroelectric phases have spontaneous polarization confined to a symmetry axis along 4-fold <001>, 2-fold <011>, and 3-fold <111> directions with respect to the cubic axis, respectively. The polarization directions in the monoclinic and triclinic phases are less restricted leading to higher numbers of possible domain states (see Section 2.3).

1.2 Lead-based perovskite relaxor ferroelectrics

A study of different perovskite compositions quickly revealed that some complex perovskites, specifically of the $Pb(B'_{1-y}B''_{y})O_3$ type, show peculiar dielectric behaviour in comparison to conventional ferroelectrics. Pioneering studies by Smolenskii *et al.* (e.g. 1959 & 1961) demonstrated that some of these complex perovskites with mixed B-site cations, such as $PbMg_{1/3}Nb_{2/3}O_3$ (PMN) and $PbZn_{1/3}Nb_{2/3}O_3$ (PZN), display a broad, high, and strongly frequency dependent real part of the permittivity peak as a function of temperature (Figure 5). This behaviour is different from observations on conventional ferroelectrics, where a sharp and lower peak in the real part of the permittivity is associated with critical behaviour evidenced at the phase transition temperature and the Curie-Weiss law is followed when close to this temperature (Lines & Glass 1977).

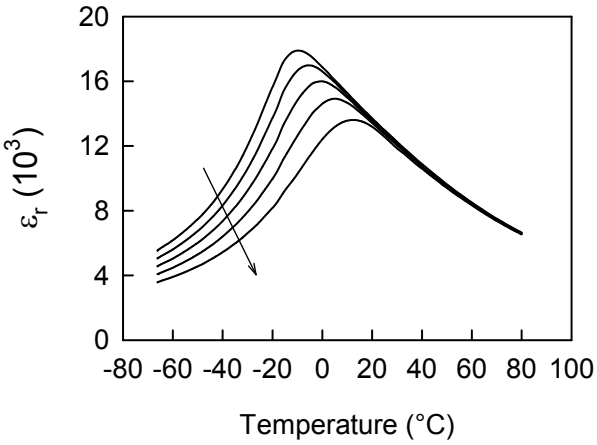

Fig. 5. Real part of the relative permittivity in PMN ceramics as a function of temperature at *f*=0.1–1000 kHz (decade intervals). Arrow indicates the direction of increasing frequency.

Due to their peculiar dielectric behaviour, the studied materials were first referred to as "ferroelectrics with diffused phase transition" or "dirty ferroelectrics" as a departure from conventional ferroelectrics. The first model by Smolenskii *et al.* (1959) suggested that the diffused phase transition behaviour was caused by compositional heterogeneity in B-sites giving rise to local fluctuations in the Curie point. Further investigations showed that the optical index of refraction deviates from a linear response around the Burns temperature (T_B) (~340 °C for

PMN and ~480 °C for PZN) far above the temperature of the dielectric peak (T_m), and this peculiarity was suggested to originate from a quadratic electro-optic effect induced by some local polarization clusters forming around that temperature (Burns & Scott 1973, Burns & Dacol 1983 and 1990). A hypothesis of small polar regions combined with analogies to superparamagnetism led to the description of a superparaelectric model, where locally ordered polar regions with correlated ions shifts are dynamically disordered due to thermal motion and no long range correlation occurs between these regions at high temperatures, i.e. $T_m < T < T_B$ (Cross 1987). Additionally, these materials adopted a more descriptive name of "relaxor ferroelectrics" due to their aforementioned peculiar relaxation properties and close relation to conventional ferroelectrics (Cross 1987). In reality, interactions between polar regions become significant at lower temperatures, and an extended dipolar-glass model was proposed by Viehland *et al.* (1990 & 1991). The increasing interaction of polar regions on cooling leads to a deviation from Curie-Weiss behaviour, and an increasing frustration of their dynamics eventually freezes them out at 'freezing' temperature, T_f ($\leq T_m$), in a way analogous to magnetic spin glasses (Viehland *et al.* 1990 & 1992). This leads to the formation of a wide permittivity peak at around T_m (see Figure 5) and the dielectric relaxation (i.e. T_m vs. f) can be described by the Vogel-Fulcher relationship (Viehland *et al.* 1990). The characteristic relaxation time of the corresponding relaxation process involves a wide distribution of times but the longest relaxation time diverges at T_f (Levstik *et al.* 1998).

A hypothesis of local polar clusters with short-range order below the specific temperature T_B was later confirmed by many experiments including scattering techniques and transmission electron microscopy (Vakhrushev *et al.* 1989 & 1996, Yoshida *et al.* 1998). It has also been stated that actual polar regions form at lower temperatures around T^* ($< T_B$) where correlated behaviour leads to the rise of a truly static component of polarization/distortion and the onset of their aforementioned relaxation (Toulouse 2008, Dkhil *et al.* 2009). These forming polar regions are commonly called polar nanoregions (PNRs), and their size is characteristically on a scale from a few to tens of nanometres. The constituent ions are mainly displaced along the [111] direction of the $Pb(B'_{1-y}B''_y)O_3$ cubic perovskite unit cell, and these correlated displacements create PNRs with a rhombohedral structure (Vakhrushev *et al.* 1995, Takesue *et al.* 2001). After their formation, the number of these ellipsoidal nanoregions starts to grow first with decreasing temperature, but a rapid decrease in number is observed at the freezing temperature T_f where nanoregions seem to combine into larger clusters (Xu *et al.*

2004a). Below the freezing temperature the relaxor transforms from the ergodic relaxor phase to a non-ergodic phase due to increasing correlations between the polar dipoles (Bokov & Ye 2006). In the non-ergodic phase, the free energy has several minima with similar depths but different separating energy barriers. The system cannot go through all the minima (different dipole configurations) in a practical time scale, which leads to a difference between thermodynamic and time averages. Practically, changes of state of a new free energy minimum may be increasingly slow and the equilibrium may not be attained, making the properties of a non-ergodic phase largely history-dependent. At low temperatures, the polar nanoregions constitute a significant portion of the material; for example in a PMN crystal their volume can cover up to ~25% (de Mathan *et al.* 1991, Uesu *et al.* 1996). It is now commonly believed that the increasing interaction of polar regions under decreasing temperature and freezing at T_f qualitatively explains the main dielectric characteristics (the high and diffused dielectric peak with strong frequency dispersion) of the complex lead-based perovskite relaxor ferroelectrics shown in Figure 5. However, the dielectric behaviour of different $Pb(B'B'')O_3$-based perovskites may differ significantly due to their different B-site occupations.

In addition to polar order, another characteristic ordering effect in $Pb(B'B'')O_3$-based perovskite materials occurs in its B-site sublattice where different configurations among the B-site cations are possible after equilibrium between the elastic and electric energies is reached. An adopted B-site configuration is critically dependent on the valence and size of the involving B-site cations. (Davies & Akbas 2000). A large chemical difference (e.g. difference in size, valence, or coordination preference) between B' and B'' cations usually stabilizes an ordered B-site arrangement (Ye *et al.* 1998, Davies *et al.* 2008). A complete ordering of B-site cations leads to a superstructure with a built-in 1:1 type long-range order (Figure 6(a)). This type of behaviour is observed for example in $Pb(Mg_{1/2}W_{1/2})O_3$ and $Pb(Co_{1/2}W_{1/2})O_3$ with ordered B^{2+} and B^{6+} cations, and typically these materials exhibit normal ferroelectric or antiferroelectric phase transitions (Baldinozzi *et al.* 1993, Ye *et al.* 1998). Some intermediate $Pb(B'_{1/2}B''_{1/2})O_3$-type compounds, such as $Pb(Sc_{1/2}Ta_{1/2})O_3$ (PST), have B-site cations with an intermediate chemical difference so that the 1:1 type B-site ordering occurs by enhanced diffusion in kinetically active region near the order-disorder phase transition temperature T_t (Stenger & Burggraaf 1980, Setter & Cross 1980). Thus, a structure with variable degrees of spatial order can be achieved by different thermal annealing and quenching procedures. In general, the

1:1 ordered regions are called chemically or compositionally ordered (nano)regions (CORs).

$Pb(B^{2+}_{1/3}B^{5+}_{2/3})O_3$ type relaxors may also exhibit some degrees of chemical ordering. Small regions (few nanometres) with unique 1:1 type order have been found for example in PMN and PZN, and these regions have the same overall stoichiometry in comparison to the surrounding disordered matrix (Krause *et al.* 1979, Randall & Bhalla 1990, Jin *et al.* 2001). This observed similarity in stoichiometry has been explained by the random-site model (Chen *et al.* 1989, Davies & Akbas 2000), which suggests that one B-site sublattice of the ordered region consists solely of B^{5+} ions and the other sublattice is randomly occupied by B^{2+} and B^{5+} cations (Figure 6(b)). The ratio of ions in the random sublattice is B^{2+}:B^{5+}=2:1 so that the overall stoichiometry of CORs is preserved. In other words, the formula of PMN in the ordered regions can be written as $Pb[(Mg_{2/3}Nb_{1/3})_{1/2}Nb_{1/2}]O_3$. Interestingly, the B-site arrangement in $Pb(B^{2+}_{1/3}B^{5+}_{2/3})O_3$ would naturally imply a stoichiometric 1:2 type ordered structure. A tendency for the observed 1:1 type rather than 1:2 type ordering is believed to be related to the interaction between B^{2+} bonded oxygen ions and the lone-pair of Pb^{2+} (Burton 2000). In some $Pb(B^{2+}_{1/3}B^{5+}_{2/3})O_3$ type relaxors, such as PMT, the ordering can also be enhanced by thermal annealing. Otherwise, thermal motion tends to destroy the B-site order in PMN at relatively low temperatures (T_f~900 °C) and the temperature region for ordering (i.e. $T < T_f$) shows slow kinetics so that the degree of compositional order cannot be changed by thermal annealing. (Davies & Akbas 2000). Otherwise, the chemically ordered regions in $Pb(B^{2+}_{1/3}B^{5+}_{2/3})O_3$ type relaxors can be increased by a combination of chemical doping and suitable high temperature treatment (Davies & Akbas 2000, Zhao *et al.* 2009).

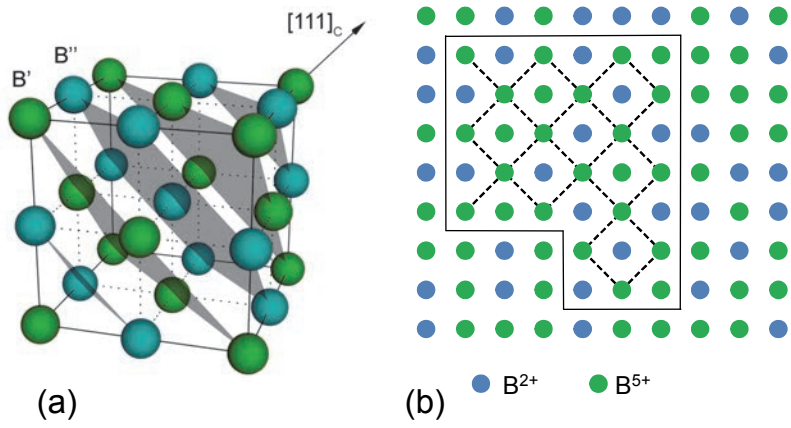

Fig. 6. Compositional order in $Pb(B'B'')O_3$ perovskite relaxors: (a) 1:1 B-site ordered supercell with alternating (111) planes occupied solely by either B' or B'' cations, and (b) two dimensional presentation of a chemically ordered nanoregion (bounded by solid line) in a disordered matrix of $Pb(B^{2+}_{1/3}B^{5+}_{2/3})O_3$ type relaxor according to the random-site model. For the sake of clarity A-site (Pb^{2+}) and oxygen ions are not shown. Figures modified from Kiat & Dkhil (2008) and Bokov & Ye (2006).

The compositional B-site order/disorder in complex $Pb(B'B'')O_3$ perovskites is an especially important factor for relaxor behaviour since the dispersion in dielectric properties can only be observed in disordered crystals. For example, a disordered PST shows relaxor ferroelectric behaviour, while the ordered structure experiences a sharp phase transition behaviour (Setter & Cross 1980). On the other hand, no clear difference in relaxation behaviour is observed between PMN (COR size ~2–5 nm) and La-modified PMN (COR size ~100 nm) despite the clear difference in degrees of compositional order (the cation ordering parameters were ~0 and ~0.4), but the diffuseness of the phase transition is considerably higher in more disordered samples (Zhao *et al.* 2009). This influence of chemical order on relaxor dielectric properties indicates that chemical and polar orders are intimately connected, at least to some extent. Essentially, there exist chemically different A- and B-sites in the $Pb(B'B'')O_3$ perovskite lattice due to chemical disorder and therefore the polar order is disturbed.

In the ergodic phase of relaxors (i.e. in the range of $T_f < T < T_B$) the CORs have been suggested to act as sites of nucleation for emerging PNRs (Randall & Bhalla 1990). However, some relaxation caused by dynamic PNRs has also been observed in compositions without CORs, such as in solid-solution of PMN with

55% $PbTiO_3$ (Bokov *et al.* 2011), and PNRs have also been related to disordered regions in PSN (Laguta *et al.* 2004). Additionally, some PNRs appear to be already naturally static in the ergodic state so that they don't contribute to the relaxation (Vakhrushev *et al.* 2005, Blinc 2006, Stock *et al.* 2010, Bokov *et al.* 2011). It seems that the static PNRs are necessarily pinned by chemically ordered regions since they grow with increasing COR size and disappear without CORs (Stock *et al.* 2006, Long *et al.* 2008). The general picture arising from these studies describes an ergodic relaxor phase with the coexistence of dynamic and static PNRs, where static PNRs locate inside CORs and dynamic PNRs can exist in both ordered and disordered regions (Bokov *et al.* 2011). With this viewpoint in mind, different effects of increasing structural order on dielectric properties in $Pb(B'_{1/2}B''_{1/2})O_3$ and modified $Pb(B'_{1/3}B''_{2/3})O_3$ relaxors are believed to relate to their aforementioned distinct natures of ordering (Davies & Akbas 2000, Bokov *et al.* 2011). As the ordered state of $Pb(B'_{1/2}B''_{1/2})O_3$ consists of two B-site sublattices both filled solely by one type of B-site ion, the ordered regions of $Pb(B'_{1/3}B''_{2/3})O_3$ still include one B-site sublattice with a random distribution of B-ions and associated random fields (Davies & Akbas 2000).

Although relaxors are known to involve polar regions, their actual formation and fragmentation are not completely understood. The compositional disorder evidently destroys an otherwise general tendency for long-range ferroelectric or antiferroelectric order met in compositionally ordered relaxors but exact mechanisms are unclear (Bokov & Ye 2006). Basically, there are two main aspects to consider with respect to the formation and nature of the polar order (Samara 2003, Bokov & Ye 2006). As already briefly mentioned, the first aspect regards relaxor ferroelectric as a glassy state similar to magnetic dipolar glasses with randomly interacting polar nanodomains in the presence of random fields (Cross 1987, Viehland *et al.* 1991, Levstik *et al.* 1998). Polar nanoregions are then considered as results of local phase fluctuations in an otherwise cubic matrix. The second aspect describes relaxor ferroelectrics as ferroelectrics where domains are broken up to nanoscale so that the material only consists of small domains and surrounding domain walls (Westphal *et al.* 1992). The main idea is that the long-range polar order is destroyed by quenched random fields caused by disordered distribution of heterovalent B-site ions. Experimental distinction between these two aspects using structural measurements is exceedingly complicated due to their spatial equivocalities − the cubic matrix in the first aspect is only an average symmetry with different expected local symmetry and domain walls of undefined symmetry constituting a significant portion in the second aspect (Bokov & Ye

2006). There are a number of other experimental results in favour of both the aforementioned aspects and therefore no clear consensus is found (see e.g. Samara 2003, Fu *et al.* 2009, Novak *et al.* 2012). A sort of combination of these aspects is drawn with the spherical random-bond-random-field (SRBRF) model developed by Pirc & Blinc (1999), which describes the static relaxor behaviour by considering the interactions between different PNRs (i.e. random bonds) as well as action between PNRs and random fields. The strength of random fields then decides whether the ground state is relaxor or long-range ordered ferroelectric phase.

When $Pb(B'B'')O_3$-type relaxors are combined with other ferroelectric perovskites to make relaxor ferroelectric solid-solutions, their polar structure is largely affected and properties start to more closely resemble those of ordinary ferroelectrics. Especially, relaxor ferroelectric solid-solutions with ferroelectric $PbTiO_3$ have been extensively studied due to their extraordinary electromechanical behaviour, which has even led to the birth of an important family of relaxor-PT materials. In general, this material group shares some factors, such as MPB region, large polarization, and proper range of B-site ionic size and mass, which could be universal signs for underlying high electromechanical coupling and piezoelectricity (Yamashita & Ichinose 1996, Yamashita *et al.* 2002). The effect of PT on some properties of relaxors is reviewed in Chapter 2 from the viewpoint of PMN-PT and PZN-PT systems which are the most studied relaxor-PT systems and particularly relevant materials considering this Thesis work.

As a summary of this section, Figure 7 schematically presents the main stages in the formation of polar order in both conventional ferroelectrics and lead-based relaxor ferroelectrics. While the nonpolar paraelectric phase transforms at T_C to the ferroelectric polar phase with a complex domain pattern, the development of polar order in relaxor ferroelectrics is more complex and subtle. The uncorrelated ion shifts form correlated polar nanoregions around T_B and these random regions grow in size on decreasing temperature. An increasing interaction of PNRs leads to a freezing of their dynamics at T_f and some regions combine into larger groups. Depending on the type of relaxor and its chemical order, some lead-based relaxors spontaneously transform into the long-range ferroelectric or antiferroelectric phase at T_C while other relaxors show a limited polar order embedded into a cubic average lattice.

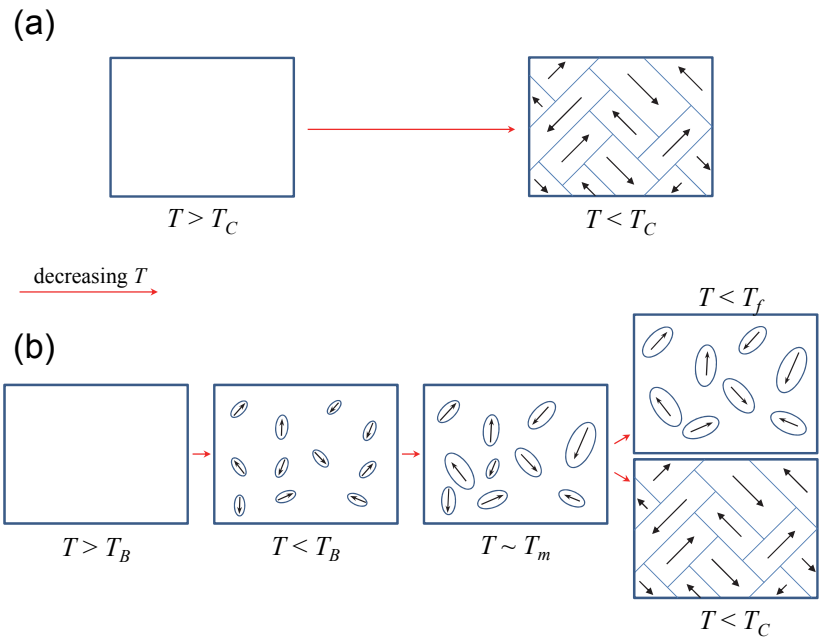

Fig. 7. Schematic presentation of the evolving of polar order in (a) conventional ferroelectrics and (b) relaxor ferroelectrics.

Although the great majority of relaxor ferroelectrics are based on perovskite Pb(B'B'')O_3-type materials with varying non-isovalent B-site cations, similar relaxor like properties have also been found in other types of material systems. These materials include, for example, nonstoichiometric $Pb_{1-x}La_x(Zr_{1-y}Ti_y)_{1-x/4}O_3$ (PLZT) perovskite, homovalent substituted perovskites of $Ba(Ti_{1-x}Sn_x)O_3$ and $Ba(Ti_{1-x}Zr_x)O_3$, tungsten bronze -type $Sr_{1-x}Ba_xNb_2O_6$, and modified polyvinylidene fluoride (PVDF) polymers. A common factor for all these materials seems to be the presence of a broken polar order which gives rise to peculiar relaxational properties.

1.3 Application areas for relaxor ferroelectrics

Many relaxor ferroelectric materials show enhanced electromechanical properties (see Section 2.2) and for this reason a majority of their applications are based on piezoelectric and electrostrictive effects. In general, the piezoelectric effect is utilized in various applications involving mechanical actuation and transduction.

These applications include accelerometers, valves, pumps, hydrophones, oscillators, motors and energy harvesters, to name just a few. Specifically, an enhanced electromechanical behaviour in relaxor-PT single crystals provides unequalled improvements in bandwidth, sensitivity and energy density for advanced transducer and actuator applications (Park & Hackenberger 2002). To date, ultrasound transducers for medical and sonar applications, accelerometers, and different actuators have been studied most extensively since these applications are considered to gain significant benefit from the enhanced electromechanical coupling factors, strain levels, and piezoelectric coefficients of relaxor-based single crystals (Park & Hackenberger 2002, Hackenberger *et al.* 2008, Zhang & Li 2012). For example, an ultrasound imaging system developed by Philips utilizes relaxor-PT single crystal (PureWave crystal) arrays in its transducer probes to provide higher sensitivity and efficiency as well as larger bandwidth so that a single probe can be used to generate high quality 3D images (Gururaja *et al.* 1999, Chen *et al.* 2006). Besides the piezoelectricity, pure relaxors and relaxor-PT (with low PT content) materials show beneficial electrostrictive behaviour around their permittivity maximum. In PMN-PT systems, for instance, the electromechanical behaviour is predominantly electrostrictive with $x < 0.20$ and piezoelectric with $x > 0.20$ (Kelly *et al.* 1997). In the electrostrictive effect the coupling between the field-induced strain and electric field (or induced polarization) is nonlinear while in the piezoelectric effect the coupling is linear. The sign of the induced electrostrictive strain does not change when the field is reversed and it is proportional to the square of the applied electric field. (Nye 1980). Contrary to many piezoelectrics, where domain reorientation introduces considerable hysteretic and aging effects, an electrostrictive strain-electric-field relation is practically anhysteretic and does not suffer from aging (Cross *et al.* 1980, Uchino 2010). This makes it possible to fabricate specific electromechanical devices with a highly accurate and reproducible response. As a remarkable example, electrostrictive PMN-based multilayer actuators have been utilized in the Hubble Space Telescope to drive its correction tilt mirrors remotely (Cross 2008).

Besides electromechanical applications, the peculiar structural properties of relaxor ferroelectrics lead to high permittivity, as well as remarkable electro-optic and pyroelectric effects. These properties are exploited for example in multi-layered ceramic capacitors, pyroelectric heat sensors, and electro-optic valves and displays (Shrout & Halliyal 1987, Wan *et al.* 2004, Uchino 1994 & 2010).

1.4 Motivation and organization of the Thesis

After the gradual revelation of many beneficial couplings between electrical, mechanical, thermal, and optical properties over the past 50 years, relaxor ferroelectrics have become an important material group for many applications. A more rapid growth of interest has been experienced especially during the last 25 years folllowing the discovery of an extraordinary electromechanical behaviour. Despite the long and successfully history of relaxor ferroelectric research spanning the past 50 years, many properties of prototypic $Pb(Mg_{1/3}Nb_{2/3})_{1-x}Ti_xO_3$ and $Pb(Zn_{1/3}Nb_{2/3})_{1-x}Ti_xO_3$ solid solution relaxor ferroelectric systems are still unclear or not known, especially under an applied electric field. Although many new materials are constantly being developed, their properties hardly match those of PMN-PT and PZN-PT, particularly in terms of electromechanical and pyroelectric performance. Therefore it is very important to study these basic relaxor ferroelectric systems in detail to gradually reveal the relations behind their versatile behaviour. A resulting more comprehensive understanding is the key to the improvement of their properties, not to mention the discovery and development of new applications and materials.

The objective of this work was to study different electric-field-induced dielectric and thermal effects in relaxor ferroelectric $Pb(Mg_{1/3}Nb_{2/3})_{1-x}Ti_xO_3$ and $Pb(Zn_{1/3}Nb_{2/3})_{1-x}Ti_xO_3$ systems in polycrystalline and single-crystalline forms. The electrocaloric effect, which links the entropy and electric field, is studied in detail since its behaviour strongly reflects the electrically induced structural changes in these materials. Importantly, related electric-field-induced polarization rotation and phase transitions are also closely connected to the mechanisms behind other phenomena, such as an enhanced piezoelectricity. Additionally, the electrocaloric effect is also a potential phenomenon to be utilized in future solid-state cooling applications. There are indications that relaxor ferroelectrics have substantial and advantageous electrocaloric properties, but the great scarcity of available data restricts our understanding of their behavior and technological potential. As a major objective, this scarcity of results is addressed in the Thesis by studying electrocaloric effect in PMN-PT and PZN-PT in great detail by means of direct measurements. Rather than evaluating their technological potential, the scope of the Thesis is to study the behaviour of the electrocaloric effect as a function of electric field, temperature and composition. A general summarized objective of this work is to provide more information for a better understanding of underlying

complex structural and electrothermal properties in relaxor ferroelectric types of materials from a new perspective.

This Thesis work involves a review of the related scientific literature and the empirical part arranged in the following way. Chapter 1 reviews first some basics of ferroelectricity and perovskite ferroelectrics in general. The remainder of the chapter is dedicated to description and current understanding of special lead-based relaxor ferroelectrics and their applications. Chapter 2 concentrates on studied ferroelectric systems of PMN-PT and PZN-PT by reviewing some of their key properties regarding the Thesis work. The main focus concentrates on previous studies of the PMN-PT system, but some references are given to the analogous PZN-PT system. In more detail, Chapter 2 deals first with phase diagrams of PMN-PT and PZN-PT systems. Then an extraordinary high piezoelectricity observed in these systems is reviewed by making connection with closely related electric-field-induced phase transitions and polarization rotation. Finally, an electrocaloric effect is considered by starting from basic definitions while some attention is also paid to previous research results and potential future application. All the essential experimental techniques and methodologies used in this Thesis are introduced in Chapter 3. The main experimental results are presented and discussed in Chapter 4. In Section 4.1, a development of ferroelectric order is studied in PMN-13PT ceramics by measuring dielectric and thermal responses to isothermally applied electric fields. The effect of different polarization rotation routes and electric-field-induced phase transitions on dielectric and thermal characteristics of PMN-PT single crystals close to the MPB region is reviewed in Section 4.2. Experimental electrocaloric measurements on PZN-8PT single crystal are performed and a simple lattice model is used to predict the main experimental findings in Section 4.3.1. An evolution of the directly measured electrocaloric effect in PMN-*x*PT systems as a function of temperature, electric field and composition is investigated in Section 4.3.2. Finally, the main conclusions of this Thesis work are given in Chapter 5.

2 Special characteristics related to studied relaxor ferroelectric systems

The studied material systems, PMN-PT and PZN-PT, and some of their special characteristic properties, particularly from the Thesis work point of view, are reviewed in this chapter. The main focus is on the PMN-PT system and some deviations related to the isostructural PZN-PT system are additionally referred to. Special attention is given to some electric-field-induced phenomena, such as polarization rotation, piezoelectricity, phase transitions and the electrocaloric effect, which are of particular interest.

2.1 Pseudobinary PMN-PT and PZN-PT phase diagrams

The structure of PMN-PT and PZN-PT has proven, over the years, to be exceedingly complex and different characterization techniques have revealed unique structural features on both the microscopic and macroscopic scales. In this chapter, the phase diagrams are considered more from the macroscopic or average point of view, although macroscopic phases may have different symmetries on a more microscopic scale. Other inhomogeneities and complexities commonly encountered in the PMN-PT and PZN-PT systems include phase-coexistence, concentration gradients, skin-effect, random-fields, grain size etc. Therefore, it is reasonable to point out at first that these factors greatly complicate the formation of unambiguous phase diagrams for these systems and also for other relaxors. Additionally, the PZN-*x*PT system with low *x* suffers from a scarcity of results since it cannot be fabricated by conventional ceramic processing, and therefore most of the available data comes from single crystals.

The canonical relaxor $Pb(Mg_{1/3}Nb_{2/3})O_3$ has an average cubic structure, but the local structure is distorted (Bonneau *et al.* 1989 & 1991, de Mathan *et al.* 1991). Already at high temperatures, especially Pb^{2+} and O^{2-} ions are permanently but randomly displaced from their ideal cubic positions in the paraelectric phase (Bonneau *et al.* 1989, Vakhrushev *et al.* 1994, Dkhil *et al.* 2001). Some signs of correlated displacements and developing ferroelectric order are observed below $T_f \approx 220$ K in PMN, but this order seems to be of short-range only (Tu *et al.* 1995, Gehring *et al.* 2001, Dhkil *et al.* 2001, Wakimoto *et al.* 2002, Ye *et al.* 2003). The situation with PZN seems to be even more complicated because different low-temperature structures are observed. For example, a region of coexistence with cubic and FE phases (Fujishiro *et al.* 2000, Lebon *et al.* 2002, Bing *et al.* 2005),

difference in skin (rhombohedral) and bulk (nearly cubic ‘X’ phase) structures (Xu *et al.* 2003a & 2004b), and a clear rhombohedral phase (Kisi & Forrester 2005) have all been reported for PZN.

Following the successful exploitation of highly piezoelectric $PbZr_{1-x}Ti_xO_3$ ceramic solid solutions, further research on solid solutions between relaxors and conventional ferroelectrics has also been performed. Most notably, lead titanate with its high Curie point (T_C~490 °C) has been widely used in many solid-solutions, which has led to the formation of a unique family of relaxor-PT materials, including PMN-PT and PZN-PT. A gradual occupation of the original B-site cation site by ferroelectrically active titanium ions in PMN-PT and PZN-PT decreases the size of chemically ordered regions and tends to trigger a macroscopic ferroelectric order at low temperatures (Randall & Bhalla 1990, Ye & Dong 2000, Ye *et al.* 2003). While the high temperature phase remains cubic, a clear low-temperature rhombohedral ferroelectric phase is shown already in PMN-5PT composition (Ye *et al.* 2003). Then, an increasing PT concentration tends to increase the rhombohedral distortion and domain size as well as to decrease the lattice constant (Ye *et al.* 2003, Xu *et al.* 2004c, Bai *et al.* 2004b & 2005). However, strict and definite compositional boundaries separating ferroelectric and averagely cubic regions at low temperatures cannot be drawn because the low-temperature ferroelectric phase is clearly different from conventional ferroelectrics in many ways. Essentially, the low-temperature rhombohedral structure in PMN-PT appears to be only an average since Pb cations are shifted towards the <001> direction while Ti, Mg, and Nb cations are displaced along the <111> direction (Dkhil *et al.* 2001). This indicates that the local symmetry is monoclinic although the average structure is rhombohedral. Additionally, regions of macroscopic cubical average symmetry with variously sized PNRs embedded in the low-temperature FE phase are observed in PMN-*x*PT even with reasonably high *x* values (Jiang & Kojima 2000, Shvartsman & Kholkin 2004). The aforementioned very unusual ‘X’ phase discovered in PZN has actually been observed also in both PZN-PT and PMN-PT compositions (Ohwada *et al.* 2003, Xu *et al.* 2003b & 2004c, Gehring *et al.* 2004). This nearly cubic ‘X’ phase is a bit mysterious since it does not show detectable rhombohedral distortion but some structural instabilities (e.g. large strain) are still observed below T_C. Remarkably, the ferroelectric polarization is established by the ionic displacements even in the undistorted lattice. (Xu *et al.* 2003b, Xu 2010). This exceptional decoupling of lattice distortion and polarization breaks down with higher concentrations of PT (Xu *et al.* 2003b). Another structural anomaly

met in PZN-PT and PMN-PT crystals is the skin-effect. In compositions where the abnormal 'X' phase is detected in the bulk, the surface of the crystal (~10–100 μm) shows a normal rhombohedral distortion instead. Even in the case of compositions with rhombohedral phase all over the crystal, the lattice parameters (the rhombohedral angle and lattice constant) are found to be different in bulk and surface. (Xu *et al.* 2004c & 2006).

Eventually the $PbTiO_3$ addition leads to more structural changes at temperatures below the universal cubic region. A morphotropic phase boundary (MPB) similar to PZT also exists in phase diagrams of PMN-PT and PZN-PT solid solutions (Kuwata *et al.* 1981 & 1982, Choi *et al.* 1989a & 1989b). A certain amount of PT causes a compositional phase transition from rhombohedral to tetragonal phase at the MPB, which literally means "the boundary between two forms". As in the case of regions with lower x, this morphotropic phase boundary is more complex than a simple phase boundary. As a matter of fact, the morphotropic boundary proves to be more like a morphotropic phase region since additional lower symmetry monoclinic phases exist between the rhombohedral and tetragonal phases. In the PMN-PT system the ferroelectric rhombohedral phase seems to develop into the tetragonal phase through two different monoclinic phases, M_B and M_C (space groups of *Cm* and *Pm*), within the region of x~0.27–0.35 (Noheda *et al.* 2002a, Kiat *et al.* 2002, Singh & Pandey 2003, Singh *et al.* 2006). The observation of lower-symmetry phases in the MPB region is rather difficult due to the small differencies and special high resolution equipement and techniques are usually needed for a detailed characterization. One interesting sign of phase complexity is that monoclinic *Cm* phases have been found even from PMN-20PT, and more remarkably, this phase changes to rhombohedral with decreasing grain size (Carreaud *et al.* 2006).

A similar picture arises in the case of PZN-PT where the orthorhombic O phase is reported in the morphotropic phase boundary region (Cox *et al.* 2001, La-Orauttapong *et al.* 2002). In contrast, monoclinic M_C phase is also observed instead of orthorhombic in PZN-PT (Kiat *et al.* 2002, Bertram *et al.* 2003). In many cases the observed phases coexist in the MPB region and a single phase is only rarely observed. Figure 8 shows recent refined phase diagrams for polycrystalline PMN-PT and singlecrystalline PZN-PT systems close to the MPB regions with labeled major phases. Phase diagram frames are mainly adopted from the works of Singh *et al.* (2006) and La-Orauttapong *et al.* (2002). Remarkably, the M_B phase in Figure 8(a) has only been observed in a few studies and is not shown in the majority of previous phase diagrams.

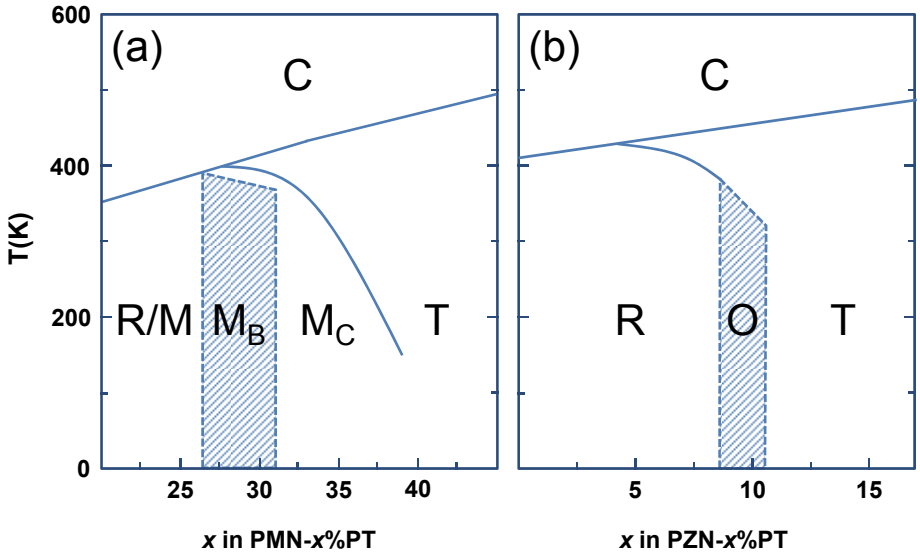

Fig. 8. Schematic pseudobinary phase diagrams for (a) PMN-PT, and (b) PZN-PT solid-solution systems around the morphotropic phase boundary regions. Figure modified from Singh *et al.* (2006) and La-Orauttapong *et al.* (2002).

2.2 High piezoelectricity and polarization rotation

Already in the 1980's PMN-PT and PZN-PT systems were found to show enhanced dielectric and piezoelectric properties with compositions approaching the newly discovered MPB region as in the case of the famous PZT (Kuwata *et al.* 1981, Choi *et al.* 1989b), and it seemed clear that electromechanical properties were maximized close to the MPB. These early investigations already showed some indications of an extraordinary piezoelectricity in single crystals of PMN-PT and PZN-PT (Kuwata *et al.* 1982, Shrout *et al.* 1990), and more detailed studies by Park & Shrout (1997) on these crystals finally confirmed an extraordinary high electromechanical behaviour. Remarkably, high strain levels (> 0.6%) as well as high piezoelectric and electromechanical coupling coefficients (d_{33} ~ 2500 pC/N, k_{33} > 90%) were observed close to the MPB region when an electric field was applied to a non-polar [001] direction (with respect to the cubic lattice) in rhombohedral crystals. More significantly these observations greatly renewed the interest in PMN-PT and related relaxor-based materials with MPB with a view to understanding the physical origin for such peculiar

electromechanical behaviour. Additionally, the development and search for new piezoelectric materials was directed towards materials with similar kinds of structural instabilities, and this trend continues to dominate the research field today, especially in the development of new lead-free piezoelectric materials. A general trend for piezoelectric materials development is sketched in Figure 9, where characteristic room-temperature d_{33} piezoelectric coefficient values are presented against the reporting years. This figure clearly illustrates the discovery of an enhanced piezoelectricity in single crystals of PMN-PT and PZN-PT. The basis for this diagram is adapted from the works of Yamashita & Ichinose (1996) and Ye (2009) and some values are added from the publications by Park & Shrout (1997) and Zhang *et al.* (2001).

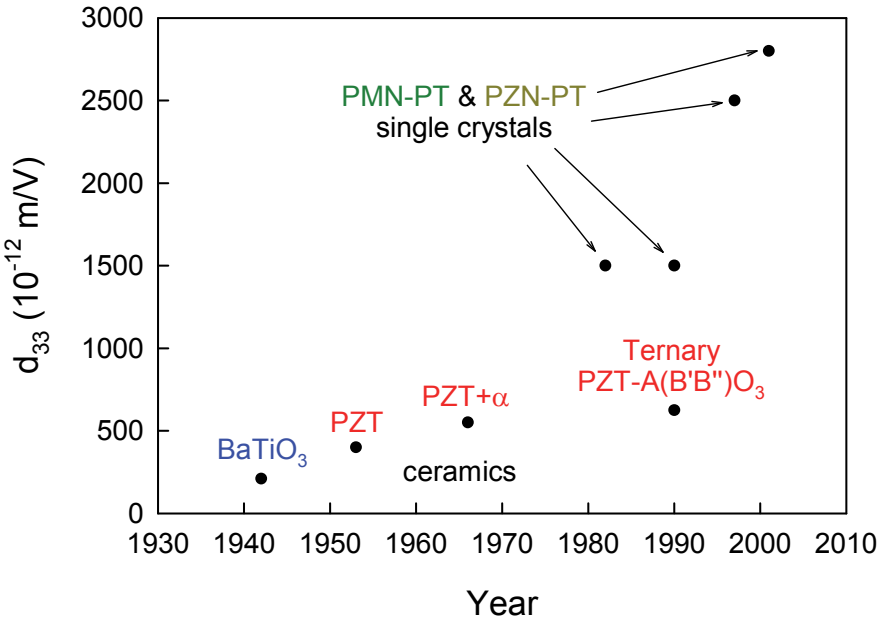

Fig. 9. General development trend of piezoelectric characteristics (as a form of d_{33}) with references to some notable piezoelectric materials. Figure modified from works of Yamashita & Ichinose (1996) and Ye (2009).

The discovery that the highest piezoelectric activity in relaxor-PT single crystals was observed in non-polar directions raised some questions. The previous assumptions (e.g. Jaffe *et al.* 1971), that a possible two-phase coexistence at the MPB and the resulting increased ease of polarization reorientation give rise to

strong piezoelectric effects, could not explain this finding (Davis 2007). While observing the high piezoelectricity in PMN-PT and PZN-PT, Park and Shrout (1997) assumed that a <001>-directional poling favours a stable engineered domain structure with four equivalent <111>-oriented domain variants in a rhombohedral crystal. The polar direction is expected to incline closer to the electric-field direction in each degenerate domain with an increasing <001>-directed electric field. The abruptly increasing strain at higher electric fields was believed to be associated with an electric-field-induced rhombohedral-tetragonal phase transition, where all polarizations collapse into the <001> direction. (Park & Shrout 1997).

The possible origin of high piezoelectricity in PMN-PT and related perovskites was greatly clarified at the turn of the new millennium when Noheda *et al.* (1999) found by means of high-resolution synchrotron x-ray diffraction (XRD) that there exists an undiscovered monoclinic phase in the ceramic $PbZr_{0.52}Ti_{0.48}O_3$ composition. Further investigations into PZT revealed that this monoclinic phase occupies a small region between rhombohedral and tetragonal phases close to the MPB (Noheda *et al.* 2000). As already described in Section 2.1, this finding proved to be somewhat universal since similar types of intermediate phases were discovered later in the MPB regions of PMN-PT and PZN-PT. When more high resolution structural studies were carried out on other related solid-solution systems, similar low symmetry monoclinic phases were found for example in PSN-PT (Haumont *et al.* 2003). Remarkably, all the experimentally observed monoclinic phases are also predicted theoretically through the expansion of the Landau-based free-energy expression (Vanderbilt & Cohen 2001).

The actual role of the monoclinic phase in explaining high piezoelectricity is emphasized in the polarization rotation model by Fu & Cohen (2000). The first-principle calculations show that a large piezoelectric response can be achieved by electric-field-induced polarization rotation in these types of materials. More precisely, it was shown that the high piezoelectricity in rhombohedral $BaTiO_3$ under a [001] directed electric field was due to polarization rotation in a plane between the [111] and [001] directions. As can be seen from the presentation of the lattice parameters of the observed monoclinic M_A phase in relation to the tetragonal lattice setting (Figure 10(a)), the inclination of a monoclinic cell naturally provides a rotation route for polarization between [111] and [001] directions (Figure 10(b)). In contrast to the rhombohedral and tetragonal phases, the polarization of the monoclinic phase is not limited to a specific

crystallographic direction but is free to rotate within its mirror plane. Therefore, in this picture the discovered monoclinic phase acts as a structural bridge with polarization lying in a plane between the higher symmetry rhombohedral and tetragonal phases (Noheda 2002, Noheda & Cox 2006). One important point to notice here is that piezoelectric usage of these materials is restricted to the region, where hysteretic transitions are not yet electrically induced (see Section 2.3) and a high low-hysteretic piezoelectric behaviour can be attained.

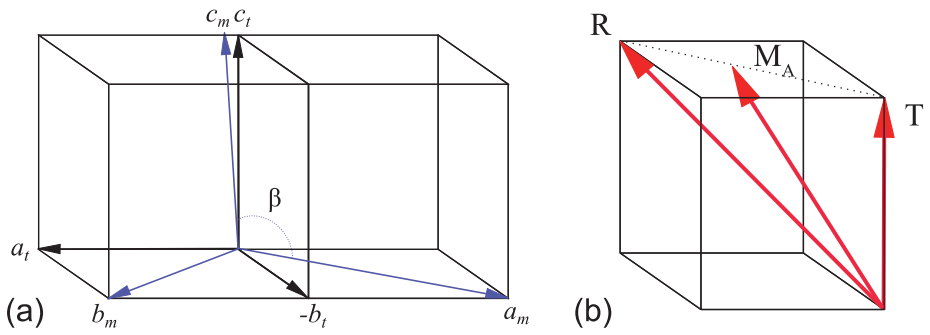

Fig. 10. (a) Monoclinic M_A lattice parameter presentation (angle β and lattice constants a_m, b_m, and c_m) in relation to tetragonal T unit cells (a_t, b_t, and c_t) (Modified from Noheda *et al.* 1999). (b) Principle of polarization rotation through a monoclinic M_A phase between rhombohedral <111> and tetragonal <001> directions.

Discoveries of lower symmetry MPB phases and polarization rotation paths in many perovskite materials have indeed given an increasing support for the polarization rotation model. All this information has led to a common statement that the high piezoelectricity of single-crystal PMN-PT and related materials of morphotropic phase boundary composition is explained by the polarization rotation from the polar direction to the direction of the electric field in the presence of one or more monoclinic phases (Davis 2006). This statement, however, is not fully adopted and there remains some debate over the issue. For example, the true nature of monoclinic phases is still somewhat mysterious. There are indications that monoclinic phases could actually be composed of very fine scale twins of rhombohedral and tetragonal phases (Khachaturyan *et al.* 1991, Jin *et al.* 2003, Viehland 2000, Wang 2006). Another viewpoint is to treat monoclinic phases as field-distorted higher symmetry phases, which also implies that monoclinic phases are not real stable phases (Durbin *et al.* 2000, Rajan *et al.* 2003, Lim *et al.* 2003). A more universal approach to explain high piezoelectricity in

many ferroelectrics is the idea of free energy instability, which is present also in the case of another mechanism of polarization extension leading to high piezoelectricity (Damjanovic 2009 & 2010). A similar argument was proposed already as an aspect of the polarization rotation model, when it was stated that the ease of polarization rotation is favoured by the flat energy surface (Fu & Cohen 2000). Furthermore, in the case of polarization rotation, the angle of rotation is directly related to strong anisotropy in a material's dielectric susceptibility (Budimir *et al.* 2003, Davis *et al.* 2007, Damjanovic *et al.* 2008, Damjanovic 2009). Moreover, experimental evidence indicates that the intrinsic crystal anisotropy accounts only for part of the electromechanical response in PMN-PT and PZN-PT (Bokov & Ye 2002, Zhang *et al.* 2003, Damjanovic *et al.* 2003, Dammak *et al.* 2003). More specifically, it seems that a significant amount of the enhanced electromechanical response can be governed by the extrinsic contribution from the domain structure and possible interphase boundaries (Pramanick *et al.* 2011).

2.3 Electric-field-induced phase transitions

Being naturally dielectric polar materials, the structure and related properties of PMN-PT and PZN-PT can be greatly influenced by the application of an external electric field. The phase diagrams described in Section 2.1 are derived from macroscopically non-polar ceramic materials and an applied electric field not only causes macroscopic polarization but also alters the stability regions and symmetry of the observed phases. Especially, the phase structure around the MPB region is highly unstable with nearly degenerate phase energies and even a low applied electric field can induce phase transitions by changing the respective free energies. Since the phase stability is highly dependent on both electric field and temperature, two different procedures are employed to study electric-field-induced phase transitions. Either an electric field is applied to a material at constant temperature or the temperature of the material is varied under fixed electric field values.

With low concentrations of $PbTiO_3$, the application of a high enough electric field induces a long-range ferroelectric rhombohedral order (Arndt *et al.* 1988, Ye & Schmid 1993, Vakhrushev *et al.* 1997). Depending on the temperature region, this transition to the rhombohedral phase is basically reversible or irreversible (Ye & Schmid 1993). The lower symmetry morphotropic phases can also be observed with low $PbTiO_3$ concentrations under the electric field application. For example,

a constant electric field E=0.5 kV/cm applied to the <001> direction enforces PMN-15PT single crystal to the M_A monoclinic phase at low temperatures (Cao *et al.* 2006). Generally, an applied constant electric field tends to favour a ferroelectric phase with polarization axis closer to the field direction and therefore phase stability regions are altered as a function of temperature. In PMN-xPT crystals close to the MPB region the polarization can rotate through three different monoclinic M_A, M_B, and M_C phases depending on the electric field direction (Bai *et al.* 2004a, Chien *et al.* 2004, Cao *et al.* 2005 & 2006). Polarization directions in these monoclinic phases are confined into separate planes instead of lying along particular crystallographical directions. These mirror planes for M_A, M_B, and M_C phases are collectively shown in Figure 11 in relation to higher symmetry R, O, and T phases. As can be seen, monoclinic M_A, M_B and M_C planes provide bridges between R–T, R–O and O–T end member pairs, respectively. Due to restrictions of the polarization directions imposed by the symmetry, perovskite rhombohedral (point group 3*m*), orthorhombic (*mm*2), and tetragonal (4*mm*) phases have 8, 12, and 6 possible polar directions while all three monoclinic phases (*m*) have 24 possible polar directions (Aizu 1970), as schematically shown in Figure 12. An electric field application inclines polarization directions closer to the field direction, and in single crystals specific domain-engineered structures are formed where certain possible domain variants remain depending on the field direction. Since the polarization is free to rotate in a monoclinic plane, its angle is not restricted but varies with temperature and electric field.

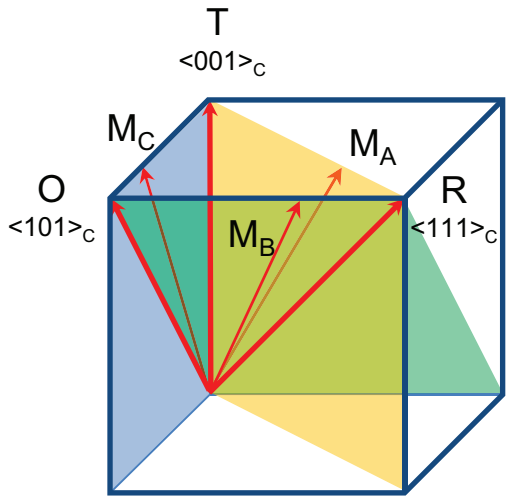

Fig. 11. Presentation of polarization directions for rhombohedral R, orthorhombic O, and tetragonal T in a pseudocubic cell. Monoclinic polarization planes for M_A, M_B, and M_C phases are presented as yellow, green, and blue, respectively.

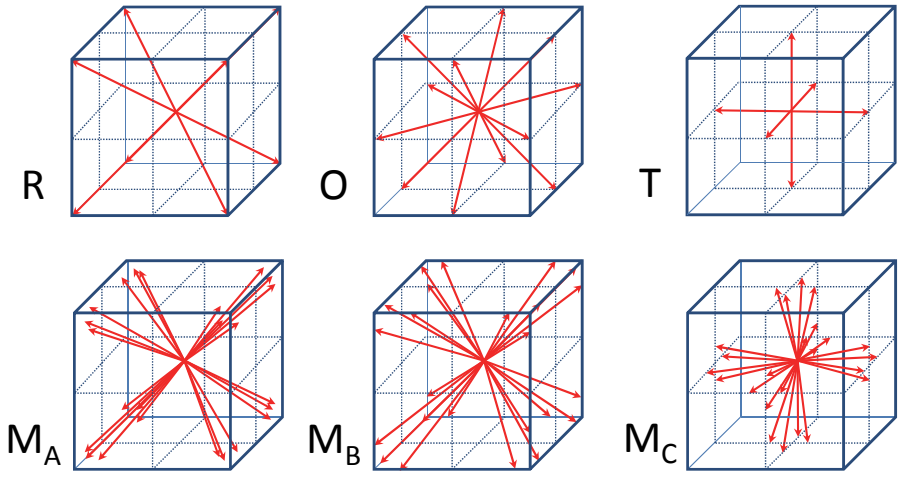

Fig. 12. Possible polar variants in a pseudocubic cell for ferroelectric rhombohedral R (3*m*), orthorhombic O (*mm*2), tetragonal T (4*mm*), and monoclinic M_A, M_B, and M_C (*m*) perovskite phases. Polarization directions in monoclinic phases are free to rotate within each plane while in R, O, and T phases the polarization lies along <111>, <110>, and <001> directions, respectively.

In-situ structural investigations reveal that a phase sequence in PMN-PT and PZN-PT at fixed temperature can be R→M_A→T, R→M_A→M_C→T or M_C→T with increasing *E* parallel to the <001> and R→M_B→O or M_C→O with increasing *E* parallel to the <011> depending on the temperature and composition (Noheda *et al.* 2001 & 2002b, Ohwada *et al.* 2003, Bai *et al.* 2004a, Chien *et al.* 2004, Cao *et al.* 2005 & 2006, Fang *et al.* 2009b). Application of an electric field to the <111> direction tends to stabilize the rhombohedral phase and a phase sequence of O→M_B→R can be induced in pseudo-orthorhombic PZN-PT (Davis *et al.* 2005). Some of these phase transition routes are described in Figure 13. Electric-field-induced phase transitions within different phases generally exhibit reversible and discontinuous first-order characteristics with hysteretic behaviour although a limited reversibility and phase coexistence are also evidenced (Durbin *et al.* 1999, Noheda *et al.* 2002a and 2002b, Ren *et al.* 2002, Ohwada *et al.* 2003, Bai *et al.* 2004a, Davis *et al.* 2006, Fang *et al.* 2009b, Paper III, Paper IV). Additionally, above T_C a reversible phase transition from the macroscopically non-polar relaxor phase to the polar ferroelectric state may occur, which is also typical in conventional ferroelectrics with first-order phase transition. The symmetry of the induced low-temperature metastable phase again depends on the direction of the applied electric field.

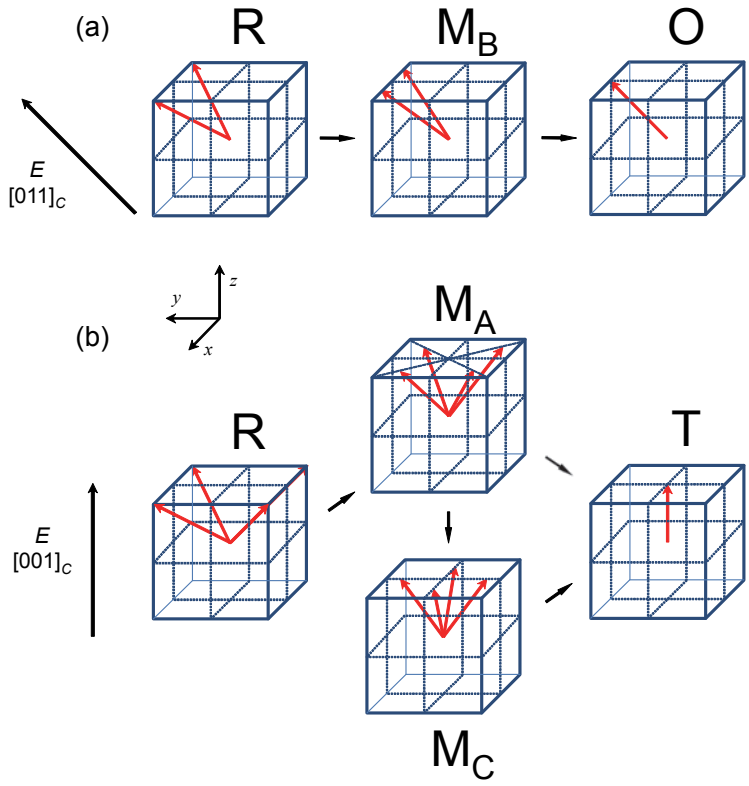

Fig. 13. Schematic description of some previously evidenced polarization rotation pathways and phases shown in pseudocubic cell during electric-field-induced phase transitions in PMN-PT and/or PZN-PT single crystals from domain-engineered R phase: (a) phase sequence R→M_B→O with increasing electric field along <011>$_C$, (b) phase sequence R→M_A→T, or R→M_A→M_C→T with increasing electric field along <001>$_C$.

A first-order transition line in the PMN-PT phase diagram (E vs. T) may terminate at the critical end point beyond which the adjacent phases become indistinguishable in the same way as in the pressure vs. temperature phase diagram of water (Kutnjak *et al.* 2006 & 2007). Latent heat gradually vanishes when approaching the critical end point and supercritical evolution is observed after that point. In the PMN-PT system the first-order nonpolar-polar phase transition and lower temperature ferroelectric-ferroelectric phase transitions terminate at critical end points (E=E_{CP} and T=T_{CP}) at least when the electric field

is applied to the [111]- or [110]-directions (Kutnjak *et al.* 2006 & 2007). These phase transitions in PMN-PT single crystals are generally found to show weakly first-order characteristics (Kutnjak 2008, Novak *et al.* 2012). Discontinuity in the order parameter (polarization P in this case) describing the phase transition vanishes beyond the critical end point where it shows continuous change as a function of temperature without hysteresis (see e.g. Brokate & Sprekels 1996). Additionally, signs of the critical end point have been observed by dc biased dielectric spectroscopic measurements in PZN-PT single crystal (Iwata *et al.* 2011). It was also suggested that the giant electromechanical activity of PMN-PT and related materials could be naturally explained by the approaching critical point (Kutnjak *et al.* 2006).

2.4 Electrocaloric effect

The electrocaloric effect can be described as a change of temperature as a function of an adiabatically applied electric field in a dielectric material (Lines & Glass 1977). This temperature change results from the field-induced change in dipolar entropy of the dielectric material (see Figure 1). Basically, all dielectric materials show an electrocaloric effect but high reversible entropy changes are required as a function of temperature and electric field in order to induce an electrocaloric effect sufficiently large to be of any potential interest for applications.

Although the electrocaloric effect has been known for a reasonably long time, it did not attract much research interest until quite recently. Only a few experimental measurements were carried out in the early days after the first study by Kobeco & Kurtchatov (1930) on Rochelle salt. More extensive studies were undertaken much later within the period of 1960–1990 but the effect still seemed to be too small to be succesfully exploited using the contemporary technology. A complete renewal of interest began in 2006 when Mischenko *et al.* (2006a) estimated a high electrocaloric temperature change in PZT thin films (ΔT~12 K) comparable to values achieved by the magnetocaloric effect. After this discovery a series of papers have reported a ‘giant’ electrocaloric effect in various ferroelectric-based thin film materials.

2.4.1 Thermodynamics of electrocaloric effect

A system in thermodynamic equilibrium may be described by a set of intensive and extensive variables. The expression for the electrocaloric temperature change can be derived from basic thermodynamic relations by starting from a total differential of entropy S. A change of this extensive variable is related to changes of chosen intensive parameters of temperature T, stress X, and electric field E in an elastic dielectric as follows (Lines & Glass 1977)

$$dS = \left(\frac{\partial S}{\partial T}\right)_{X,E} dT + \left(\frac{\partial S}{\partial X_{ij}}\right)_{T,E} dX_{ij} + \left(\frac{\partial S}{\partial E_i}\right)_{X,T} dE_i \,. \tag{1}$$

All the differential coefficients in Equation (1) are measures of physical effects shown in the Figure 1 (Nye 1980). The first differential term describing a change of entropy as a function of temperature is related to the heat capacity. The other two differentials, where entropy changes as a function of stress and electric field, indicate piezocaloric and electrocaloric effects, respectively. For simplicity one usually assumes material to be isotropic and under constant stress so that the second term in Equation (1) and tensor presentation can be omitted. Furthermore, it is considered that the thermodynamic process is reversible adiabatic (isentropic), where no heat exchange takes place and entropy change is zero, i.e. dS=0. This also means that the relation dQ=TdS holds for a reversible process. Using these assumptions, an infinitesimal temperature change from Equation (1) is given by

$$\begin{aligned} dT &= -\left(\frac{\partial T}{\partial S}\right)_E \left(\frac{\partial S}{\partial E}\right)_T dE = -\left(T\frac{\partial T}{\partial Q}\right)_E \left(\frac{\partial S}{\partial E}\right)_T dE \\ &= -\frac{T}{C_{p,E}} \left(\frac{\partial S}{\partial E}\right)_T dE. \end{aligned} \tag{2}$$

When using temperature, electric field and stress as independent variables, the differential of the Gibbs free energy dG of the system is expressed as (Damjanovic 1998)

$$dG = -SdT - x_{ij}dX_{ij} - D_i dE_i, \tag{3}$$

where x_{ij} is the strain tensor and D_i is the electric displacement tensor. Then the physical electrocaloric effect $(\partial S/\partial E)_T$ in Equation (2) can be replaced by another physical effect $(\partial D/\partial T)$ since they are related by the Maxwell relation

$$\left(\frac{\partial S}{\partial E_i}\right)_T = -\frac{\partial}{E_i}\left(\frac{\partial G}{\partial T}\right)_{X,E} = -\frac{\partial}{\partial T}\left(\frac{\partial G}{\partial E_i}\right)_{X,T} = \left(\frac{\partial D_i}{\partial T}\right)_E \tag{4}$$

derived from Equation (3). After the replacement, the electrocaloric temperature change is expressed as

$$\Delta T = -\frac{T}{C_{p,E}}\int_{E_1}^{E_2}\left(\frac{\partial D}{\partial T}\right)_E dE = -\frac{T}{C_{p,E}}\int_{E_1}^{E_2}\left(\frac{\partial P}{\partial T}\right)_E dE\,. \tag{5}$$

The application of Equation (5) is the most widely used method for an indirect evaluation of the electrocaloric effect in ferroelectric-based materials. The isothermal hysteresis loops are measured at desired temperatures and the obtained polarization data $P(E,T)$ values are fitted with high-order polynomials to derive the $P(T)$ dependence at distinct fixed E values. The calculated differentials $(\partial P/\partial T)_E$ are then fitted as a function of E so that the integration gives the values for ΔT.

Although the indirect method described above is known to give reasonably realistic values for the electrocaloric effect, there are some limitations for its applicability (Scott 2011, Valant 2012). For instance, relaxors are known to show non-ergodic behaviour and an application of statistical thermodynamic equilibrium relations may be questionable. Moreover, the dynamics of polarization may have significant effects on the indirect values evaluated at different frequencies (Starkov *et al.* 2010). The above treatment also omits the secondary effect where temperature is changed by the deformation of material through the converse piezoelectric effect (see Figure 1).

More generally, the physical picture of the electrocaloric effect can be explained by changes in dipolar and other forms of entropy, e.g. phonons, electrons, etc. (Dunne *et al.* 2008, Pirc *et al.* 2011a & 2011b). Application of electric field into dielectric material tends to promote polarization and reorientate any existing dipolar entities (Figure 14). The field-induced ordering of dipoles leads to a decreased dipolar entropy ($\Delta S_{dip} < 0$), and since under adiabatic conditions the total entropy does not change ($\Delta S = 0$), the decrease in dipolar entropy is compensated for by other forms of entropy (i.e. lattice phonon-related contributions). This causes an increase in temperature of the dielectric material under adiabatic conditions. Since the electrocaloric temperature change is reversible, this process is reversed on decreasing the electric field.

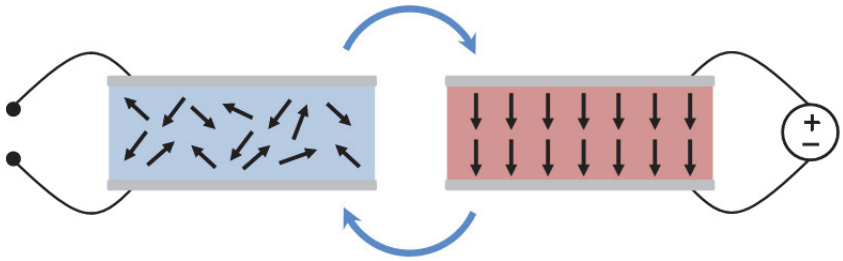

Fig. 14. Schematic presentation of the reversible dipolar ordering/disordering by an applied electric field leading to the electrocaloric temperature change under adiabatic conditions.

By assuming that the entropy can be divided into two largely independent contributions due to dipolar and other field-independent degrees of freedom so that $S(E,T) = S_{dip}(E,T) + S_{ph}(T)$, the adiabatic conditions yield (Pirc *et al.* 2011b)

$$S_{ph}(T_2) - S_{ph}(T_1) = -\left\{S_{dip}(E_2,T_2) - S_{dip}(E_1,T_1)\right\}, \tag{6}$$

when changing state from (E_1, T_1) to (E_2, T_2). The lattice entropy change on the left hand side can be resolved by integrating $C_{ph}(T)/T$ between T_1 and T_2. If the lattice heat capacity per unit volume $C_{ph}(T)$ is assumed to be constant over the temperature range of $\Delta T = T_2 - T_1$, Equation (6) leads to a following expression for the final temperature T_2 (Pirc *et al.* 2011b)

$$T_2 = T_1 \exp\left\{-\frac{S_{dip}(E_2,T_2) - S_{dip}(E_1,T_1)}{C_{ph}(T_1)}\right\}, \tag{7}$$

which is reached by changing the electric field from E_1 to E_2. This equation is equally suitable for both ferroelectrics and relaxors (Pirc *et al.* 2011b). Basically different models can be used to implement system configurational entropies and the corresponding electrocaloric temperature can then be extracted. Naturally the dipolar entropy can be extracted from the free-energy instead of using the specific Maxwell relation of Equation (4). For ferroelectrics the free-energy can be expressed by a well-known phenomenological Landau-based mean field free-energy expansion in terms of polarization (the order parameter) as the following simplified form of

$$G = G_0 + \frac{1}{2}aP^2 + \frac{1}{4}bP^4 + \frac{1}{6}cP^6 + \ldots - EP, \tag{8}$$

where a, b, c, … are temperature dependent coefficients and G_0 is the free-energy without polarization. Usually the mean-field approach assumes that only the coefficient a is regarded as a temperature dependent factor. By applying the equilibrium conditions (i.e. $[\partial G/\partial P]_E = 0$), the dipolar entropy $S_{dip} = -(\partial G/\partial T)_E$ can be extracted and the final temperature of Equation (7) takes the form of (Pirc *et al.* 2011b)

$$T_2 = T_1 \exp\left\{\frac{1}{2C_{ph}}\left[a_1(T_2)P^2(E,T_2) - a_1(T_1)P^2(0,T_1)\right]\right\}, \tag{9}$$

where $a_1 = da/dT$ is the differential of the coefficient a for the P^2 term in the free-energy expansion and the electric field is assumed to change from 0 to E (Pirc *et al.* 2011b). A simpler expression is obtained when Equation (9) is linearized and the right-hand side T_2 is replaced by T_1 (i.e. isothermal approximation) before extracting the entropy change from the free-energy expansion. That simplification gives

$$\Delta T \cong -\frac{T}{C}\Delta S = \frac{T}{2C}a_1 \Delta P^2 , \tag{10}$$

which was often used in many earlier treatments of the electrocaloric effect in ferroelectrics (see e.g. Lines & Glass 1977). In this way it is possible to estimate the electrocaloric temperature change by determining the coefficient a_1 and the polarization change. However, this method is largely limited and gives very rough estimates with accuracy of around 50% or less (Scott 2011).

When the dipolar entropy is linked with polarization reorientation under an applied electric field, the maximum saturated alignment of dipolar entities (the minimum dipolar entropy) is naturally expected above a certain electric field value. From this point of view, the maximum electrocaloric temperature change is achieved when all the dipoles are aligned. Pirc *et al.* (2011a) used this idea to derive a relation for the saturated electrocaloric temperature change ΔT_{sat}. When the number of equivalent orientational states is known for each dipolar entity, the maximum and minimum dipolar entropies can be derived from the Gibbs-Shannon entropy of mixing. Then the saturated electrocaloric temperature change is expressed as (Pirc *et al.* 2011a)

$$\Delta T_{sat} = \frac{T \ln \Omega}{3\varepsilon_0 \Theta C_E} P_{sat}^2 , \tag{11}$$

where Ω, Θ, P_{sat} are the number of orientational states, the Curie constant, and saturation polarization, respectively. This equation allows for a simple estimation of the maximum electrocaloric effect caused by dipole orientation. The values for P_{sat} and Θ can be derived from actual physical measurements of polarization and permittivity (Pirc *et al.* 2011a). Although some other factors, such as first order phase transitions and mechanical boundary conditions, may also have significant impacts on ECE, this expression can still be used for an initial estimation of the magnitude of ECE in different systems.

2.4.2 Electrocaloric solid-state cooling and specific material requirements

Increasing economical and environmental concerns over the currently used refrigeration technologies have created an emerging interest in alternative cooling technologies especially over the past decades. More efficient, versatile, and eco-friendly solutions are urgently needed to reduce the emissions and the use of natural resources. A promising way to address the problems encountered with conventional vapour-compression cooling is to provide solid-state cooling with few moving parts and without working fluids (Dieckmann *et al.* 2011a). The currently existing solid-state cooling and generator devices utilize the thermoelectric Peltier effect. Although Peltier devices are used in small-scale coolers, such as chip-cooling applications and handheld refrigerators, their coefficient of performance is currently too low to challenge conventional vapour-compression cycles (Dieckmann *et al.* 2011a). Other solid-state cooling solutions utilizing, for example, electron tunnelling, thermoelasticity and different coupling effects in ferroic materials, have been more actively studied during recent years (Dieckmann *et al.* 2011b, Fähler *et al.* 2012). Especially, some ferroic materials offer large caloric effects induced either by magnetic, electrical or mechanical fields. Of these caloric effects in ferroics, the magnetocaloric effect is the most studied for cooling applications and high magnetic entropy change values have been observed for example in ferromagnetic Gd-based alloys close to room temperature (Pecharsky & Gschneidner 1997). The electrocaloric effect as another ferroic-based caloric effect has become a serious alternative to the magnetocaloric effect during recent years, as already mentioned. Especially, the application and use of an electric field requires less complex components and control.

A basic principle of an electrocaloric cooling cycle is presented in Figure 15(a). When an external electric field is applied to the material at T, the temperature of an active electrocaloric element is adiabatically increased (stage transition A→B) to $T+\Delta T$ as described earlier. This additional heat can be dissipated in a heat sink, which causes the active element to decrease its temperature back to T (B→C). Then, the removal of the applied electric field further decreases the temperature to $T-\Delta T$ within the active isolated material. Now, some heat energy can be extracted from a desired heat source which increases the temperature of the active electrocaloric element to T and completes the cooling cycle. This kind of cooling cycle, which involves two constant-entropy and two constant field transitions, is only one of many possible cycle options (Scott 2011). The optimal refrigeration cycle is based on a Carnot-like cycle with two isothermal and two adiabatic processes. The Carnot-like electrocaloric cooling cycle is presented in the temperature-entropy diagram of Figure 15(b). In this case, the electrocaloric material rejects and absorbs heat at constant temperatures T_h (B→C) and T_c (D→A), respectively, while transitions between these temperatures are isentropic (Epstein & Malloy 2009). The isothermal steps in the cycle can be realized by adjusting the electric field during the heat absorption and rejection. Otherwise, if the electric field is kept constant, temperature decreases/increases during the heat rejection/absorption could lead to reduced efficiency of the refrigeration cycle (Epstein & Malloy 2009). Other ideal refrigeration cycles for electrocaloric cooling include Stirling and Ericsson cycles (He *et al.* 2002). An optimal cooling cycle should maximize the parameter called the refrigerant capacity, which is a product of the absorbed entropy ΔS and temperature difference ΔT (Wood & Potter 1985). This indicates that a high electrocaloric temperature change should also be accompanied by a high entropy change. From an application point of view, the electrocaloric cooling cycles have been considered for utilization in, for example, air conditioning, refrigeration, and heat pumping (Sinyavskii *et al.* 1989, Sinyavskii 1995, Mischenko *et al.* 2006a, Karmanenko *et al.* 2007, Neese *et al.* 2008). Electrocaloric materials could also be used in pyroelectric thermal energy harvesting cycles (Sebald *et al.* 2008 & 2009).

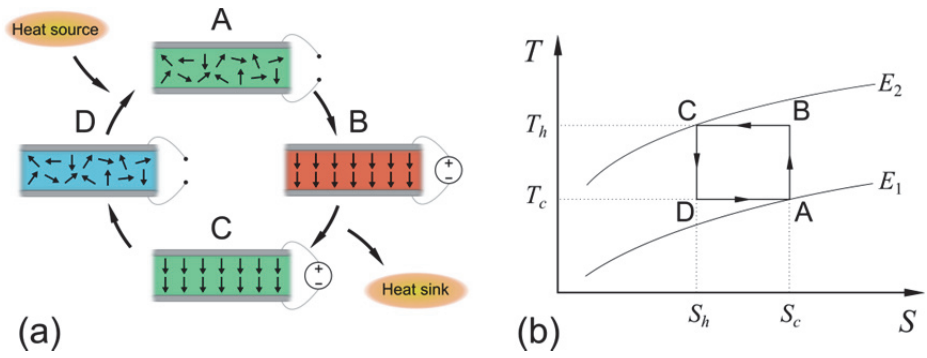

Fig. 15. (a) A schematic presentation of an electrocaloric cooling cycle. (b) A possible Carnot-type thermodynamic refrigeration cycle with adiabatic and isothermal processes (Modified from Lu & Zhang 2009).

In general, good electrocaloric materials should show high entropy changes as a function of electric field and temperature. In polar ferroelectric-based materials it is possible to induce reasonably large dipolar changes by application of an electric field, especially if phase transitions with large entropy changes are involved. Ideally, the electrocaloric effect can be large in any insulating material with a highly temperature dependent dielectric susceptibility (Rose & Cohen 2012). In addition to primary electrocaloric parameters there are some important material properties to be considered from the application point of view. If material has a particularly high dielectric breakdown field, larger fields can be applied to induce higher electrocaloric temperature changes. In fact, it has been stated that the dielectric strength is the main limiting factor for obtaining a useful electrocaloric effect (Valant *et al.* 2012). Especially, thin films are known for their high breakdown strength, which mostly explains the reported 'giant' electrocaloric effects where high electrocaloric temperature changes can simply be induced by large applied fields. The major drawback of thin films is their intrinsically small thermal mass which means that significantly higher temperature changes are required to achieve similar heat energies ($Q=mc_p\Delta T$) compared to bulk materials with a higher thermal mass (Valant *et al.* 2012). On the other hand, bulk materials are limited by their lower dielectric strength where the breakdown mechanism is dominated by electromechanical breakdown instead of by the avalanche breakdown mechanism typical for thinner films. In either case, strong fields may also introduce excessive Joule heating which should also be minimized. Furthermore, the electrocaloric effect should be strong over a wide temperature

range close to the desired working temperature, which enables the realization of effective cooling cycles.

Apart from an efficient electrocaloric material, some advanced engineering solutions are also needed, especially for a controlled heat transfer, in order to realize practical cooling cycles. For example, highly anisotropic materials, such as carbon nanotubes and liquid crystals, have been suggested to provide a potential solution for a problematic thermal transfer (Epstein and Malloy 2009). Additionally, a cooling cycle with higher overall temperature changes can be achieved by using regenerative heat exchangers, i.e., regenerators (Sinyavsky & Brodyansky 1992, Dieckmann *et al.* 2011b). These regenerators should possess high thermal anisotropy, and they have been tested and proven to be efficient in electrocaloric cooling cycle demonstrations (Sinyavsky & Brodyansky 1992, Gu *et al.* 2013a & 2013b).

2.4.3 Electrocaloric effect in PMN-PT and PZN-PT

The investigated relaxor ferroelectric systems have characteristically high polarization variations when the electric field and temperature are changed. These properties are expected to produce high dipolar entropy changes and a large electrocaloric effect. Another great advantage of PMN-PT and PZN-PT materials is that their phase transition temperatures can be altered by changes in the composition. As the highest electrocaloric effects are generally observed above the highest polar-nonpolar phase transition temperatures (i.e. the Curie point) the tunability of this temperature can be utilized to change the temperature range of the effect. Experimental and theoretical studies also suggest that polar nanodomains in relaxors make an additional contribution to the electrocaloric effect (Birks 1986, Shebanovs *et al.* 2002, Hagberg *et al.* 2008, Dunne *et al.* 2011, Shi & Soh 2011). Additionally, the responsivity of the electrocaloric effect ($\Delta T/E$) is found to reach a maximum value near the liquid-vapour type critical end point which terminates the line of field-induced first-order phase transitions (Pirc *et al.* 2011b, Rožič *et al.* 2011b).

Some experimental electrocaloric results obtained so far for bulk-type PMN-PT and PZN-PT systems are listed in Tables 1 and 2. The results of this Thesis work are presented in Chapter 4 and are thus excluded from these Tables. The values for ΔT range from 0.15 °C to 2.7 °C with electric fields of 10–90 kV/cm. The studies performed by indirect measurements are listed together with direct measurements. A significant variation is observed among the measured results

making comparisons rather difficult. Different measurement methods and experimental setups as well as the small number of measurement points may be regarded as the major sources of this variation. Especially, the majority of the direct electrocaloric measurement studies were found to involve only a very limited number of data points. While the indirect measurement method enables required polarization values to be extracted for a range of electric fields during a fast measurement cycle, the direct electrocaloric effect measurement is performed separately for each electric field with extended field application times. Therefore, the direct method places the sample under more extensive cycling in comparison to the more straightforward indirect method.

Some general trends, however, can still be drawn from the experimental results. The electrocaloric temperature change shows the highest values close to or above the Curie point. The highest electrocaloric responsivity $\Delta T/E$ is usually observed at low electric fields close to the phase transition and it tends to decrease with higher fields. This is generally to be expected since the highest responsivity is predicted to occur at the critical end point (Pirc *et al.* 2011b, Rožič *et al.* 2011b). In addition, the anisotropy of the electrocaloric effect may be significant as shown for PMN-25PT by Sebald *et al.* (2006). A more detailed review of the electrocaloric results on PMN-PT can be found elsewhere (see Peräntie *et al.* 2014).

Table 1. Experimental electrocaloric data for bulk-type PMN-PT.

Composition	ΔT (°C)	T (°C)	E (kV/cm)	ΔT/E (cm°C/MV)	Measurement details[1]	Material form[2] & thickness (μm)	Reference
PMN	0.15	-47	15	10	Thermocouple	PC n/a	Shebanovs *et al.* (1986)
PMN	2.5	67	90	28	Thermistor	PC 80	Rožič *et al.* (2011a)
PMN-8PT	1.35	23	15	90	Thermocouple	PC 3000	Xiao *et al.* (1998)
PMN-10PT	1.25	28	15	83	Thermocouple	PC 3000	Xiao *et al.* (1998)
PMN-10PT	0.45	50	29.1	16	Thermocouple	PC 500	Shebanov *et al.* (2002)
PMN-10PT	1	55	40	25	Indirect (1 Hz)	(111) SC 600	Luo *et al.* (2011)
PMN-10PT	1	10	16	63	IR detector	PC 100	Shaobo *et al.* (2004)
PMN-13PT	0.56	70	24	23	Thermocouple	PC 1000	Hagberg *et al.* (2008)
PMN-15PT	1.71	18	16	107	IR detector	PC 100	Shaobo *et al.* (2004)
PMN-25PT	0.40	32	15	27	Thermocouple	PC 3000	Xiao *et al.* (1998)
PMN-25PT	0.56[a]	120	25	22	DSC	(100) SC 1000	Sebald *et al.* (2006)
PMN-25PT	0.89[a]	100	25	36	DSC	(110) SC 1000	Sebald *et al.* (2006)
PMN-25PT	1.1[a]	100	25	44	DSC	(111) SC 1000	Sebald *et al.* (2006)
PMN-25PT	0.9[a]	110	25	36	DSC	PC 1000	Sebald *et al.* (2006)
PMN-29PT	2.3	171	50	46	Indirect (200 Hz)	(100) SC 250	Luo *et al.* (2012)
PMN-29PT	2	167	50	40	Indirect (200 Hz)	(111) SC 250	Luo *et al.* (2012)
PMN-30PT	2.7	157	90	30	Thermistor	PC 60–100	Rožič *et al.* (2011b)
PMN-30PT	2.7	127	12	230	Indirect (1 kHz)	(111) SC 200	Chukka *et al.* (2011)
PMN-30PT	0.65	135	10	65	DSC	(100) SC 1000	Le Goupil *et al.* (2012)

[a]Calculated from heat using C= 0.35 J/gK, [1]Indirect refers to evaluation from polarization measurements performed at given frequency, [2]PC = polycrystalline ceramics, (*hkl*) SC = single crystal of (*hkl*) plate.

Table 2. Experimental electrocaloric data for bulk-type PZN-PT.

Composition	ΔT (°C)	T (°C)	E (kV/cm)	ΔT/E (cm°C/MV)	Measurement details[1]	Material form[2] & thickness (μm)	Reference
PZN-8PT	0.31	165	10	31	Indirect (1 Hz)	(100) SC 340	Priya *et al.* (2003)
PZN-8PT	0.47	195	10	47	Indirect (1 Hz)	(110) SC 820	Priya *et al.* (2003)
PZN-8PT	0.21	190	10	21	Indirect (1 Hz)	(111) SC 870	Priya *et al.* (2003)

[1]Indirect refers to evaluation from polarization measurements performed at given frequency, [2]PC = polycrystalline ceramics, (*hkl*) SC = single crystal of (*hkl*) plate.

The experimental electrocaloric results obtained for thin film PMN-PT systems are listed in Table 3. One can see that all the results are obtained from indirect measurements based on polarization data. Applied electric fields are typically more than an order of magnitude higher than for bulk-type materials. Again, a great variation of results is shown with ΔT values of around 4–31 °C. Although the absolute values of ΔT are remarkably higher than those in bulk-type materials, the corresponding heat energy values are lower in thin films. Many additional effects, such as clamping and misfit, are considered to play a significant role in the electrocaloric effect of thin films (e.g. Akcay *et al.* 2008, Qiu & Jiang 2008 and 2009), which makes the result comparison even more challenging.

Table 3. Experimental electrocaloric data for PMN-PT thin films.

Composition	ΔT (°C)	T (°C)	E (kV/cm)	ΔT/E (cm°C/MV)	Measurement details[1]	Orientation[2] & thickness (μm)	Reference
PMN-7PT	9 (6.8)[a]	25 (0)[a]	723	12	Indirect (100 Hz)	PC 0.21	Correia *et al.* (2009)
PMN-10PT	5	75	895	6	Indirect (10 kHz)	PC 0.26	Mischenko *et al.* (2006b)
PMN-32PT	13.4	145	600	22	Indirect (100 Hz)	(001) 0.2	Feng *et al.* (2011a)
PMN-33PT	14.5	145	600	24	Indirect (1 kHz)	(001) 0.2	Feng *et al.* (2011b)
PMN-33PT	4.25	235	116	37	Indirect (5 kHz)	PC 0.43	He *et al.* (2011)
PMN-35PT	31	140	747	42	Indirect (200 Hz)	PC 0.24	Saranya *et al.* (2009)

[a]Values in parenthesis obtained on cooling, [1]Indirect refers to evaluation from polarization measurements performed at given frequency, [2]PC refers to polycrystalline and (*hkl*) refers to any preferred orientation.

2.4.4 Electrocaloric parameters in some other materials

Apart from PMN-PT and PZN-PT systems, the electrocaloric effect has been studied in many other materials ranging from other perovskites to polymers (see e.g. review by Valant 2012). Direct and indirect measurements have been performed for materials in the form of single crystals, thin films, thick films, multi-layered capacitors, and bulk ceramics. In addition, many theoretical investigations have been carried out to consider the electrocaloric effect in general and especially in lower dimensional structures, such as thin films, nanoparticles and rods. Details of some of the most interesting and notable experimental electrocaloric studies are given in Table 4.

The indirect electrocaloric measurements performed by Mischenko *et al.* (2006) on PZT thin film triggered a renewed interest in the electrocaloric effect. They first discovered that a 'giant' electrocaloric temperature change can be expected in PZT thin films close to the phase transition temperature. Similar measurements later suggested that a high electrocaloric ΔT is predicted in many ferroelectric thin films. In particular, ferroelectric PVDF-based co- and terpolymers, which can tolerate strong electric field strengths, were found to give indications not only of high electrocaloric temperature change but also high accompanying entropy changes closer to room temperature (Neese *et al.* 2008, Lu & Zhang 2009). Importantly, more reliable experimental evidence on these indirectly evaluated high electrocaloric temperature changes has been obtained from further direct temperature measurements. In fact, the first direct electrocaloric effect measurements on thin films of organic polymers and perovskite PLZT by IR sensor and an attached thermistor reproduced the prediction of high electrocaloric ΔT (Lu *et al.* 2010). Interestingly, the electrocaloric effect in polymers was enhanced and shifted to lower temperatures when the ferroelectric P(VDF-TrFE) copolymer was transformed to the relaxor-type polymer either by electron irradiation or formation of P(VDF-TrFE-CFE) terpolymer (Neese *et al.* 2008, Lu *et al.* 2010). To date, the highest electrocaloric temperature change ($\Delta T > 40$ °C) has been measured for a PLZT thin film at T=45 °C. This value even exceeds theoretical upper limit ΔT_{sat} estimated for this material (Pirc *et al.* 2011a). Due to the low thermal mass of thin films, other solutions based on bulk-type materials have been considered to be more practical for macroscopic electrocaloric cooling applications (Valant 2012). One interesting idea is to utilize multi-layered capacitor structures where high electric fields can be applied to relatively thin layers and the layered construction enables the

realization of a higher thermal mass. Direct measurements indeed, demonstrate that high electrocaloric temperature changes can be achieved by this method (Bai *et al.* 2011). One of the highest electrocaloric effects in bulk-type ceramics has been measured for PST-based materials (Shebanov & Borman 1992, Shebanovs *et al.* 2002). Interestingly, the electrocaloric effect in PST is strong when close to room temperature and it is largely affected by the degree of the B-site order.

Table 4. Experimental electrocaloric data for some other ferroelectric-based materials.

Composition	ΔT (°C)	T (°C)	E (kV/cm)	ΔT/E (cm°C/MV)	Measurement details[1]	Orientation[2] & thickness (μm)	Reference
PZT	12	226	480	25	Indirect	PC 0.35	Mischenko *et al.* (2006a)
PLZT	>40	45	1200	33	Thermistor	PC 0.45	Lu *et al.* (2010)
P(VDF-TrFE)	12.6	80	2090	6	Indirect	PC 0.4-2	Neese *et al.* (2008)
P(VDF-TrFE-CFE)	12	55	3070	4	Indirect	PC 1.0	Neese *et al.* (2008)
P(VDF-TrFE)[3]	20	33	1600	13	IR detector	PC 1-1.5	Lu *et al.* (2010)
$BaTiO_3$	7.1	80	800	9	DSC	PC 3[a]	Bai *et al.* (2011)
Sb-doped PST	2.3	-3	50	50	Thermocouple	PC 500	Shebanov & Borman (1992)
doped PST MLCC	3.5	18	138	25	Thermocouple	PC 64-72[a]	Shebanovs *et al.* (2002)

[a]Thickness for single layer in MLCC, [1]Indirect refers to evaluation from polarization measurements performed at given frequency, [2]PC = polycrystalline for ceramics/partially crystalline for polymers, (*hkl*) refers to preferred orientation, [3]Material irradiated by high energy electrons.

More direct and detailed studies are clearly needed to clarify the magnitude and behaviour of the electrocaloric effect in different materials. Especially this is needed for a better understanding of the phenomenon but also for testing its technological potential.

3 Experimental techniques and methodology

The material fabrication and preparation methods used in this research are introduced in this chapter together with the associated empirical methodology.

3.1 Material synthesis and preparation

3.1.1 Reactive-sintering of PMN-13PT ceramics

As with many ceramics, the most straightforward manufacturing method for PMN-based ceramics is the mixed oxide method. The reaction in a typical mixed oxide method proceeds in a complex manner involving several intermediate phases. Usually some pyrochlore-type phases are formed first, and those subsequently react with the remaining oxides to produce the perovskite phase (Inada 1977, Swartz & Shrout 1982, Guha 1999). There are a few approaches that differ slightly in the reaction sequence leading to the formation of PMN. Earlier studies suggest that PMN is formed from constituent oxides by the reactions (Inada 1977)

$$3PbO + 2Nb_2O_5 \rightarrow Pb_3Nb_4O_{13}$$
$$Pb_3Nb_4O_{13} + PbO \rightarrow 2Pb_2Nb_2O_7$$
$$Pb_2Nb_2O_7 + \frac{1}{3}MgO \rightarrow Pb(Mg_{1/3}Nb_{2/3})O_3 + \frac{1}{3}Pb_3Nb_4O_{13}\,.$$

In order to achieve high purity by the mixed oxide method, a number of repeated calcining steps are required. Another reaction route suggests the formation of an oxygen-deficient ternary pyrochlore, which reacts with remaining PbO and MgO to produce perovskite PMN (Guha 1999) as follows

$$6PbO + MgO + 3Nb_2O_5 \rightarrow Pb_6MgNb_6O_{22}$$
$$Pb_6MgNb_6O_{22} + 3PbO + 2MgO \rightarrow 9Pb(Mg_{1/3}Nb_{2/3})O_3\,.$$

The intermediate ternary pyrochlore forms a narrow homogeneity range with another pyrochlore of $Pb_7MgNb_6O_{23}$ so that the composition is $Pb_{2-x}(Mg_{0.286}Nb_{1.714})O_{6.571-x}$, and other ternary pyrochlores reported in this system usually lie within this range (Guha 1999). An excessive PbO evaporation at elevated temperatures easily drives the reaction sequence towards stable pyrochlore phases. Additionally, the perovskite phase starts to decompose at high

temperatures producing pyrochlore, which further melts and dissociates to $Mg_4Nb_2O_9$ and some liquid phase (Kim *et al.* 1997, Lu & Wen 1998, Guha 1999).

Recently, several direct reaction-sintering processes, which are modifications of the conventional mixed oxide method, have been presented mainly to decrease the number of undesired phases. The sintering is typically performed directly after the mixing of the starting powders or with an additional calcination step in these methods. The reactivity and proper phase formation have been enhanced, for example, by using magnesium in a nitrate or hydroxide form within the starting materials (Han *et al.* 1998, Chen *et al.* 2003, Liou 2003, Fang *et al.* 2005) or by the precipitation of magnesium hydroxide on the surface of niobium pentoxide particles (Gu *et al.* 2005). In addition, some more complex processes, such as molten-salt (Katayama *et al.* 1989), sol-gel (Jiwei *et al.* 2000), and ethylene glycol (Tailor & Ye 2010) based procedures, have been demonstrated to produce powders for direct sintering. Generally, these more direct routes enable a reasonably simple and straightforward preparation processes, but at the same time it is more difficult to avoid the formation of undesired secondary phases. The complex and sensitive nature of the PMN-based material systems complicates the reproduction of good electrical properties in a dense sintered structure using the minimized number of processing steps.

A specific reaction-sintering method with magnesium nitrate (Chen *et al.* 2003, Liou 2003) was used in this Thesis to prepare PMN-13PT ceramics (Papers I & II). Magnesium nitrate $Mg(NO_3)_2$ hexahydrate was used as a reactive component, and it was mixed with niobium oxide Nb_2O_5, lead oxide PbO, and titanium oxide TiO_2 directly to produce powders for sintering. Excess amounts of magnesium nitrate (5 wt.%) and lead oxide (2 wt.%) were used in order to produce the desired perovskite phase. The powder mixture was pressed into pellets and sintered at 1250 °C for 2 hours, and pure perovskite phase formation in ground samples was evidenced by XRD. The relative density of the samples was ~7.7 g/cm^3. Silver paste (W.C. Heraeus DT1402) was screen printed on parallel faces of pellets and fired at 600 °C for 10 minutes to produce electrodes for electrical measurements.

3.1.2 The columbite method for PMN-PT ceramics fabrication

The most widely used method to fabricate PMN-based ceramics is the columbite method introduced by Swartz & Shrout (1982). This route is based on a columbite-type $MgNb_2O_6$ precursor, which is first formed by reacting magnesium

oxide MgO and niobium pentoxide Nb_2O_5, which is then allowed to react with lead oxide and titanium oxide to synthesize perovskite PMN-PT, as follows:

$$MgO + Nb_2O_5 \overset{>1000\,^\circ C}{\rightarrow} MgNb_2O_6$$

$$3PbO + (1-x)MgNb_2O_6 + 3xTiO_2 \overset{>700\,^\circ C}{\rightarrow} 3Pb(Mg_{1/3}Nb_{2/3})_{1-x}Ti_xO_3.$$

The columbite precursor made of two refractory B-site oxides greatly impedes the formation of unwanted pyrochlore phases and therefore it is possible to prepare very pure perovskite phase. The final sintering is performed for precalcined powders, which are already of perovskite phase. This method typically requires three distinct mixing and calcining/firing procedures.

In the columbite method used in Paper VI, the $MgNb_2O_6$ precursor was first formed by calcination of mixed MgO (99.9%) and Nb_2O_5 (99.9%) at 1100 °C for 12 h. 1% of excess MgO was added to compensate for high temperature mass loss due to the evaporation of water and CO_2 absorbed by the MgO. $MgNb_2O_6$ was then mixed with PbO (99.9%) and TiO_2 (99.9%) powders in a ball mill for 24 h using acetone as a mixing vehicle. Stoichiometric amounts of PbO, TiO_2 and $MgNb_2O_6$ were added to produce $Pb(Mg_{1/3}Nb_{2/3})_{1-x}Ti_xO_3$ with x=0–0.2 (in 0.05 intervals), and 2% of excess PbO was used to compensate for PbO evaporation during calcination and sintering steps. The resulting powders were pressed and calcined at 900 °C for 4 h to produce pure perovskite phase. Calcined perovskite PMN-PT powders were crushed, mixed with a small amount of polyvinyl alcohol, and pressed into pellets. After 1 hour burn-off at 650 °C, the final sintering was performed at 1200–1220 °C for 4h. In XRD studies all fabricated samples showed pure perovskite phase and the relative density of the samples was 7.7–8.0 g/cm^3, depending on the composition. Aluminium or gold/chromium electrodes films (~300–500 nm in thickness) were sputtered on both sides of the pellets for electrical measurements.

3.1.3 Single-crystalline PMN-PT and PZN-PT samples

Single crystals of PMN-PT cut along the (001) and (011) crystallographical planes were used in this Thesis. (011) plates (1 mm in thickness) with nominal composition of PMN-28PT were fabricated by TRS Technologies, Inc[1], and (001) single crystal plates (0.5 mm in thickness) with compositions of PMN-27PT,

[1] TRS Technologies, Inc., PA, USA, www.trstechnologies.com

PMN-29PT and PMN-31PT were fabricated by H.C. Materials Corporation[2]. All PMN-PT crystals were grown by different modified processes based on the Bridgman method (see e.g. Han *et al.* 2008). (001) plates of PZN-8PT crystals were prepared by the solution gradient cooling technique (Dabkowski *et al.* 2004). Thin films of Au with a Cr adhesive layer (in PMN-PT) or Ag (in PZN-PT) were used as electrodes on the crystals to provide electrical connections. Depoled (001) PMN-PT crystal plates were additionally checked under cross-polarized light in order to determine the extinction angles for birefringent areas at room temperature.

3.2 Electrical and thermal characterization

3.2.1 Determination of dielectric properties

Capacitance (C) and loss tangent (tan δ) of sandwiched capacitor samples were measured using a high precision LCR meter (HP/Agilent 4284A) in the frequency range of 20–10^6 Hz at a signal amplitude of 1 V. Dielectric polarization current was determined by measuring the voltage across a reference resistor using a multimeter (Agilent 34411A). The polarization data was calculated by integrating polarization current density J (=dP/dt) in response to a triangular voltage waveform. The same measurement setup was used in polarization and electro-thermal measurements and details of this setup are described in the next subsection below. All temperature dependence measurements were performed using one of the three different thermal chambers (Espec SU-261, Memmert UFP400, and Espec BTZ175E).

3.2.2 Electro-thermal measurements

There are various methods available to measure the thermal response induced by the application of an electric field. The majority of the active research groups seem to use a modified commercial DSC equipment (e.g. Bai *et al.* 2011, Le Goupil *et al.* 2012). Thermal response is then calculated from the measured heat flow caused by the electric field under isothermal conditions. Other direct measurement methods utilize for example infrared sensors and scanning thermal microscopy which can provide more localized information but the accuracy tends

[2] H.C. Materials Corporation, IL, USA, www.hcmat.com

to be lower (Lu *et al.* 2010, Kar-Narayan *et al.* 2013). Possibly the most simple and straightforward measurement method is to record the temperature change of the sample using an attached temperature sensor. For example, different types of thermistors have been used in electrocaloric measurements (Kar-Narayan & Mathur 2010, Rožič *et al.* 2011a). The measurement method employed here utilizes a direct measurement of the temperature change of the sample registered by an attached thermocouple. A similar type of method has been used previously by Tuttle (1981).

A special sample setup was used for electric-field-induced polarization and temperature measurements (Figures 16 & 17). Thin alumel electrode wires (25 μm in diameter) were attached to both electrodes of the sample under measurement using Kapton® polyimide tape (3M Corporation). The sample was placed inside a glass beaker so that it was hanging freely by the electrode wires (Figure 16(b)). The other ends of the alumel electrode wires were soldered to metallic plates that were attached to a PTFE beaker lid. A thermocouple composed of alumel and chromel wires was attached to one side of the sample by Kapton® polyimide tape. The thermocouple outputs were soldered to other metallic plates that were fed through the PTFE beaker lid. Closing the sample inside a beaker with thin wires suppressed the change of thermal energy between the sample and its surroundings and ensured a sufficiently long thermal time constant in comparison to the measurement cycle used. The masses of tape (polyimide+silicone), electrodes and possible excess materials were determined and their effect was subtracted from the measured temperature response using Equation (12)

$$\Delta T = \Delta T_{tot} \frac{\sum_n m_n c_n}{m_s c_s}, \tag{12}$$

where ΔT_{tot} is a total measured temperature change, m_n and c_n are mass and specific heat capacity (per unit mass) for each of the involved components (sample, electrodes, tape, etc.), m_s and c_s are the mass and specific heat capacity (per unit mass) for the active material. In this way the effective temperature change ΔT in the active material was determined. This correction procedure was found to be sufficient due to the very fast internal transfer of the heat energy. The values of specific heat capacity of the involved materials are given in Table 5. The effect of thin electrode and thermocouple wires was found to be very small, and therefore their influence was omitted.

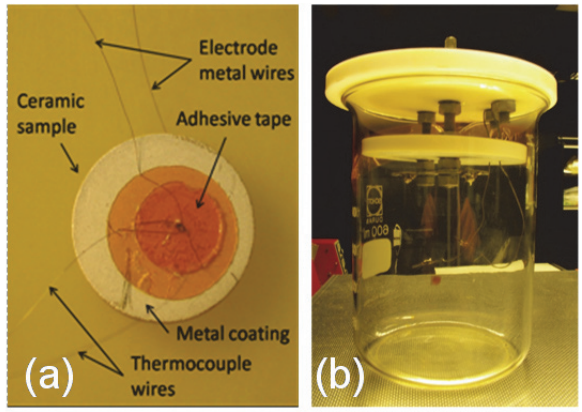

Fig. 16. (a) Electroded sample with attached voltage and thermocouple wires, and (b) a glass beaker with sample attached.

Table 5. Used specific heat capacity values for different materials.

Material	c_p (J/gK)	Reference
PMN	0.32 (at 0 °C)	Moriya *et al.* (2003)
PMN-xPT around MPB	0.30–0.35 (at 10–150 °C)	Tang *et al.* (2005)
PZN-PT	0.31	Fang *et al.* (2009a)
Silicone	1.23	Neese *et al.* (2008)
Polyimide	1.09	DuPont Kapton® HN Technical Data Sheet
Au	0.128 (at 273 K)	Tables of Physical & Chemical Constants[3]
Al	0.88 (at 273 K)	Tables of Physical & Chemical Constants[3]
Ag	0.235 (at 273 K)	Tables of Physical & Chemical Constants[3]

The measurement setup for electric-field-induced temperature measurements was also used in the polarization measurements mentioned above. A schematic diagram of this measurement setup is presented in Figure 17. The voltage stimulus for measurements was provided by a function generator (Agilent 33120A), which was connected to the sample via a high voltage amplifier (Radiant RT6000HVA). The thermocouple voltage was measured with a multimeter (HP/Agilent 3457A or 34420A). The measured difference in thermocouple voltages with and without an applied electric field was transformed

[3] Tables of Physical & Chemical Constants (16th edition 1995). 2.3.6 Specific heat capacities. Kaye & Laby Online. Version 1.0 (2005) www.kayelaby.npl.co.uk

into the corresponding temperature value by using the conversion reference table[4]. All temperature dependence measurements were performed using one of the three different thermal chambers (Espec SU-261, Memmert UFP400, and Espec BTZ175E).

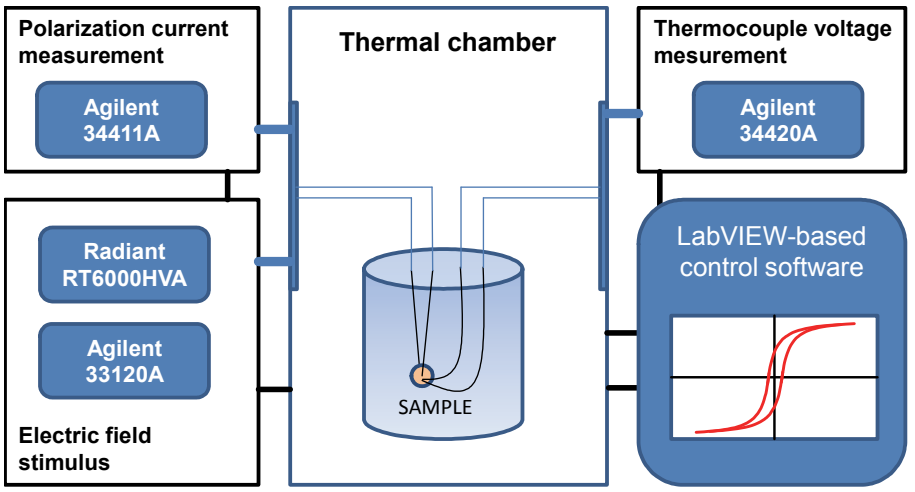

Fig. 17. The setup configuration used for electric-field-induced temperature change and polarization measurements.

Either rectangular (Papers I-III, V & VI) or a triangular (Paper IV) electric field stimulus pulses were used in the electric-field-induced dielectric and temperature measurements. All the polarization measurements were executed with triangular pulses. The rectangular pulse on-time was six seconds for thicker samples (~ 1 mm) and 1–2 seconds for thinner samples (~0.1–0.5 mm). A typical thermocouple response to the rectangular electric field pulse is shown in Figure 18. It should be mentioned that the application of relatively short pulses (1–6 seconds) in electro-thermal measurement is not customary, and the majority of other electrocaloric studies use longer pulses so that the induced temperature is allowed settle back to the initial value with constant electric field. The main reason for the use of shorter electric field pulses in this Thesis work was to minimize the time spent under the electric field. A sufficient pulse time for thermal measurements was chosen based on the measured external thermal time constant of the sample. After the application of the electric field, the thermal time constant on cooling was

[4] National Institute of Standards and Technology ITS-90 Thermocouple Database

determined to be between 15 and 40 seconds depending on the sample thickness. The actual thermal response was calculated by subtracting either an averaged or instantaneous value of the thermocouple voltages with and without the electric field. The rise times of the triangular and rectangular pulses were 0.1–10 and 0.125 seconds, respectively.

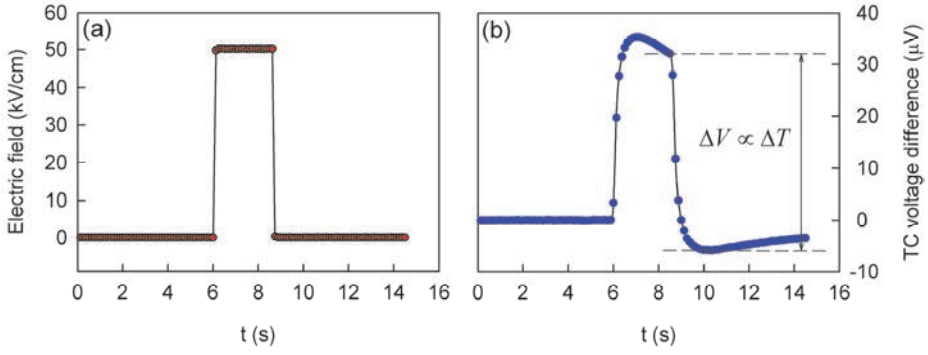

Fig. 18. Typical rectangular electric field pulse (a) and corresponding thermocouple response (b) obtained in electrothermal measurements. The extracted field-induced thermocouple voltage difference ΔV is proportional to temperature change ΔT.

4 Experimental results and discussion

This chapter introduces and discusses the main results obtained in this Thesis work. Detailed results can be found in the related publications of Papers I–VI.

4.1 Electric-field-induced dielectric and thermal response in PMN-13PT ceramics

As previously mentioned in Sections 1.2 & 2.1, it is not clear if the low-temperature phase in PMN and PMN-*x*PT with low *x* is a glassy-type frozen phase or a random-field frozen ferroelectric phase with limited ordering. Whichever the case, the application of a strong enough electric field into the low-temperature phase is known to irreversibly trigger a macroscopic long-range ferroelectric phase. However, even after electric-field application to PMN, some signs of the cubic phase are found (Vakhrushev *et al.* 1997) and only about 50% of the Pb cations are observed to displace along the polar <111> direction (Blinc *et al.* 2003). In general, the field-induced transition from the glassy phase of average cubic symmetry is expected to show some first-order characteristics (Ye & Schmid 1993) while transition from a disordered ferroelectric phase to a more long-range ordered one is expected to be a more gradual type of evolution. In addition, the PMN-*x*PT system is known to develop towards a more distinct ferroelectric phase, also with increasing *x*, although mixed and short-range ordered phases are again observed even with reasonably high *x* (Ye & Dong 2000, Jiang & Kojima 2000, Dkhil *et al.* 2001, Ye *et al.* 2003, Shvartsman & Kholkin 2004, Xu *et al.* 2006). For these reasons, the effect of electric field poling to PMN-13PT composition at fixed temperatures was investigated by dielectric studies and in-situ temperature measurements to observe the development of a macroscopic ferroelectric phase. PMN-13PT composition is particularly interesting because different results concerning the zero-field low temperature phase have been reported around this concentration. A number of structural and dielectric studies indicate that a low temperature rhombohedral ferroelectric phase spontaneously develops with PT concentrations of 5–10 mol.% (Bidault *et al.* 1996, Dkhil *et al.* 2001, Ye *et al.* 2003, Wang *et al.* 2005). However, some other studies indicate that the concentration limit for the spontaneous transition should be higher than 10–13 mol.% (Jang *et al.* 1980, Bunina *et al.* 1994, Colla *et al.* 1998, Fujishiro *et al.* 2000, Gehring *et al.* 2004, Raevski *et al.* 2005, Xu *et al.* 2006). This evident discrepancy in previous results makes it rather difficult to

form a clear picture on the nature and behaviour of low-temperature phase of PMN-*x*PT (with low *x*). The related results in this section are fully presented in the original publications of Papers I and II.

The application of an electric field pulse stronger than a specific threshold field E_{th} to a depoled PMN-13PT ceramic at low fixed temperature points below its thermal depolarization temperature T_{dp}=18 °C was found to decrease its permittivity (Figure 19). This poling effect was found to be highly irreversible so that the induced change was not recovered until thermal depolarization of the sample at $T > T_{dp}$ (Figure 19(b)). No changes in permittivity were observed after poling at constant temperatures above T_{dp} (=T_C) where field-induced changes are known to be highly reversible for both conventional and relaxor ferroelectrics (Merz 1953, Ye & Schmid 1993).

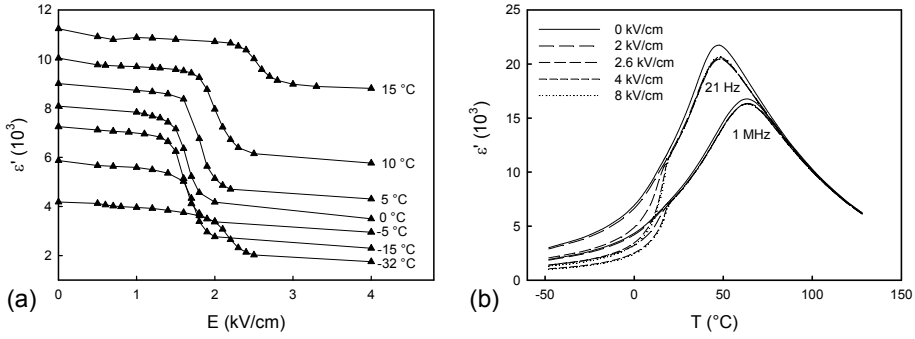

Fig. 19. (a) Real part of complex relative permittivity ε' at 21 Hz as a function of pre-poling electric field at various temperatures. (b) Temperature dependence of the real part of the complex relative permittivity ε' for PMN-13PT ceramics after poling at −48 °C and subsequent zero-field heating. (Paper I, Reprinted with permission from Applied Physics Letters. Copyright 2008, AIP Publishing LLC).

In principle, an irreversible decrease of permittivity is regarded as one sign of a field-induced transition from the relaxor phase towards the long-range ordered ferroelectric phase in PMN-PT (Raevski *et al.* 2005). However, an alignment of randomly oriented frozen polarizations by poling electric fields is also likely to decrease permittivity (see e.g. Davis 2006). A gradual rather than a discontinuous change in permittivity around E_{th} refers more to the absence of a first-order field-induced phase transition. However, the apparent gradual behaviour here is not unexpected since permittivity measurements are performed gradually after each dc field poling pulse instead of *in-situ* measurements on a continuously changing

dc field sweep. Especially, when operating with field strengths close to E_{th}, it takes a considerable time for the development of the ferroelectric phase and macroscopic polarization even with a continuous electric field (Vakhrushev *et al.* 1997). This gradual development of macroscopic polarization on poling was also observed with *P-E* hysteresis measurements when E_{max} was gradually increased (Paper I).

Further observation of the field-induced temperature effect revealed that a poling field $E>E_{th}$ induces an increase in temperature (Figure 20). Additionally, the in-situ measurement of the temperature response to a rectangular pulse revealed that the field-induced temperature change is either partially (at $T < T_{dp}$) or fully (at $T > T_{dp}$) reversible with decreasing electric field in a depoled material. When two successive electric field pulses of different signs ($|E|$=12 kV/cm > E_{th}) were further applied to an unpoled sample, the thermal response of the sample was analyzed by using the following idea (see Figue 20). The first electric field application to the unpoled sample causes a temperature rise due to hysteresis loss (*x*Hy in Figure 20(a)), the electrocaloric effect (ECE) and a possible field-induced phase transition (PT) in the temperature range below T_{dp}. Of these, the electrocaloric effect is considered to be the only reversible effect so that any temperature change is only partially recovered on electric field removal (Figure 20(a)). A successive reversed electric field pulse switches the newly formed macroscopic polarization from P_r to $-P_r$ which is accompanied by another irreversible loss through heat generation (½Hy in Figure 20(b)). In this way, the heating effect of the switching hysteresis (½Hy) was extracted first from the reversed pulse response. Furthermore, parallel dielectric hysteresis measurements were used to calculate polarization switching (½Hy) and formation (*x*Hy) losses from the corresponding hysteresis loop areas. It was assumed that a heat generation loss in an off-resonance state piezoceramics is mainly attributed to the intensive dielectric loss (Uchino & Hirose 2001) so that the area inside the *P-E* hysteresis loop corresponds to the heat energy loss. Consequently, by using two opposite field pulses in connection with dielectric hysteresis measurements, the response of each participating process was successfully extracted from the measured data.

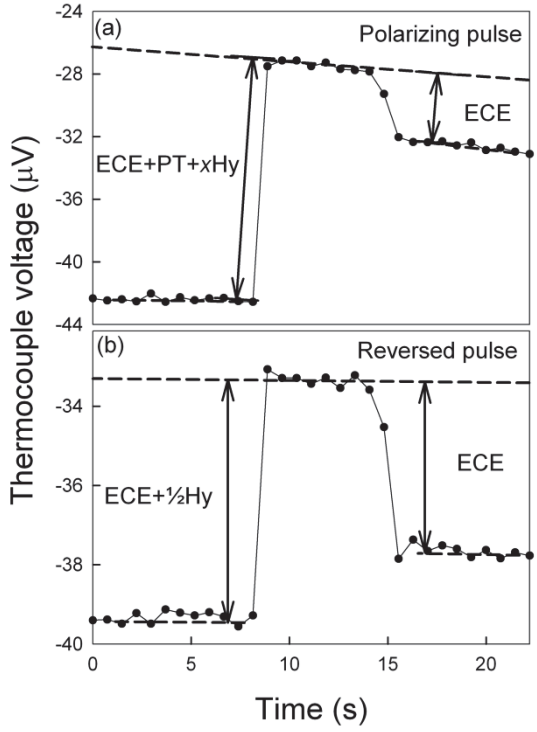

Fig. 20. Typical thermal response to the first poling (E=12 kV/cm) and following reversed (E=-12 kV/cm) electric field pulses below the thermal depolarization temperature. Temperature changes are suggested to originate from electrocaloric effect (ECE), hysteresis loss (xHy and ½Hy) and possible phase transition (PT) type response. (Paper II, Reprinted with permission from Applied Physics Letters. Copyright 2009, AIP Publishing LLC).

Figure 21 shows the measured thermal response of depoled PMN-13PT ceramics as a function of temperature for an E=12 kV/cm pulse. Above T_{dp}=18 °C the material was macroscopically depolarized and the field-induced temperature response was caused by the highly reversible electrocaloric effect dominated by the contribution of the reversible field-induced phase transition. On the other hand, the total field-induced temperature change (i.e. $\Delta T_{ECE}+\Delta T_{PT}+\Delta T_{xHy}$) was found to show a highly irreversible nature below T_{dp} and the sole reversible part (ΔT_{ECE}) decreased rapidly. Both hysteresis related irreversible temperature changes (ΔT_{xHy} and $\Delta T_{½Hy}$) increased linearly with decreasing temperature, which reflected as an increasing hysteresis loop area. However, the remaining irreversible temperature

change (ΔT_{PT}) increased rapidly from zero to a broad maximum value of ~0.25 °C just below T_{dp} before it started to decrease monotonically at lower temperatures. Interestingly, the maximum value of ΔT_{PT} was reached at around T=−4 °C where the minimum of E_{th} was also observed (see Figure 19(a)). It is noteworthy that the electrocaloric temperature change ΔT_{ECE} above T_{dp} coincides with the summed temperature response $\Delta T_{ECE}+\Delta T_{PT}+\Delta T_{xHy}$ below T_{dp}, and forms the continuous field-induced temperature response of a virgin PMN–13PT sample with a broad maximum value around T=10 °C.

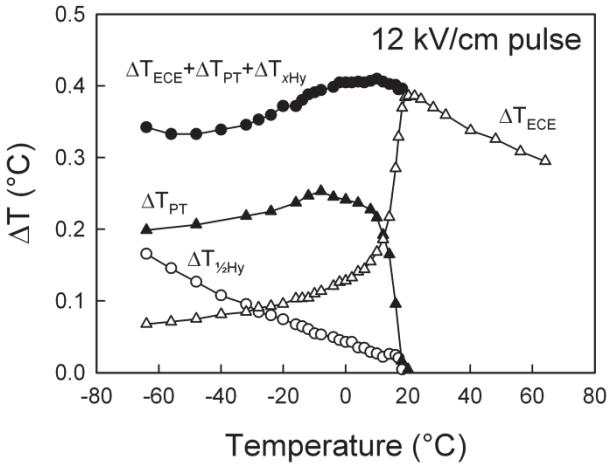

Fig. 21. Field-induced thermal response of depoled PMN-13PT as a function of temperature for E_{max}= 12 kV/cm. (Paper II, Reprinted with permission from Applied Physics Letters. Copyright 2009, AIP Publishing LLC).

These results showed that, after evaluation and subtraction of the reversible electrocaloric effect (ΔT_{ECE}) and poling hysteresis related loss (ΔT_{xHy}) from the field-induced temperature response, an additional irreversible and reasonably strong temperature response (ΔT_{PT}) was observed to remain for unpoled PMN-13PT below T_{dp}. This additional heat is clearly connected to the field-induced formation of a long-range ferroelectric order. However, as already mentioned, the nature of the low-temperature ground state of PMN-xPT (with low x) is somewhat unclear (see Chapter 2). This fact makes it difficult to estimate the origin of the additional irreversible heat energy since both aforementioned options (i.e. field-induced long-range ordering from glassy type or random-field frozen phase)

definitely involve some heat generation. A field-induced phase transition involves either a discontinuous (first-order) or a continuous (second-order) type enthalpy change which equals the heat of transition at constant pressure. Poling of unpoled and randomly oriented ferroelectric structure induce irreversible reorientation and growth of existing domains. This manifests itself as hysteresis loss transformed to heat energy.

From this viewpoint it seems that some sort of field-induced phase transition takes place in unpoled PMN-13PT below T_{dp} and this is responsible for the measured irreversible temperature change ΔT_{PT}. This would mean that unpoled PMN-13PT shows only limited ferroelectric order with mixed cubic phase at low temperatures and an electric field application is still needed to induce a fully macroscopic ferroelectric order. In general, poling of randomly oriented ferroelectric material is only expected to show hysteresis loss related to irreversible heat generation (i.e. $\Delta T_{x\mathrm{Hy}}$). However, a significant field-induced change in domain wall density, as might be expected for a random-field frozen or normal FE phase with very small domain size (see Section 1.2), can also be regarded to produce additional heat. Therefore, based on previous research and obtained results the most likely scenario is that depoled PMN-13PT produces additional irreversible field-induced heat due to an FE phase growing at the expense of some other phase. The corresponding heat energy values of $Q_{PT}=c\Delta T_{\mathrm{PT}}$~60–77 J/kg are of similar magnitude to the value (~110 J/kg) determined for the ferroelectric-to-relaxor transition of poled PMN on heating (Gorev *et al.* 2007). This could be an indication that unpoled PMN-13PT shows only partial order in unpoled form. Furthermore, this study shows that considerable irreversible thermal effects might be present during the field application. These nonreproducible effects should be avoided when searching for a highly reversible electrocaloric response.

4.2 Electric-field-induced dielectric and thermal response in PMN-PT single crystals close to the MPB region

Because the PMN-*x*PT compositions close to the morphotropic phase boundary (MPB) region show multiple phases with similar energies, the phase stability is easily altered by external means, such as temperature and electric field (see Chapter 2). The flattening of the energy profiles between different phases close to the MPB region naturally facilitates an easily enforced polarization rotation between the phases which also provides one explanation for the observed high

electromechanical activity in PMN-PT and related systems. Observations of the properties reflecting the electric-field-induced phase transitions and polarization rotation are thus important to obtain more information on their behaviour. The electric-field-induced dielectrical and temperature changes in <011>-oriented PMN-*x*PT (with *x*~28 mol%) and <001>-oriented PMN-*x*PT crystals (with *x*~27, 29, and 31 mol%) single crystals were studied as a function of temperature and the following results in this section are presented in the original publications of Papers III and IV.

4.2.1 Dielectric properties of PMN-PT single crystals

A zero-field cooled PMN-PT crystal is in a depoled state where all the polar variants of the ferroelectric phase are equally present as shown in Figure 12. According to the previous structural studies on PMN-*x*PT crystals (Bai *et al.* 2004a, Cao *et al.* 2006), studied crystal compositions of *x*=27–29 mol% have a rhombohedral ferroelectric phase at room temperature. Polarized light microscopy (PLM) inspection was performed for more questionable (due to the vicinity of the MPB) PMN-31PT crystal composition and it also indicated rhombohedral symmetry (Paper IV). When an electric-field is applied to the <011> or <001> directions at room temperature, the 8 polar variants of the low-temperature rhombohedral ferroelectric phase are affected such that either 2 variants closest to the <011> direction or 4 variants closest to the <001> direction are favoured at a sufficiently high electric field. These domain engineered states may be referred as pseudorhombohedral '2R' and '4R' states which include possible monoclinic phases ($2M_B$ or $4M_A$) with small polarization rotation angles away from the <111> directions (Bai *et al.* 2004a, Chien *et al.* 2004, Cao *et al.* 2006, Davis 2006). These poled structures had an increased permittivity and either two or three distinct changes were observed in permittivity following zero-field heating (Figures 22 & 23). The high temperature anomaly at T_d (or T_C) in the vicinity of, or at, T_m is a transition between polar and non-polar phases, and this temperature was used to determine the composition for <001>-oriented samples (Paper IV).

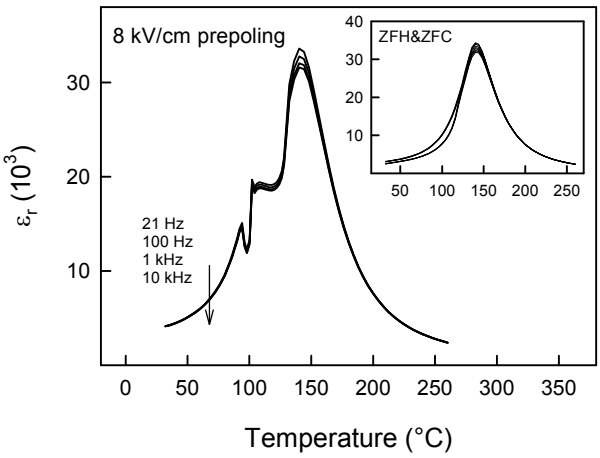

Fig. 22. Temperature dependence of the relative permittivity of poled <011>-oriented PMN-28PT single crystal upon heating. The inset shows the temperature dependence of the relative permittivity of the unpoled sample upon zero-field heating and cooling. (Paper III, Reprinted with permission from Physical Review B. Copyright 2010, the American Physical Society).

The two permittivity jumps observed at lower temperatures in the <011>-oriented PMN-28PT crystal were associated with successive phase transitions first to the ferroelectric orthorhombic phase and then to the ferroelectric tetragonal phase before the depolarization to the cubical phase takes place at T_C (Guo *et al.* 2003a, Feng *et al.* 2006, Tu *et al.* 2008). In the course of increasing x the <001>-poled crystals experienced either one or two low temperature anomalies in their dielectric properties on heating (Figure 23). The PMN-27PT composition shows a peak in dielectric properties around T=96 °C, and this peak is associated with a phase transition from a domain-engineered pseudo-rhombohedral to a tetragonal phase with reduced permittivity, and the temperature of the transition is conventionally marked as $T_{R\text{-}T}$. In PMN-29PT, a clear additional change appears in the loss curve (tan δ) adjacent to the other peak at 103 °C (inset of Figure 23(b)). A higher $PbTiO_3$ concentration PMN-31PT sample already shows two clearly distinct peaks in the relative permittivity and loss tangent (Figure 23(c)). A similar dual peak in the temperature dependence of dielectric properties has been previously observed in <001>-poled PMN-PT single crystals close to the MPB region (Guo *et al.* 2003b, Tu *et al.* 2004, Feng *et al.* 2006, Slodczyk *et al.* 2008, Lin *et al.* 2010, Li *et al.* 2010). This additional peak in dielectric properties is

caused by a phase transition where the polarization jumps between two different rotational routes. More specifically, the intial rotation route between the R and T phase changes to the route lying between the O and T phases, as can be seen from Figures 11 & 13(b). The overall phase sequence can then be described as $R/M_A \rightarrow M_C \rightarrow T$ with increasing temperature. In fact, this very same phase transition sequence is observed in <001>-oriented PMN-30%PT crystals, also during an isothermal application of an electric field (Bai *et al.* 2004a).

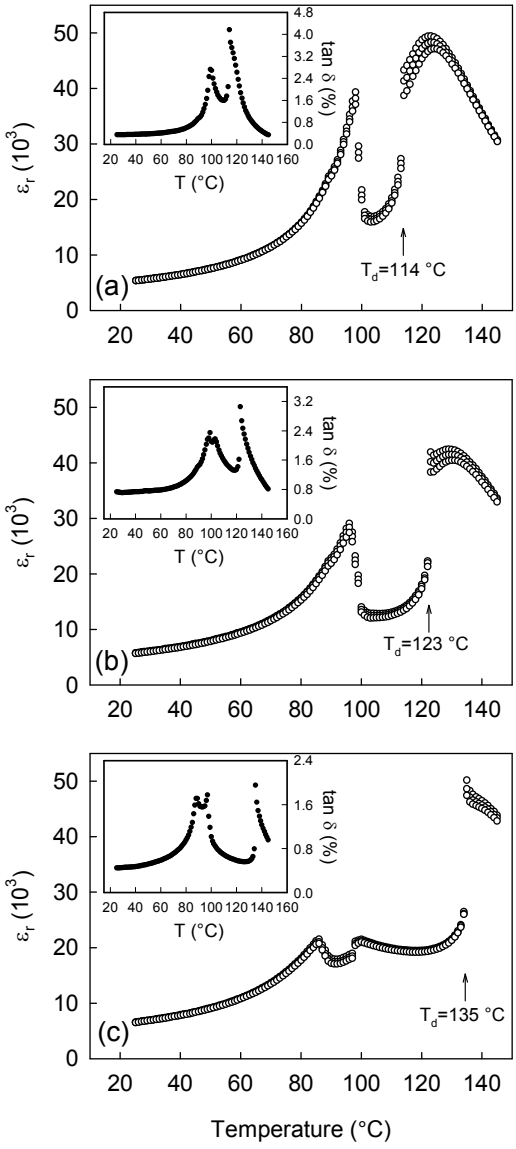

Fig. 23. Temperature dependence of the relative permittivity (at 0.1, 1, and 10 kHz) and loss tangent (at 1 kHz) on heating for <001>-poled (a) PMN-27PT, (b) PMN-29PT, and (c) PMN-31PT single crystals. (Paper IV, Reprinted with permission from Journal of Applied Physics. Copyright 2012, AIP Publishing LLC).

A clear hysteresis was additionally observed in the permittivity behaviour of low temperature phase transitions (M_A-M_C and M_C-T) of <001>-poled PMN-31PT crystals (Figure 24). On heating the permittivity changes were observed at T=86 °C and T=95 °C, while on cooling these changes took place at T=79 °C and T=52 °C, correspondingly. Especially, the clear difference in the magnitude of the hysteresis indicates that these are two separate phase transitions.

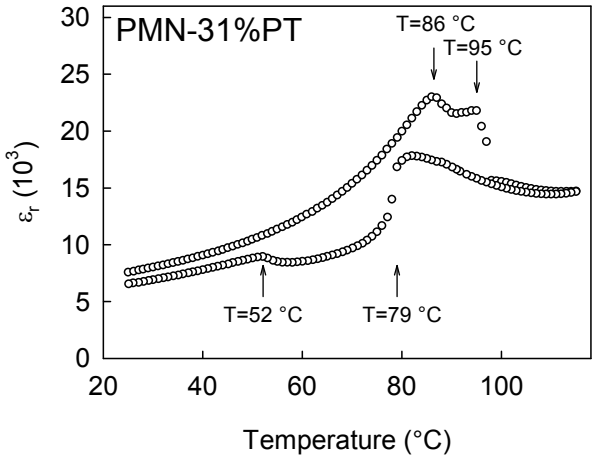

Fig. 24. Temperature dependence of of the relative permittivity on heating and cooling for a <001>-poled PMN-31PT crystal at 1 kHz. (Paper IV, Reprinted with permission from Journal of Applied Physics. Copyright 2012, AIP Publishing LLC).

4.2.2 Polarization rotation and phase stability under electric field in PMN-PT single crystals

Observation of the polarization response to bipolar and unipolar electric fields revealed different types of polarization changes depending on the crystal composition, temperature and direction of the electric field. From the behaviour of the polarization response to an applied bipolar electric field up to E=9 kV/cm, four distinct temperature regions (Regions I–IV) were identified for <011>-oriented PMN-28PT crystals, and typical ferroelectric hysteresis loops representing these regions are shown in Figure 25. Within Regions I (below 68 °C) and III (96–128 °C) the polarization shows similar qualitative behaviour where reversible jumps in polarization with accompanying hysteresis were observed at certain temperature-dependent electric field strengths after first poling. Narrow

ferroelectric hysteresis loops with locally lower coercive fields were measured in the intermediate Region II (68–94 °C) whereas double loop hysteresis characteristics were found just above the depolarization temperature.

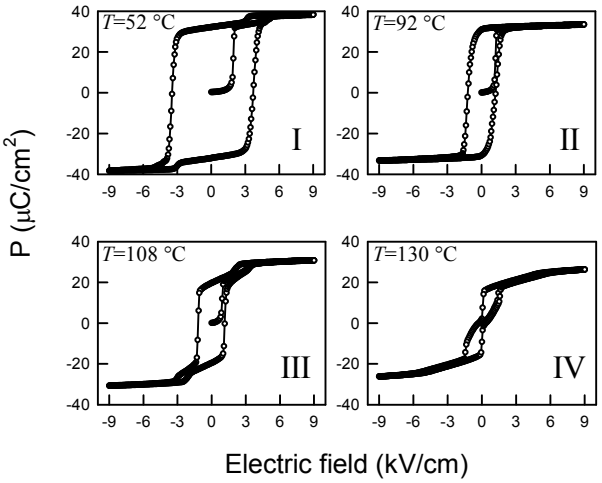

Fig. 25. Series of dielectric hysteresis loops in <011>-oriented PMN-28PT taken at fixed temperatures after zero-field cooling from 180 °C. (Paper III, Reprinted with permission from Physical Review B. Copyright 2010, the American Physical Society).

Qualitatively similar findings were observed for <001>-poled PMN-PT single crystals when a unipolar electric field up to E=20 kV/cm was applied along the <001> direction. In this case, the investigations were performed below T_C so that three different temperature regions were identified. All the compositions were found to show a complex polarization rotation route with two reversible and hysteretic jumps in polarization at lower temperatures (Figure 26). This kind of behaviour is very uncommon and similar characteristics have been observed, in both electric-field-induced strain and polarization measurements, in only a few <001>-poled PMN-xPT crystal compositions (Davis *et al.* 2006, Herklotz *et al.* 2010, Li *et al.* 2010). When the temperature was increased, two other temperature regions emerged and these regions showed only one or zero sudden polarization changes.

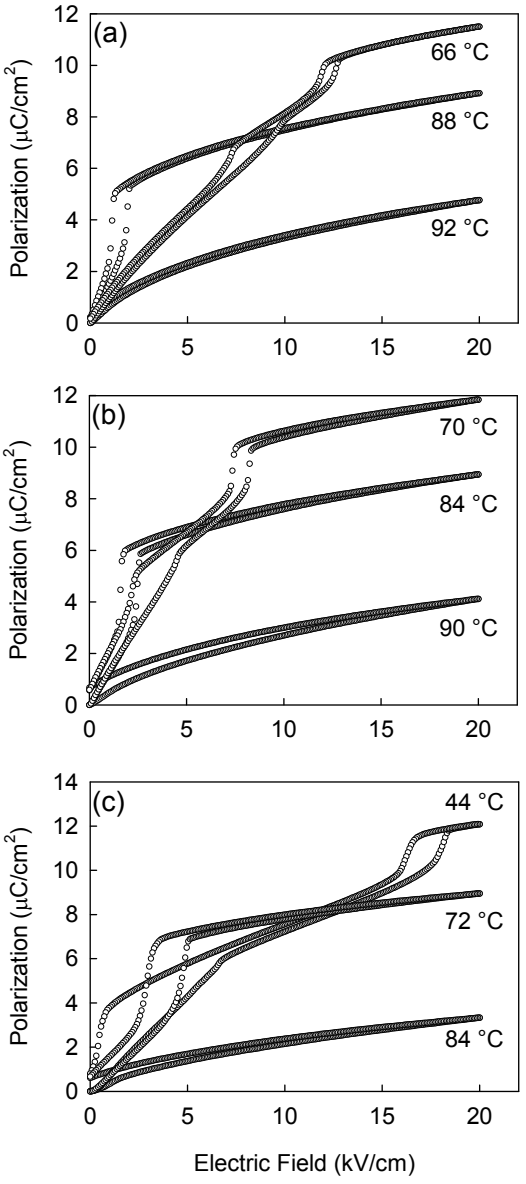

Fig. 26. Series of dielectric polarization curves for <001>-poled (a) PMN-27PT, (b) PMN-29PT, and (c) PMN-31PT single crystal as a function of unipolar electric field. Each curve was measured isothermally on cooling. (Paper IV, Reprinted with permission from Journal of Applied Physics. Copyright 2012, AIP Publishing LLC).

All the electric field strengths causing sudden changes in polarization were determined (with increasing and decreasing fields) from the *P-E* measurements of PMN-*x*PT single crystals (see Figures 25 & 26) and these are collectively presented in Figures 27 and 28 as functions of temperature. The aforementioned temperature regions with different polarization behaviours are easily distinguished here. All the observed reversible electric-field-induced jumps in polarization with increasing and decreasing fields represent significant corresponding changes in the lattice of PMN-*x*PT crystals. As mentioned in Chapter 2, the polarization in different ferroelectric phases of perovskite lies along certain crystallographical axes (except for the monoclinic and triclinic symmetries). Therefore the application of an electric field along the <011> and <001> directions favours the stabilization of orthorhombic (with polarization along <011>) and tetragonal (with polarization along <001>) phases, respectively. Polarization can rotate continuously under the electric field within the particular ferroelectric phase, but some discontinuous jumps are expected when first-order phase transitions take place between the phases. By following the measured results in combination with earlier results, the observed reversible polarization changes as a function electric field were assigned to different electric-field-induced phase transitions.

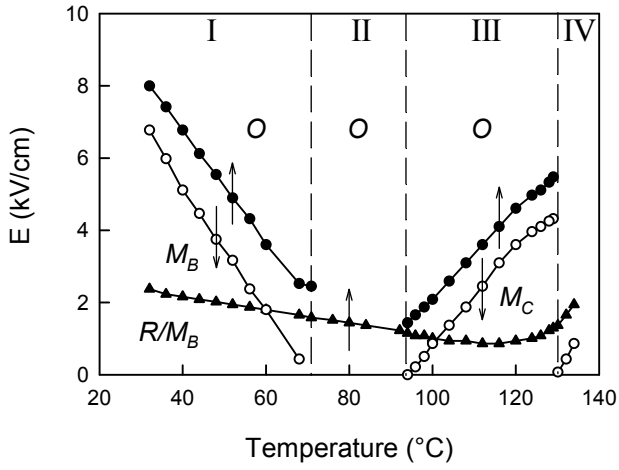

Fig. 27. Temperature dependence of threshold electric fields of induced polarization changes and proposed phase stability ranges in <011>-oriented PMN-28PT. The first polarization changes from a depoled crystal are depicted as triangles. Black (white) circles indicate threshold fields for reversible changes with an increasing (decreasing)

electric field after the initial poling. The direction of the electric field is marked with arrows. (Modified from Paper III, Reprinted with permission from Physical Review B. Copyright 2010, the American Physical Society).

Previous structural studies showed that the phase transition sequence of $R \rightarrow M_B \rightarrow O$ with increasing field takes place at room temperature in PMN-*x*PT ($x < 0.3$) crystals with $E \| [011]$. It was also shown that the M_B phase is recovered after the field removal. (Cao *et al.* 2006, Fang *et al.* 2009b). Therefore, the reversible phase transition $M_B \leftrightarrow O$ is considered to be responsible for the observed reversible polarization behaviour in Region I, as depicted in Figure 25. The only irreversible change of polarization is observed on first poling from a depoled state (Figure 25) which means that an irreversible $R \rightarrow M_B$ phase transition should take place in the course of this macroscopic polarization formation (triangular symbols in Figure 27). In accordance with our findings, previous electric-field-induced strain measurements (Feng *et al.* 2003, Shanthi & Lim 2009) indicated that this phase transition has a considerable hysteresis, which is a sign of first order characteristics. The required electric field strengths for the $M_B \leftrightarrow O$ transition are decreasing with increasing temperature and the back-inducing field finally decays towards zero when entering Region II (Figure 27). Since there are no other anomalies in polarization after the initial poling and a well-defined hysteresis loop is established, an orthorhombic phase is assumed to be stable after the first field application in Region II. In other words, the field-induced phase transition to the orthorhombic phase can then be considered to become irreversible. In fact, it has been observed that an electric field poling to the <011> direction in PMN-PT crystals with x=33% induces the orthorhombic phase to be stable already at room temperature (Lu *et al.* 2001, Feng *et al.* 2006, Shanthi & Lim 2009). However, it seems that the ground state phase (zero-field cooled after thermal depolarization) in Region II is not an orthorhombic one and a field application is always needed to induce it. This idea is also supported by the fact that the orthorhombic phase in PMN-PT is always observed after poling or during the field application (Cao *et al.* 2005 & 2006, Tu *et al.* 2008). Another reversible transition appearing in Region III has a linearly increasing threshold field with increasing temperature which differs from the behaviour in Region I. Presumably, this implies a new field-induced phase transition taking place in this region. As the dielectric measurements of Figure 22 already indicated, the polarization rotation route involving an underlying tetragonal phase can now be considered. A reversible phase transition sequence of $M_C \rightarrow O$ with increasing field has been observed previously in PMN-*x*PT compositions with higher x

values ($0.3 < x \leq 0.35$) and with E||[110] (Cao *et al.* 2006). In this case with lower x, the same reversible transition may appear now at higher temperature range (Region III) and is responsible for the polarization response in that region. As in the case of an R→M_B↔O transition, the M_C↔O transition path involves a third phase so that it is fully expressed as T→M_C↔O where the M_C phase is recovered after the first poling field removal. When entering Region IV, the crystal depolarizes and turns to averagely cubic phase where the electric field can reversibly induce phase changes to the polar O phase close to the Curie point, T_C. This transition line (C→O) is presented by the traced first polarization changes (black triangles in Figure 27) above T_C.

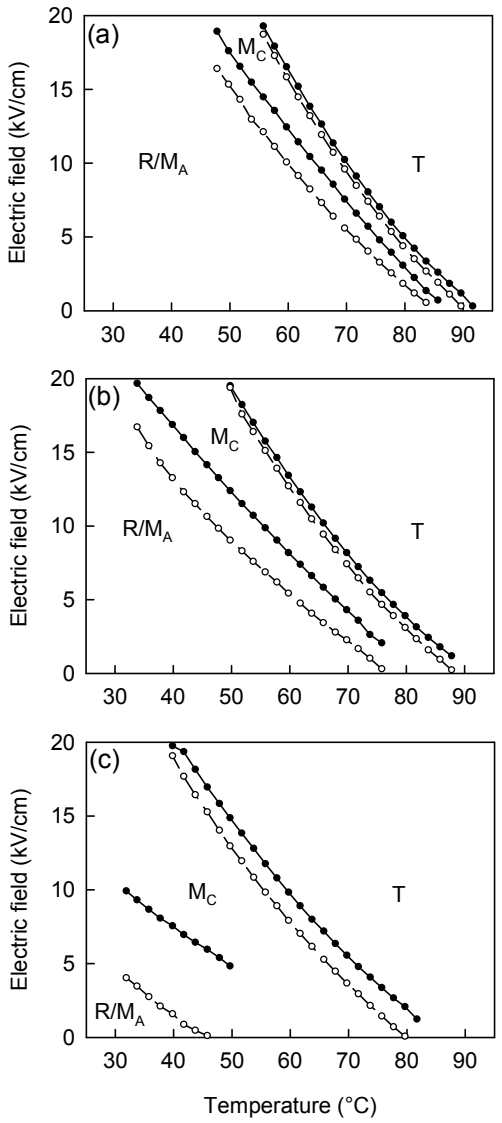

Fig. 28. Electric field-temperature diagrams showing locations of measured sudden changes in field-induced isothermal polarization with increasing and decreasing electric fields for (001)-poled (a) PMN-27PT, (b) PMN-29PT, and (c) PMN-31PT single crystals. Black (white) circles indicate threshold electric fields with increasing (decreasing) electric field. (Paper IV, Reprinted with permission from Journal of Applied Physics. Copyright 2012, AIP Publishing LLC)

The complex polarization rotation route in poled PMN-*x*PT crystals at low temperatures with E||[001] can be attributed to a phase sequence of $R \rightarrow M_A \rightarrow M_C \rightarrow T$ which has been identified by high-resolution diffraction (HRD) techniques (Bai *et al.* 2004a, Cao *et al.* 2006). Here, the first transition from R to M_A is considered to be irreversible so that the phase transition path of $M_A \leftrightarrow M_C \leftrightarrow T$ is responsible for the observed polarization behaviour. Despite the fact that similar field-induced behaviour with two successive and reversible phase transitions has been evidenced indirectly in PMN-*x*PT with x=28, 30, 30.5, 31 mol% (Davis *et al.* 2006, Herklotz *et al.* 2010, Li *et al.* 2010), the structural evidence for this phase transition sequence has been found only in PMN-30%PT composition. In addition, the fact that many studies within the same composition region fail to observe this complex polarization rotation route raises some questions. Basically, two phase coexistence in the crystal (due to variance in x) should be expected to show a similar type of polarization/strain response. However, complex polarization rotation routes similar to $R \rightarrow M_A \rightarrow M_C \rightarrow T$ have also been detected by HRD in analogous PZN-PT (Noheda *et al.* 2002b, Ohwada *et al.* 2003), predicted theoretically for PZT (Bellaiche *et al.* 2001), and observed even for strained $BiFeO_3$ (Christen *et al.* 2011). Evidently this complex phase transition behaviour is very sensitive to variations in composition. From the above discussion, the low temperature field-induced phase transition in the studied <001>-poled PMN-*x*PT crystals was assigned as $R/M_A \rightarrow M_C \rightarrow T$ and the corresponding phase stability regions are depicted in Figure 28. When the other polarization change disappeared at higher temperatures, it was interpreted as a stabilization of the M_C phase. Therefore, the field-induced phase transition is the $M_C \leftrightarrow T$ in this temperature range. Finally, the tetragonal phase is stabilized in <001>-poled crystals at high temperatures. Because the electric field was applied in the <001> direction, a tetragonal phase with <001> directed polarization tended to expand into lower temperatures with increasing electric field. Importantly, the obtained phase stability boundaries in <001>-poled PMN-31PT (Figure 28(c)) are in agreement with the observed permittivity changes on cooling (Figure 24).

When temperature and composition x are increased, it is also shown that the monoclinic M_C phase is favoured over the M_A phase (Figures 28 & 29). There is a temperature region where the field-induced phase transition is simply $M_C \leftrightarrow T$ so that the M_C phase is the ground state of the poled crystal. This behaviour is expected since the phase diagram also indicates the stabilization of the M_C phase with increasing x close to the MPB region (Noheda *et al.* 2002a). An electric field

must still be applied to induce the M_C phase at room temperature in the studied composition range but a clear trend of M_C stabilization is shown. Interestingly, the M_C phase can be first stabilized by an irreversible field-induced phase transition (i.e. by overpoling) close to the MPB region before it becomes the ground state phase with further increase of *x*. This phase boundary region is particularly important because piezoelectric properties show significant deterioration when the M_C phase is induced (the term 'overpoling' refers to this deterioration). At high enough temperatures each poled PMN-*x*PT crystal composition shows a tetragonal ground phase and electric field application to the <001> direction shows no anomalies.

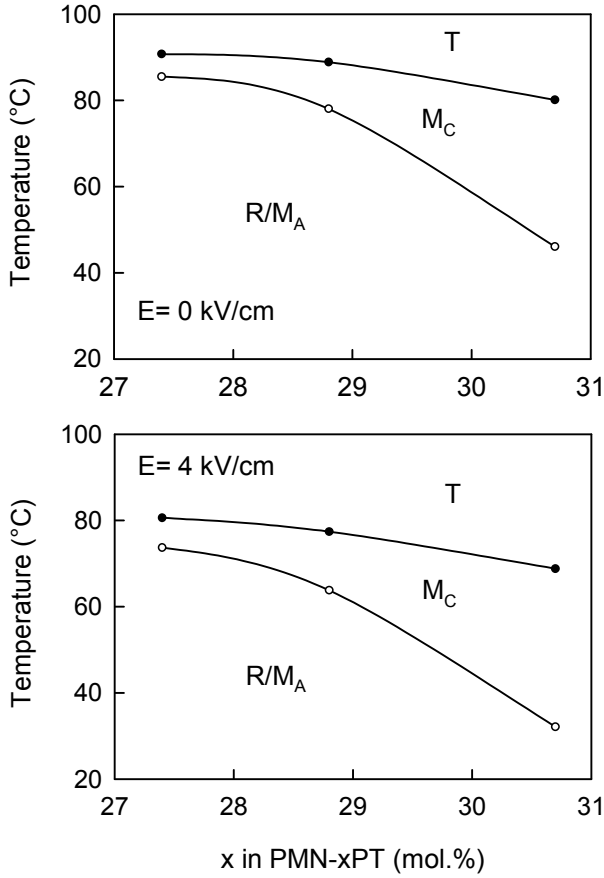

Fig. 29. Phase stability regions in <001>-poled PMN-*x*PT single crystals for electric fields of 0 and 4 kV/cm. The values are extracted from isothermal polarization measurements on cooling. (Paper IV, Reprinted with permission from Journal of Applied Physics. Copyright 2012, AIP Publishing LLC)

4.2.3 Field-induced temperature changes

In order to clarify the suggested phase stability ranges and polarization behaviour within, direct electrocaloric measurements were performed using electric field and temperature parameters similar to those of the polarization measurements (Figures 25 & 26). Evidently different phases present in the different temperature regions provide their unique thermal response to the applied electric field and

clear changes with critical electric fields were observed in the vicinity of the transition regions. The critical electric field strengths and temperature characteristics were generally in good agreement with results from the polarization measurements.

Figure 30 shows the measured electrocaloric effect of a <011>-oriented PMN-28PT single crystal as a function of temperature for different electric field strengths. Especially, the electrocaloric behaviours in Regions I and III differ significantly from each other, which further supports the suggested idea that the orthorhombic phase is field-induced through two different routes. The crystal temperature is decreased in Region I and increased in Region III when the electric field is increased to the critical electric field strength of the phase transition. Evidently this shows that these phase transitions are of a different kind and involve prominent enthalpy changes of opposite sign. Furthermore, these abrupt changes show a partially discontinuous nature and clear hysteresis which are signs of first-order-like behaviour. Interestingly, the behaviour in Region I means that an effectively negative electrocaloric effect is present. Normally, when an increasing electric field tends to align polar dipoles, the dipolar entropy is decreased and compensated for by an increase in temperature. However, a field-induced transition to a phase with higher dipolar entropy can cause the temperature to decrease, as is shown here. This may take place when starting from a phase with its polar direction non-colinear to the direction of the applied electric field (Ponomareva & Lisenkov 2012, Axelsson *et al.* 2013). A significant enhancement of the ECE was observed in temperature Region IV where the material turns to non-polar.

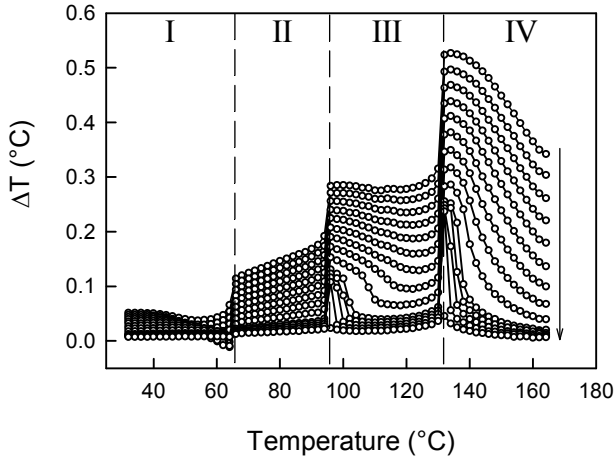

Fig. 30. Temperature dependence of electrocaloric effect in <011>-poled PMN-28PT for a series of electric field pulses of 9−1 kV/cm. An arrow is drawn to indicate the direction of the decreasing electric field. (Paper III, Reprinted with permission from Physical Review B. Copyright 2010, the American Physical Society)

The field-induced temperature of <001>-poled PMN-*x*PT crystals was measured simultaneously with polarization in response to a unipolar triangular electric field of E_{max}=20 kV/cm. This was done to emphasize the thermal behaviour of the crystal around the threshold electric fields leading to sudden polarization changes. Figure 31 shows the results of these field-induced temperature change measurements for selected temperatures (same as in Figure 26) in different PMN-PT compositions. In general, the continuous rotation of polarization leads to a linear change in the material's dipolar entropy and temperature. Then, at certain electric field values, the temperature of the crystal decreased in a sudden manner due to electric-field-induced phase transitions evidenced also in polarization measurements. As in the case of polarization, these temperature changes were highly reversible with decreasing field apart from a small hysteresis loss. The decrease of temperature was found to be very similar to that observed at low temperatures for <011>-oriented PMN-28PT. In this case both transitions of $M_A \rightarrow M_C$ and $M_C \rightarrow T$ showed a decreasing temperature with increasing electric field. Interestingly, all transitions showed signs of both continuous and discontinuous transitions, which are expected when transitions are weak first order phase transitions.

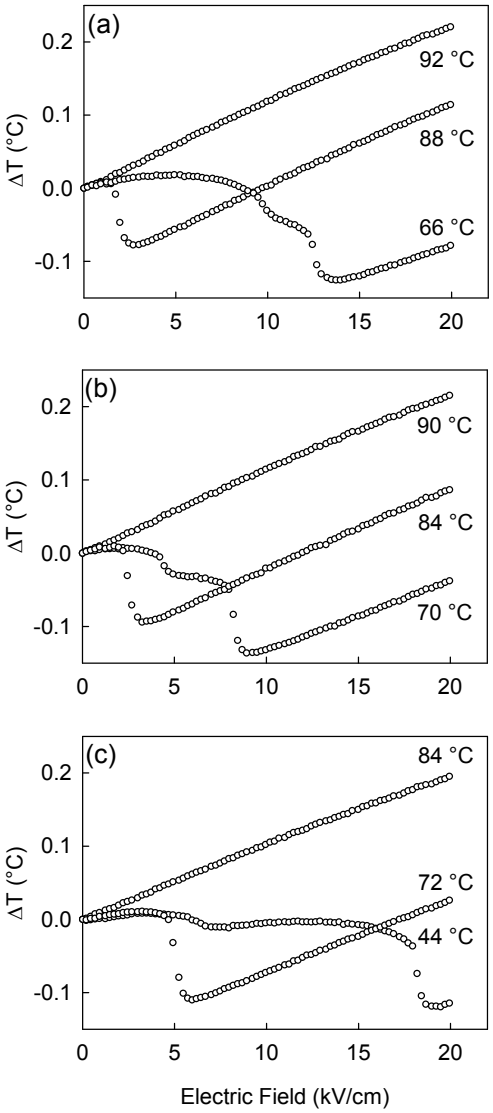

Fig. 31. Series of in-situ temperature responses with an increasing electric field measured from the crystal surface during unipolar polarization measurement for <001>-poled (a) PMN-27PT, (b) PMN-29PT, and (c) PMN-31PT single crystals. (Paper IV, Reprinted with permission from Journal of Applied Physics. Copyright 2012, AIP Publishing LLC).

4.3 Electrocaloric effect in PZN-PT single crystal and PMN-PT ceramics

The experimental electrocaloric studies performed have indicated that relaxor ferroelectric materials show promising and peculiar electrocaloric behaviour. Especially, the unique feature of relaxor ferroelectrics, a presence of PNRs, seems to provide a significant contribution to the electrocaloric effect (Birks 1986, Hagberg *et al.* 2008, Dunne *et al.* 2011, Shi & Soh 2011, Valant 2012). In order to better understand the behaviour of ECE and evaluate its technological potentiality in relaxor ferroelectrics, detailed direct measurements were necessarily needed. Direct measurements of the electrocaloric effect were performed for PZN-8PT single crystal and a series of polycrystalline PMN-*x*PT compositions ($0 \leq x \leq 0.30$) to study the behaviour of the effect as a function of temperature and electric field. The related results in this section are presented in the original publications of Papers V and VI.

4.3.1 Direct electrocaloric measurements on PZN-PT crystal

Measurement of the electrocaloric effect in <001>-oriented PZN-8.4PT single crystal was performed on cooling within the temperature range 60–200 °C with electric fields of 1–12 kV/cm, and the results are presented in Figure 32. The electrocaloric temperature change shows small values at lower temperatures but starts to increase when approaching the higher phase transition temperature T_C. The peak value of ΔT=0.25 °C was measured at T= 180 °C with an electric field of 12 kV/cm. In contrast to the studied PMN-PT single crystals (see Section 4.2.3), no additional anomalies in ΔT were found at lower temperatures despite the clear peak in permittivity at T=90 °C on heating. The lower temperature phase transition is likely to be induced below the lowest measurement temperature of T=60 °C on cooling due to hysteresis of the phase transition. This is supported by the dielectric and Raman spectroscopy results on PZN-9PT crystals where a phase transition from tetragonal to monoclinic phase takes place at around T=27 °C under field-cooling (El Marssi & Dammak 2007).

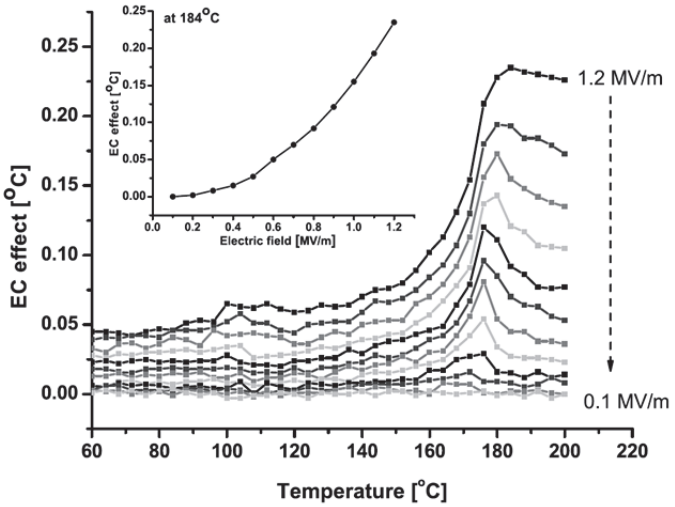

Fig. 32. Electrocaloric effect as a function of PZN-PT sample temperature for external fields of 1–12 kV/cm (1 kV/cm increments). The inset shows the maximum electrocaloric Δ*T* as a function of temperature. (Paper V, Reprinted with permission from Physical Review B. Copyright 2010, the American Physical Society).

The main intention of this study was to reproduce the essential features of the experimental electrocaloric findings by means of a simple lattice model and mean-field approximation. More specifically, the model was only intended to describe the ECE behaviour around the transition at T_C. In the model, each ion inside a domain can occupy two different states (i.e. up/down) within the potential produced by the effective field of neighbouring ions. When N out of M ions in the domain adopt the up orientation and the effective interaction energy between the nearest neighbour pairs of dipoles is $\pm J$ (+/− refers to like and unlike states, and J was parametrized to be $-113.25k$), the mean-field approximation gives a configurational energy of

$$E_c = \frac{zJ}{2M}(2N - M)^2 + (M - 2N)\mu E\,, \tag{13}$$

where z is an average coordination number (taken to be 4), μ is the dipole moment associated with each dipole (parametrized to be 0.96×10^{-30} Cm), and E is the applied electric field. For this canonical ensemble with discrete values of energy E_c and constant values for the number of ions M and the volume V, the canonical partition function Q can be written down. The Helmholtz energy f_c is then

expressed by the partition function as $f_c = -kT\ln(Q)$. When the fraction of ions in the up direction is used as a variable (i.e. $x=N/M$) and the logarithm of the sum present in Q is replaced by the logarithm of the maximum term, the Helmholtz free energy is given by

$$f_c = kT\left[\ln(1-x) - x\ln(1-x) + x\ln x\right] - 2x\mu E + \mu E + \frac{zJ}{2}(2x-1)^2 - kT\ln\left(\frac{e^{-\Theta/2T}}{1-e^{-\Theta/T}}\right), \quad (14)$$

where k is the Boltzmann constant and Θ is the Debye temperature (~300 K). The equilibrium values of x were extracted by numerically solving the minimum free energy condition (i.e. $\partial f_c/\partial x=0$). The corresponding configurational entropy per ion, S/k, is given by

$$\frac{S}{k} = -\frac{1}{k}\frac{\partial f_c}{\partial T} = -\left[(1-x)\ln(1-x) + x\ln x\right] + \frac{\Theta/T}{e^{\Theta/T}-1} - \ln(1-e^{-\Theta/T}) \quad (15).$$

As mentioned in Section 2.4.1, the corresponding electrocaloric temperature change is given by the adiabatic condition $S(E_1,T_1)=S(E_2,T_2)$, from which it is solved by a numerical search procedure. Figure 33 shows the calculated electrocaloric effect as a function of electric field and temperature. The polar regions in PZN-PT are considered to show continuous transition behaviour and the average interaction energy is then weighted assuming a variation that follows the Gaussian distribution.

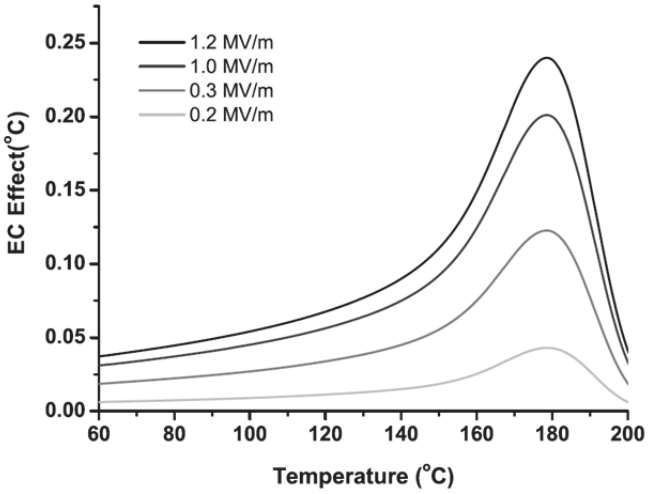

Fig. 33. Calculated EC effect as a function of sample temperature and electric field for PZN-PT crystal. (Paper V, Reprinted with permission from Physical Review B. Copyright 2010, the American Physical Society).

Because the mean-field approach breaks down close to the phase transition temperature, an accurate shape representation of properties is not reproduced around this temperature. Significant deviations are also observed at high electric fields above T_C. However, despite the crudeness of this model, it predicts the main experimental trends satisfactorily. Therefore the idea that the electric field drives the EC effect mainly by lowering the dipolar entropy of the system is nicely demonstrated here. Interestingly, an improved agreement between experimental and calculated results was obtained when the dipole moment was assumed to be linearly dependent on electric field.

4.3.2 Evolution of electrocaloric effect in polycrystalline PMN-PT system

The directly measured electrocaloric effect (ΔT) as a function of temperature and electric field is shown in Figures 34 & 35 for different PMN-*x*PT compositions. First, with small applied electric fields the electrocaloric effect shows a distinct peak in the vicinity of the depolarization temperature T_d or the Curie temperature T_C (see Figure 34(a)). A smaller additional ECE peak is also observed for PMN-30PT below its T_C. Close to the phase transition temperatures the electric field is

able to produce notable reversible polar changes more easily due to the flatter energy landscape (see Sections 2.2 & 2.3). When the electric field is increased, another broader peak in the electrocaloric effect arises gradually at temperatures above T_d (=T_C) (Figures 34–36). This behaviour has been observed only in a few detailed ECE measurements of PMN-PT (Shebanovs *et al.* 2002, Hagberg *et al.* 2008). However, it is often ignored in many studies due to a lack of detailed and direct electrocaloric effect measurements and therefore its emergence and behaviour are largely unknown. Since this enhancement of the ECE peak has only been observed in relaxor ferroelectrics, it is natural to assume that it arises from the contribution of polar nanoregions (PNRs) as has been suggested by Dunne *et al.* (2011) and Shi & Soh (2011). Critically, this would mean that the appearance of second ECE peaks is a universal property of relaxors. In addition, the aligning and growing PNRs may also play a significant role in the "giant" electrocaloric temperature changes observed in many relaxor-based thin films under very high electric fields.

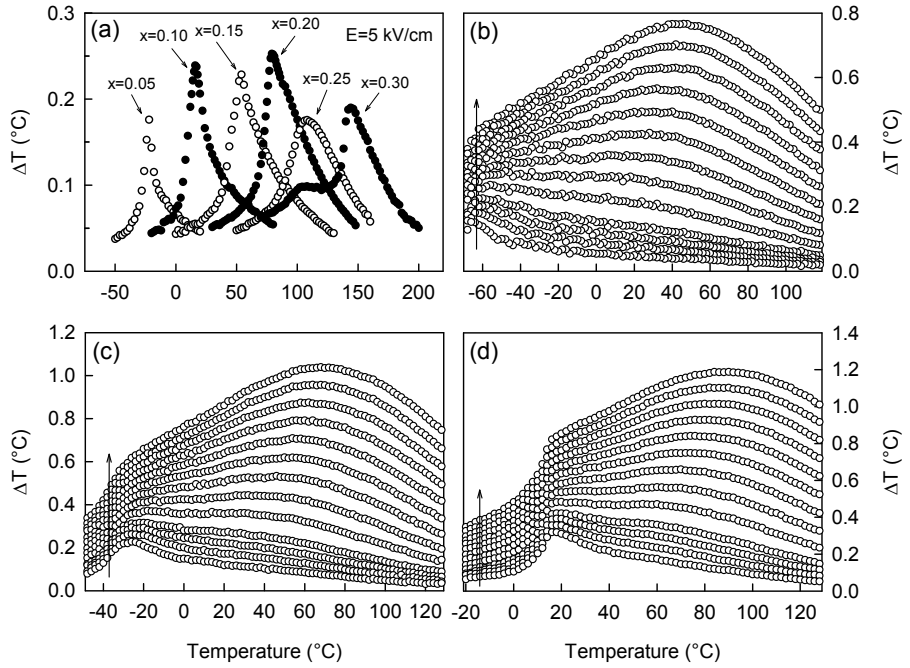

Fig. 34. (a) Electrocaloric effect in different PMN-*x*PT compositions with *x*=5–30 mol% and electric field of 5 kV/cm. Electrocaloric temperature change in (b) PMN, (c) PMN-5PT, and (d) PMN-10PT as a function of temperature and electric fields of 8–14 kV/cm (2 kV/cm intervals) and 18–50 kV/cm (4 kV/cm intervals). The direction of the increasing electric field is marked with arrows. (Paper VI, Reprinted with permission from Journal of Applied Physics. Copyright 2013, AIP Publishing LLC).

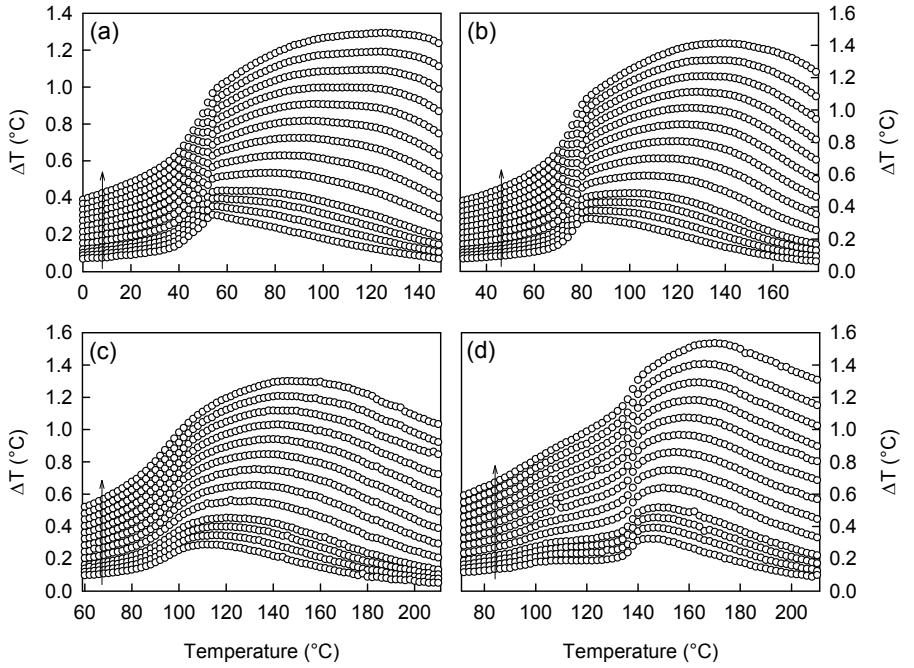

Fig. 35. Electrocaloric temperature change in (a) PMN-15PT, (b) PMN-20PT, (c) PMN-25PT, and (d) PMN-30PT as a function of temperature and electric fields of 8–14 kV/cm (2 kV/cm intervals) and 18–50 kV/cm (4 kV/cm intervals). The direction of the increasing electric field is marked with arrows. (Paper VI, Reprinted with permission from Journal of Applied Physics. Copyright 2013, AIP Publishing LLC).

Table 6 presents the essential electrocaloric properties that were measured from different PMN-*x*PT compositions. The electrocaloric temperature change ΔT varied between 0.77 °C (at 46 °C for PMN) and 1.55 °C (at 170 °C for PMN-30PT) with an electric field of 50 kV/cm. Some compositions (e.g. PMN and PMN-5PT) were able to withstand higher electric fields within their lower measurement temperatures. Table 6 also shows the measurement results for PMN when an electric field of 90 kV/cm was applied and it is seen that the slope of the temperature change (i.e. $\Delta T/E$) remains similar (Figure 36(b)). Approximately a half of the previous direct EC measurements on polycrystalline PMN-PT system are in close agreement with these results (see Table 1). For example, a clear difference between PMN and PMN-30PT compositions was found here in terms

of ΔT and $\Delta T/E$ (Table 6), but these values were found to be much closer in another direct measurement by Rožič *et al.* (2011a & 2011b).

Table 6. Electrocaloric properties measured in a series of PMN-*x*PT compositions.

Composition	ΔT (°C)	T (°C)	E (kV/cm)	ΔT/E (cm°C/MV)	Measurement details	Material form & thickness (μm)
PMN	1.42	68	90	15.8	Thermocouple	Polycrystal, 110
PMN	0.77	46	50	15.4	Thermocouple	Polycrystal, 110
PMN-5PT	1.04	68	50	20.8	Thermocouple	Polycrystal, 110
PMN-10PT	1.2	90	50	24	Thermocouple	Polycrystal, 120
PMN-15PT	1.3	112	50	26	Thermocouple	Polycrystal, 120
PMN-20PT	1.41	134	50	28.2	Thermocouple	Polycrystal, 120
PMN-25PT	1.3	148	50	26	Thermocouple	Polycrystal, 120
PMN-30PT	1.55	170	50	31	Thermocouple	Polycrystal, 110

When the evolution of the maximum electrocaloric effect is observed, it is shown that the temperature of the maximum ECE (T_{ECmax}) is shifted from the proximity of T_d (=T_C) to higher temperatures above a specific electric field value (Figure 36(a)). This shift was especially clear with low x and it effectively increases the broadness of the active temperature range. However, the temperature of the second ECE peak approaches T_C with increasing x and a continuous evolution of T_{ECmax} with electric field was observed for $x > 20$ mol%. This great enhancement of ECE above T_C is not shown in conventional ferroelectrics, such as $BaTiO_3$ (see e.g. Moya *et al.* 2013, Novak *et al.* 2013), where a field-induced phase transition is possible only within a limited temperature range above T_C (Merz 1953).

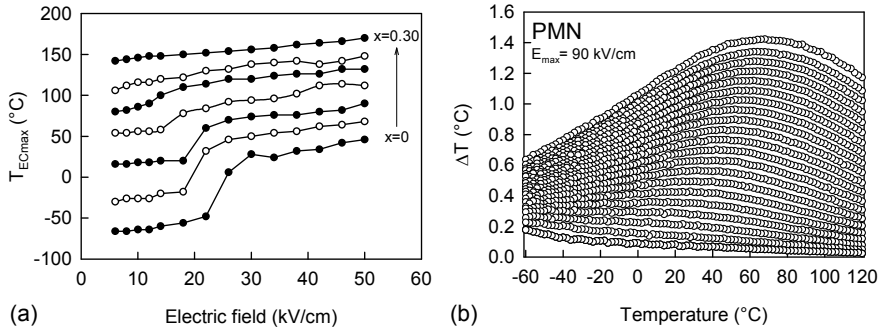

Fig. 36. (a) Temperature of maximum electrocaloric effect T_{ECmax} as a function of applied electric field 4–50 kV/cm in the PMN-*x*PT system with *x*=0–0.3. (b) Electrocaloric effect as a function of temperature in PMN for electric fields of 10–90 kV/cm (4 kV/cm intervals). (Paper VI, Reprinted with permission from Journal of Applied Physics. Copyright 2013, AIP Publishing LLC).

When an electric field is applied to a relaxor ferroelectic PMN-PT in the ergodic relaxor phase, the existing PNRs can be thought to be responsible for the enhanced temperature range of ECE. Therefore it is justifiable to assume that the evolution of ECE with electric field and temperature in the ergodic phase of different PMN-PT compositions effectively correlates with concentration, size, and dynamics of PNRs. The concentration of gradually forming PNRs in the ergodic phase just above T_C is considered to decrease with increasing x in a PMN-xPT system (Ye *et al.* 2003). Since every PNR is regarded as an obstacle for growth of FE nuclei, a lower number of PNRs leads to less restricted isothermal growth and the easier formation of a low temperature FE phase at T_C. In addition, many PNRs can be reoriented and merged into other growing PNRs more easily so that larger domains are observed in the FE phase with higher x. (Ye *et al.* 2003, Bai *et al.* 2004b). Also, a larger proportion of the PNRs are expected to be static (i.e. cannot be reoriented by thermal motion) in a PMN-xPT with lower x due to pinning by CORs (Bokov *et al.* 2011). Then, from the electrocaloric point of view, the growth of the polar phase in the ergodic phase close to T_C is more difficult with lower x, and higher electric fields are required for the activation of high temperature ECE. On the other hand, a higher concentration of PNRs with lower x may enable the field-induced formation of critical sized nuclei and the activation of PNRs within a wider temperature range above T_C. With increasing concentration of $PbTiO_3$ the second ECE peak is observed closer to T_C when its

relaxor nature is gradually diminished. Therefore, it is expected that only a single ECE peak exists with high enough x.

In comparison to the obtained experimental results, a qualitatively similar type of ECE behaviour has been obtained theoretically by Pirc *et al.* (2011b). By using Equation (9) and extracting the terms a_1 and $P(E,T)$ according to the SRBRF model of relaxors (Pirc & Blinc 1999), they were able to model the electrocaloric effect in relaxor ferroelectrics. These model calculations show a similar enhancement of the electrocaloric effect to higher temperatures with increasing electric fields. However, the response at higher electric fields did not produce a separate ECE peak at high temperatures but a continuous evolution of $T_{ECmax}(E)$ was extracted. Additionally, Pirc *et al.* (2011b) predicted that the electrocaloric response (i.e. $\Delta T/E$) of relaxor ferroelectrics with first-order field-induced phase transitions shows its maximum value close to the critical point (E_{CP},T_{CP}) (see Section 2.4). When low electric fields of 1–20 kV/cm were used to measure the electrocaloric effect in the PMN-xPT series, the temperature of maximum responsivity was observed to lie just above the depolarization temperature, as shown in Figure 37. The depolarization temperature was approximated by the extrapolating $T_{ECmax}(E)$ dependence to a value at E=0. Both these temperatures are approaching the temperature of maximum permittivity T_m (measured at 1 kHz) when increasing x strengthens the ferroelectric nature in PMN-xPT. This is expected since it is well known that in ordinary ferroelectrics T_C equals T_m (Bokov *et al.* 2005).

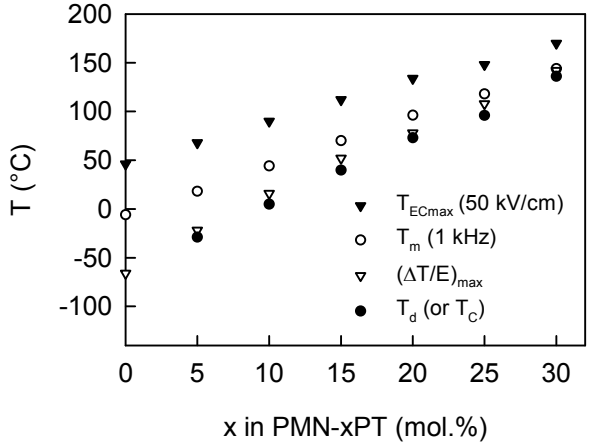

Fig. 37. Temperatures of maximum electrocaloric effect T_{ECmax} (E=50 kV/cm), maximum permittivity T_m (at 1 kHz), maximum ECE responsivity, and depolarization T_d as a function of composition x in the PMN-xPT system. (Paper VI, Reprinted with permission from Journal of Applied Physics. Copyright 2013, AIP Publishing LLC)

The extracted electric field values at the maximum ECE responsivity points were found to decrease as a function of x (Paper VI) as is to be expected if these values correspond to the critical point values E_{CP} (Kutnjak *et al.* 2007). However, an exception was observed with PMN-25PT composition which showed a significantly higher electric field at the maximum responsivity point. This fact, in combination with a diffuse ECE behaviour (Figure 34(a) & 35(c)), may indicate that the nature of the phase transition changes around this concentration. In fact, some behaviour characteristics of a second order phase transition have been observed in PMN-25PT by dielectric spectroscopy (Bokov & Ye 2000) and this composition is known to lie close to a possible tricritical point in the x-T phase diagram (Wu *et al.* 2012).

5 Conclusions

The main purpose of this Thesis work was to investigate electric-field-induced changes in PMN-PT and PZN-PT relaxor ferroelectric materials by means of dielectric and temperature measurements. The most important results obtained during this research work are summarized in the following paragraphs.

Measurements on depoled PMN-13PT ceramics showed that isothermal electrical poling induced an irreversible decrease in permittivity and an increase in temperature when operating below its thermal depolarization temperature. At higher temperatures the field-induced thermal response was found to be highly reversible in nature. This behaviour was attributed to the development of a long-range ferroelectric order at low temperatures. A detailed analysis of the field-induced in-situ temperature change at low temperatures revealed that unpoled PMN-13PT exhibits an irreversible thermal response that exceeds the evaluated dielectric loss. It was suggested that this additional thermal response originates from an irreversible field-induced phase transition similar to that observed for PMN. This suggestion therefore assumes that the low temperature phase of depoled PMN-13PT composition is not a conventional ferroelectric phase with single symmetry but a phase with different coexisting symmetries.

Studies on PMN-PT single crystals close to the MPB region revealed various electric-field-induced phase transitions as evidenced by changes in field-induced dielectric and temperature measurements. This prompted the proposition of a new *E-T* phase diagram for PMN-28PT crystal with *E* along the <011> direction. In addition to the well-known low temperature $R \rightarrow M_B \leftrightarrow O$ phase transition, another phase transition of $T \rightarrow M_C \leftrightarrow O$ was proposed to take place at higher temperatures with the electric field along the <011> due to its different electric-field-induced thermal (i.e. electrocaloric) behaviour. Despite the similarities in polarization measurements, the reversible M_B-O transition produced a decrease in temperature while the M_C-O transition instead produced an increase in temperature with increasing electric field. Critically, the behaviour of the low temperature phase transition led to an unusual situation where an effectively "reversed" or "negative" electrocaloric effect takes place. The electrocaloric measurement of <011>-oriented PMN-28PT single crystals gave the first direct evidence of this reversed electrocaloric effect.

A highly complex polarization rotation route with two discontinuous type reversible changes was evidenced in PMN-*x*PT single crystals with *x*=27–31 mol% when an electric field was applied along the <001> direction. By following the

temperature and composition dependence of the field-induced polarization/temperature changes, this complex rotation route was attributed to a phase sequence of R/M_A↔M_C↔T. This has previously been observed only rarely within a narrower composition range. Constructed phase diagrams showed that M_C and T phases tended to stabilize with increasing temperature and x in agreement with previous studies. Therefore, an intermediate temperature region with a field-induced M_C↔T phase transition was observed for all studied compositions. All evidenced field-induced phase transitions (i.e. M_A→M_C and M_C→T) showed a decreased temperature as was observed for <011>-oriented PMN-28PT. In general, the observed field-induced polarization and temperature changes showed features of both discontinuous and continuous type transitions.

The electrocaloric effect in PZN-8PT single crystals was measured with reasonably low electric fields of $E \leq 12$ kV/cm and was observed to show a single maximum value of ΔT=0.25 °C just above its Curie point. The essential properties of the measured electrocaloric effect were reproduced in the vicinity of the transition temperature by using a simple lattice model and mean-field approximation. The successful use of this model demonstrated that the electrocaloric effect is driven by the field-induced entropy lowering of the dipolar system.

Direct measurements of the electrocaloric effect in the polycrystalline PMN-xPT system showed that the maximum electrocaloric temperature change was obtained in the vicinity of the thermal depolarization temperature with low electric fields. The use of higher electric fields significantly enhanced the temperature range of the effect when an additional electrocaloric maximum appeared at higher temperatures. The behaviour of a high temperature electrocaloric effect as a function of temperature, electric field, and composition refers to an increasing field-induced contribution from aligning and growing polar nanoregions of the ergodic relaxor phase. The maximum electrocaloric temperature change ΔT varied between 0.77 °C (at 46 °C for PMN) and 1.55 °C (at 170 °C for PMN-30PT) with an electric field of 50 kV/cm. These electrocaloric results suggested that the intrinsic Curie temperature of relaxor ferroelectric material should be significantly lower than any desired working temperature range in order to maximize its electrocaloric properties especially with high electric fields.

References

Aizu K (1966) Possible species of ferroelectrics. Phys Rev 146: 423–429.

Aizu K (1970) Possible species of ferromagnetic, ferroelectric, and ferroelastic crystal. Phys Rev B 2: 754.

Akcay G, Alpay SP, Rossetti GA Jr & Scott JF (2008) Influence of mechanical boundary conditions on the electrocaloric properties of ferroelectric thin films. J Appl Phys 103: 024104.

Arndt H, Sauerbier F, Schmidt G & Shebanov LA (1988) Field-induced phase transition in $Pb(Mg_{1/3}Nb_{2/3})O_3$ single crystals. Ferroelectrics 79: 145.

Axelsson A-K, Le Goupil F, Dunne LJ, Manos G, Valant M & Alford NMcN (2013) Microscopic interpretation of sign reversal in the electrocaloric effect in a ferroelectric $Pb(Mg_{1/3}Nb_{2/3})O_3$-$30PbTiO_3$ single crystal. Appl Phys Lett 102: 102902.

Bai F, Wang N, Li J, Viehland D, Gehring PM, Xu G & Shirane G (2004) X-ray and neutron diffraction investigations of the structural phase transformation sequence under electric field in $0.7Pb(Mg_{1/3}Nb_{2/3})O_3$-$0.3PbTiO_3$ crystal. J Appl Phys 96: 1620.

Bai F, Li J & Viehland D (2004) Domain hierarchy in annealed (001)-oriented $Pb(Mg_{1/3}Nb_{2/3})O_3$-x%$PbTiO_3$ single crystals. Appl Phys Lett 85: 2313.

Bai F, Li J & Viehland D (2005) Domain engineered states over various length scales in (001)-oriented $Pb(Mg_{1/3}Nb_{2/3})O_3$-x%$PbTiO_3$ crystals: electrical history dependence of hierarchal domains. J Appl Phys 97: 054103.

Bai Y, Zheng G-P, Ding K, Qiao L, Shi S-Q & Guo D (2011) The giant electrocaloric effect and high effective cooling power near room temperature for $BaTiO_3$ thick film. J Appl Phys 110: 094103.

Baldinozzi G, Sciau Ph & Buffat PA (1993) Investigation of the orthorhombic structures of Pb_2MgWO_6 and Pb_2CoWO_6. Sol State Commun 86: 541.

Bellaiche L, García A & Vanderbilt D (2001) Electric-field induced polarization paths in $Pb(Zr_{1-x}Ti_x)O_3$ alloys. Phys Rev B 64: 060103.

Bertram R, Reck G & Uecker R (2003) Growth and correlation between composition and structure of $(1-x)Pb(Zn_{1/3}Nb_{2/3})O_3$-$xPbTiO_3$ crystals near the morphotropic phase boundary. J Crystal Growth 253: 212.

Bhalla AS, Guo R & Roy R (2000) The perovskite structure – a review of its role in ceramic science and technology. Mat Res Innovat 4: 3.

Bidault O, Licheron M, Husson E, Calvarin G & Morell A (1996) Experimental evidence for a spontaneous relaxor to ferroelectric phase transition in $Pb(Mg_{1/3}Nb_{2/3})O_3$ – 10% Ti. Sol State Commun 98: 765.

Bing Y-H, Bokov AA, Ye Z-G, Noheda B & Shirane G (2005) Structural phase transition and dielectric relaxation in $Pb(Zn_{1/3}Nb_{2/3})O_3$ single crystals. J Phys Condens Matter 17: 2493.

Birks EH (1986) The electrocaloric effect in $Pb(Sc_{0.5}Nb_{0.5})O_3$ ceramic. Phys Stat Sol A 94: 523.

Blinc R, Laguta V & Zalar B (2003) Field cooled and zero field cooled ^{207}Pb NMR and the local structure of relaxor $PbMg_{1/3}Nb_{2/3}O_3$. Phys Rev Lett 91: 247601.

Blinc R (2006) Polar nano-clusters in relaxors on the atomic level. Ferroelectrics 330: 1.
Bokov AA & Ye Z-G (2000) Dielectric dispersion and critical behavior in relaxor ferroelectric $Pb(Mg_{1/3}Nb_{2/3})O_3$-$PbTiO_3$. Appl Phys Lett 77: 1888.
Bokov AA & Ye Z-G (2002) Giant electrostriction and stretched exponential electromechanical relaxation in $0.65Pb(Mg_{1/3}Nb_{2/3})O_3$-$0.35PbTiO_3$ crystals. J Appl Phys 91: 6656.
Bokov AA, Luo H & Ye Z-G (2005) Polar nanodomains and relaxor behaviour in $(1-x)Pb(Mg_{1/3}Nb_{2/3})O_3$-$xPbTiO_3$ crystals with x=0.3-0.5. Mat Sci Eng B 120: 206.
Bokov AA & Ye Z-G (2006) Recent progress in relaxor ferroelectrics with perovskite structure. J Mater Sci 41: 31.
Bokov AA, Rodriguez BJ, Zhao X, Ko J-H, Jesse S, Long X, Qu W, Kim TH, Budai JD, Morozovska AN, Kojima S, Tan X, Kalinin SV & Ye Z-G (2011) Compositional disorder, polar nanoregions and dipole dynamics in $Pb(Mg_{1/3}Nb_{2/3})O_3$-based relaxor ferroelectrics. Z Kristallogr 226: 99.
Bonneau P, Garnier P, Husson E & Morell A (1989) Structural study of PMN ceramics by X-ray diffraction between 297 and 1027 K. Mater Res Bull 24: 201.
Bonneau P, Garnier P, Calvarin G, Husson E, Gavarri JR, Hewat AW & Morell A (1991) X-ray and neutron diffraction studies of the diffused phase transition in $Pb(Mg_{1/3}Nb_{2/3})O_3$ ceramics. J Solid State Chem 91: 350.
Brokate M & Sprekels J (1996) Hysteresis and phase transitions. In: Applied Mathematical Sciences 121, New York, Springer-Verlag.
Budimir M, Damjanovic D & Setter N (2003) Piezoelectric anisotropy-phase transition relations in perovskite single crystals. J Appl Phys 94: 6753.
Bunina O, Zakharchenko I, Yemelyanov S, Timonin P & Sakhnenko V (1994) Phase transitions in $PbMg_{1/3}Nb_{2/3}O_3$-$PbTiO_3$ system. Ferroelectrics 157: 299.
Burns G & Scott BA (1973) Index of refraction in 'dirty' displacive ferroelectrics. Solid State Commun 13: 423.
Burns G & Dacol FH (1983) Glassy polarization behavior in ferroelectric compounds $Pb(Mg_{1/3}Nb_{2/3})O_3$ and $Pb(Zn_{1/3}Nb_{2/3})O_3$. Solid State Commun 48: 853.
Burns G & Dacol FH (1990) Ferroelectrics with a glassy polarization phase. Ferroelectrics 104: 25.
Burton BP (2000) Long-range vs short-range interactions and the configurational energies of $Ba(B,B')O_3$ and $Pb(B,B')O_3$ perovskites. Model Simul Mater Sci Eng 8: 211.
Cao H, Bai F, Wang N, Li J, Viehland D, Xu G & Shirane G (2005) Intermediate ferroelectric orthorhombic and monoclinic M_B phases in [110] electric-field-cooled $Pb(Mg_{1/3}Nb_{2/3})O_3$-30%$PbTiO_3$ crystals. Phys Rev B 72: 064104.
Cao H, Li J, Viehland D & Xu G (2006) Fragile phase stability in $(1-x)Pb(Mg_{1/3}Nb_{2/3})O_3$-$xPbTiO_3$ crystals: A comparison of [001] and [011] field-cooled phase diagrams. Phys Rev B 73: 184110.
Carreaud J, Kiat JM, Dkhil B, Algueró M, Ricote J, Jiménez R, Holc J & Kosec M (2006) Monoclinic morphotropic phase and grain size-induced polarization rotation in $Pb(Mg_{1/3}Nb_{2/3})O_3$-$PbTiO_3$. Appl Phys Lett 89: 252906.

Chen J, Chan HM & Harmeer MH (1989) Ordering structure and dielectric properties of undoped and La/Na-doped $Pb(Mg_{1/3}Nb_{2/3})O_3$. J Am Ceram Soc 72: 593.

Chen J, Panda R & Savord B (2006) Realizing dramatic improvements in the efficiency, sensitivity and bandwidth of ultrasound transducers – Philips PureWave crystal technology. URI: http://www.healthcare.philips.com/pwc_hc/main/shared/ Assets/ Documents/Ultrasound/Solutions/technologies/Philips_PureWave_crystal_technology .pdf. Cited 2013/8/24.

Chen J-H, Liou Y-C & Tseng K-H (2003) Stoichiometric perovskite lead magnesium niobate ceramics produced by reaction-sintering process. Jpn J Appl Phys 42: 175.

Chien RR, Schmidt VH, Tu C-S, Hung L-W & Luo H (2004) Field-induced polarization rotation in (001)-cut $Pb(Mg_{1/3}Nb_{2/3})_{0.76}Ti_{0.24}O_3$. Phys Rev B 69: 172101.

Choi SW, Shrout TR, Jang SJ & Bhalla AS (1989) Morphotropic phase boundary in $Pb(Mg_{1/3}Nb_{2/3})O_3$-$PbTiO_3$ system. Mater Lett 8: 253.

Choi SW, Shrout TR, Jang SJ & Bhalla AS (1989) Dielectric and pyroelectric properties in the $Pb(Mg_{1/3}Nb_{2/3})O_3$-$PbTiO_3$ system. Ferroelectrics 100: 29.

Christen HM, Nam JH, Kim HS, Hatt AJ & Spaldin NA (2011) Stress-induced R-M_A-M_C-T symmetry changes in $BiFeO_3$ films. Phys Rev B 83: 144107.

Chukka R, Cheah JW, Chen Z, Yang P, Shannigrahi S, Wang J & Chen L (2011) Enhanced cooling capacities of ferroelectric materials at morphotropic phase boundaries. Appl Phys Lett 98: 242902

Cohen R (1992) Origin of ferroelectricity in perovskite oxides. Nature 358: 136.

Colla EV, Yushin NK & Viehland D (1998) Dielectric properties of $(PMN)_{(1-x)}(PT)_x$ single crystals for various electrical and thermal histories. J Appl Phys 83: 3298.

Correia TM, Young JS, Whatmore RW, Scott JF, Mathur ND & Zhang Q (2009) Investigation of the electrocaloric effect in a $PbMg_{2/3}Nb_{1/3}O_3$-$PbTiO_3$ relaxor thin film. Appl Phys Lett 95: 182904

Cox DE, Noheda B, Shirane G, Uesu Y, Fujishiro & Yamada Y (2001) Universal phase diagram for high-piezoelectric perovskite systems. Appl Phys Lett 79: 400.

Cross LE, Jang SJ, Newnham RE, Nomura S & Uchino K (1980) Large electrostrictive effects in relaxor ferroelectrics. Ferroelectrics 23: 187.

Cross LE (1987) Relaxor Ferroelectrics. Ferroelectrics 76: 241.

Cross LE (2008) Relaxor ferroelectrics. In: Heywang W, Lubitz K & Wersing W (eds) Piezoelectricity - Evolution & Future of a Technology, Springer Series in Material Science 114: 131.

Dabkowski A, Dabkowska HA, Greedan JE, Ren W & Mukherjee BK (2004) Growth and properties of single crystals of relaxor PZN-PT materials obtained from high-temperature solution. J Cryst Growth 265: 204.

Damjanovic D (1998) Ferroelectric, dielectric and piezoelectric properties of ferroelectric thin films and ceramics. Rep Prog Phys 61: 1267.

Damjanovic D (2009) Comments on Origins of Enhanced Piezoelectric Properties in Ferroelectrics. IEEE Trans Ultrason Ferroelectr Freq Control 56: 1574.

Damjanovic D (2010) A morphotropic phase boundary system based on polarization rotation and polarization extension. Appl Phys Lett 97: 062906.

Damjanovic D, Budimir M, Davis M & Setter N (2003) Monodomain versus polydomain piezoelectric response of $0.67Pb(Mg_{1/3}Nb_{2/3})O_3$-$0.33PbTiO_3$ single crystals along nonpolar directions. Appl Phys Lett 83: 527.

Damjanovic D, Davis M & Budimir M (2008) Enhancement of piezoelectric properties in perovskite crystals by thermally, compositionally, electric field and stress induced instabilities. In: Ye Z-G (ed.) Handbook of Advanced Dielectric Piezoelectric and Ferroelectric Materials – Synthesis, Properties and Applications. Cambridge, Woodhead: 304–332.

Dammak H, Renault A-E, Gaucher P, Thi MP & Calvarin G (2003) Origin of the giant piezoelectric properties in the [001] domain engineered single crystals. Jpn J Appl Phys Pt 1 42: 6477.

Davies PK & Akbas MA (2000) Chemical order in PMN-related relaxors: structure, stability, modification, and impact on properties. J Phys Chem Solids 61: 159.

Davies PK, Wu H, Borisevich AY, Molodetsky IE & Farber L (2008) Crystal chemistry of complex perovskites: new cation-ordered dielectric oxides. Annu Rev Mater Res 38: 369.

Davis M, Damjanovic D & Setter N (2005) Electric-field-induced orthorhombic to rhombohedral phase transition in $[111]_C$-oriented $0.92Pb(Zn_{1/3}Nb_{2/3})O_3 - 0.08PbTiO_3$. J Appl Phys 97: 064101.

Davis M, Damjanovic D & Setter N (2006) Electric-field-, temperature-, and stress-induced phase transitions in relaxor ferroelectric single crystals. Phys Rev B 73: 014115.

Davis M (2006) Phase transitions, anisotropy and domain engineering: the piezoelectric properties of relaxor-ferroelectric single crystals. PhD Thesis. Swiss Federal Institute of Technology in Lausanne–EPFL, Ceramics Laboratory.

Davis M (2007) Picturing the elephant: Giant piezoelectric activity and the monoclinic phases of relaxor-ferroelectric single crystals. J Electroceram 19: 23.

Davis M, Budimir M, Damjanovic D & Setter N (2007) Rotator and extender ferroelectrics: Importance of shear coefficient to the piezoelectric properties of domain-engineered crystals and ceramics. J Appl Phys 101: 054112.

de Mathan N, Husson E, Calvarin G & Gavarri JR, Hewat AW & Morel A (1991) A structural model for the relaxor $PbMg_{1/3}Nb_{2/3}O_3$ at 5 K. J Phys Condens Matter 3: 8159.

Dieckmann J, Cooperman A & Brodrick J (2011) Solid-state cooling, Part 1. ASHRAE J 53(3): 82.

Dieckmann J, Cooperman A & Brodrick J (2011) Solid-state cooling, Part 2. ASHRAE J 53(4): 66.

Dkhil B, Kiat JM, Calvarin G, Baldinozzi G, Vakhrushev SB & Suard E (2001) Local and long range polar order in the relaxor-ferroelectric compounds $PbMg_{1/3}Nb_{2/3}O_3$ and $PbMg_{0.3}Nb_{0.6}Ti_{0.1}O_3$. Phys Rev B 65: 024104.

Dkhil B, Gemeiner P, Al-Barakaty A, Bellaiche L, Dul'kin E, Mojaev E & Roth M (2009) Intermediate temperature scale T^* in lead-based relaxor systems. Phys Rev B 80: 064103.

Dunne LJ, Valant M, Manos G, Axelsson A-K & Alford NM (2008) Microscopic theory of the electrocaloric effect in the paraelectric phase of potassium dihydrogen phosphate. Appl Phys Lett 93: 122906.

Dunne LJ, Valant M, Axelsson A-K, Manos G & Alford NM (2011) Statistical mechanical lattice model of the dual-peak electrocaloric effect in ferroelectric relaxors and the role of pressure. J Phys D Appl Phys 44: 375404.

Durbin M, Jacobs EW, Hicks JC & Park S-E (1999) In situ x-ray diffraction study of an electric field induced phase transition in the single crystal relaxor ferroelectric, 92% $Pb(Zn_{1/3}Nb_{2/3})O_3$-8% $PbTiO_3$. Appl Phys Lett 74: 2848.

Durbin MK, Hicks JC, Park S-E & Shrout TR (2000) X-ray diffraction and phenomenological studies of the engineered monoclinic crystal domains in single crystal relaxor ferroelectrics. J Appl Phys 87: 8159.

El Marssi M & Dammak H (2007) Orthorhombic and monoclinic ferroelectric phases investigated by Raman spectrocscopy in PZN-4.5%PT and PZN-9.5%PT crystals. Sol State Commun 142: 487.

Epstein RI & Malloy KJ (2009) Electrocaloric devices based on thin-film heat switches. J Appl Phys 106: 064509.

Erhart J (2004) Domain wall orientations in ferroelastics and ferroelectrics. Phase Transit 77: 989.

Fang X, Li B & Gu H (2005) Low-temperature single-step reactive sintering methods for lead magnesium niobate. Mater Lett 59: 3262.

Fang B, Du Q, Zhou L, Zhao X, Xu H & Luo H (2009) Structural phase transition and physical properties of tetragonal $0.85Pb(Zn_{1/3}Nb_{2/3})O_3$-$0.15PbTiO_3$ single crystals. J Appl Phys 106: 074110.

Fang F, Yang W & Luo X (2009) [101]-oriented $Pb(Mg_{1/3}Nb_{2/3})O_3$-$PbTiO_3$ single crystals under electric field loadings: polarization rotation linking M_B, O, and R phases. J Am Ceram Soc 93: 3916.

Feng Z, Luo H, Guo Y, He T & Xu H (2003) Dependence of high electric-field-induced strain on the composition and orientation of $Pb(Mg_{1/3}Nb_{2/3})O_3$-$PbTiO_3$ crystals. Sol State Commun 126: 347.

Feng Z, Zhao X & Luo H (2006) Composition and orientation dependence of dielectric and piezoelectric properties in poled $PbMg_{1/3}Nb_{2/3}O_3$-$PbTiO_3$ crystals. J Appl Phys 100: 024104.

Feng Z, Shi D, Zeng R & Dou S (2011) Large electrocaloric effect of highly (100)-oriented $0.68PbMg_{1/3}Nb_{2/3}O_3$-$0.32PbTiO_3$ thin films with a $Pb(Zr_{0.3}Ti_{0.7})O_3/PbO_x$ buffer layer. Thin Solid Films 519: 5433.

Feng Z, Shi D & Dou S (2011) Large electrocaloric effect in highly (001)-oriented $0.67PbMg_{1/3}Nb_{2/3}O_3$-$0.33PbTiO_3$ thin films. Sol State Commun 151: 123.

Fousek J & Janovec V (1969) The orientation of domain walls in twinned ferroelectric crystals. J Appl Phys 40: 135.

Fu H & Cohen RE (2000) Polarization rotation mechanism for ultrahigh electromechanical response in single-crystal piezoelectrics. Nature 403: 281.

Fu D, Taniguchi H, Itoh M, Koshihara S, Yamamoto Y & Mori S (2009) Relaxor $Pb(Mg_{1/3}Nb_{2/3})O_3$: A ferroelectric with multiple inhomogeneities. Phys Rev Lett 103: 207601.

Fujishiro K, Iwase T, Uesu Y, Yamada Y, Dkhil B, Kiat J-M, Mori S & Yamamoto N (2000) Optical and structural studies of long-range order development in relaxor ferroelectrics. J Phys Soc Jpn 69: 2331.

Fähler S, Rößler UK, Kastner O, Eckert J, Eggeler G, Emmerich H, Entel P, Müller S, Quandt E & Albe K (2012) Caloric effects in ferroic materials: new concepts for cooling. Adv Eng Mater 14: 10.

Gehring PM, Wakimoto S, Ye Z-G & Shirane G (2001) Soft mode dynamics above and below the Burns temperature in the relaxor $Pb(Mg_{1/3}Nb_{2/3})O_3$. Phys Rev Lett 87: 277601.

Gehring PM, Chen W, Ye Z-G & Shirane G (2004) The non-rhombohedral low-temperature structure of PMN-10%PT. J Phys Condens Matter 16: 7113.

Goldschmidt VM (1926) Die Gesetze der Krystallochemie. Naturwissenschaften 14: 477.

Gorev MV, Bondarev VS & Aleksandrov KS (2007) Heat capacity of PMN near an electric-field-induced phase transition. JETP Lett 85: 283.

Gu H, Shih WY & Shih W-H (2005) Low-temperature, single step, reactive sintering of lead magnesium niobate using $Mg(OH)_2$-coated Nb_2O_5 powders. J Am Ceram Soc 88: 1435.

Gu H, Craven B, Qian X, Li X, Cheng A & Zhang QM (2013) Simulation of chip-size electrocaloric refrigerator with high cooling-power density. Appl Phys Lett 102: 112901.

Gu H, Qian X, Li X, Craven B, Zhu W, Cheng A, Yao SC & Zhang QM (2013) A chip scale electrocaloric effect based cooling device. Appl Phys Lett 102: 122904.

Guha JP (1999) Reaction chemistry and subsolidus phase equilibria in lead-based relaxor systems: Part I Formation and stability of the perovskite and pyrochlore compounds in the system PbO-MgO-Nb_2O_5. J Mater Sci 34: 4985.

Guo Y, Luo H, Xu H, Zhou X, Pan X & Yin Z (2003) Ultra-high piezoelectric response in <110>-oriented polydomain $Pb(Mg_{1/3}Nb_{2/3})O_3$-$PbTiO_3$ single crystals. Appl Phys A 77: 707.

Guo Y, Luo H, Ling D, Xu H, He T & Yin Z (2003) The phase transition sequence and the location of the morphotropic phase boundary region in $(1-x)Pb(Mg_{1/3}Nb_{2/3})O_3$-$x PbTiO_3$ single crystal. J Phys Condens Matter 15: L77.

Gururaja TR, Panda RK, Chen J & Beck H (1999) Single crystal transducers for medical imaging applications. Proc IEEE Ultrasonics Symposium. Lake Tahoe, USA 2: 969.

Hackenberger WS, Luo J, Jiang X, Snook KA, Rehrig PW, Zhang S & Shrout T (2008) Recent developments and applications of piezoelectric crystals. In: Ye Z-G (ed.) Handbook of Advanced Dielectric Piezoelectric and Ferroelectric Materials – Synthesis, Properties and Applications. Cambridge, Woodhead: 73–100.

Hagberg J, Uusimäki A & Jantunen H (2008) Electrocaloric characteristics in reactive sintered 0.87 $Pb(Mg_{1/3}Nb_{2/3})O_3$-0.13 $PbTiO_3$. Appl Phys Lett 92: 132909.

Han KR, Kim S & Koo HJ (1998) New preparation method of low-temperature-sinterable perovskite $0.9Pb(Mg_{1/3}Nb_{2/3})O_3$-$0.1PbTiO_3$ powder and its dielectric properties. J Am Ceram Soc 81: 2998.

Han P, Tian J & Yan W (2008) Bridgman growth and properties of PMN-PT-based single crystals. In: Ye Z-G (ed.) Handbook of Advanced Dielectric Piezoelectric and Ferroelectric Materials – Synthesis, Properties and Applications. Cambridge, Woodhead: 3–37.

Haumont R, Dkhil B, Kiat JM, Al-Barakaty A, Dammak H & Bellaiche L (2003) Cationic-competition-induced monoclinic phase in high piezoelectric $(PbSc_{1/2}Nb_{1/2}O_3)_{1-x}$-$(PbTiO_3)_x$ compounds. Phys Rev B 68: 014114.

He J, Chen J, Zhou Y & Wang JT (2002) Regenerative characteristics of electrocaloric Stirling or Ericsson refrigeration cycles. Energy Conv Manag 43: 2319.

He Y, Li XM, Gao XD, Leng X & Wang W (2011) Enhanced electrocaloric properties of PMN-PT thin films with LSCO buffer layers. Funct Mater Lett 4: 45.

Herklotz A, Plumhof JD, Rastelli A, Schmidt OG, Schultz L & Dörr K (2010) Electrical characterization of PMN-28%PT(001) crystals used as a thin-film substrates. J Appl Phys 108: 094101.

Hill NA (2000) Why there are so few magnetic ferroelectrics? J Phys Chem B 104: 6694.

Inada M (1977) Analysis of the formation process of the piezoelectric PCM ceramics. Jpn Natl Tech Rept 23: 95.

Itoh M & Taniguchi H (2008) Ferroelectricity in perovskite-type oxides. Ferroelectrics 369: 127.

Iwata M, Kato S & Ishibashi Y (2011) The critical end point in $Pb(Zn_{1/3}Nb_{2/3})O_3$-8%$PbTiO_3$. Ferroelectrics 415: 20.

Jaffe B, Cook WR & Jaffe H (1971) Piezoelectric Ceramics. London, NY, Academic Press.

Jang SJ, Uchino K, Nomura S & Cross LE (1980) Electrostrictive behavior of lead magnesium niobate based ceramic dielectrics. Ferroelectrics 27: 31.

Jiang FM & Kojima S (2000) Microheterogeneity and relaxation in $0.65Pb(Mg_{1/3}Nb_{2/3})O_3$-$0.35PbTiO_3$ relaxor single crystals. Appl Phys Lett 77: 1271.

Jin HZ, Zhu J, Miao S, Zhang XW & Cheng ZY (2001) Ordered domains and polar clusters in lead magnesium niobate $Pb(Mg_{1/3}Nb_{2/3})O_3$. J Appl Phys 89: 5048.

Jin YM, Wang YU & Khachaturyan AG (2003) Adaptive ferroelectric states in systems with low domain wall energy: tetragonal microdomains. J Appl Phys 94: 3629.

Jiwei Z, Bo S, Liangying Z & Xi Y (2000) Preparation and dielectric properties by sol-gel derived PMN-PT powder and ceramic. Mater Chem Phys 64: 1.

Karmanenko SF, Pakhomov OV, Prudan AM, Starkov AS & Eskov A (2007) Layered ceramic structure based on the electrocaloric elements working as a solid state cooling line. J Eur Ceram Soc 27: 3109.

Kar-Narayan S & Mathur ND (2010) Direct and indirect electrocaloric measurements using multilayer capacitors. J Phys D Appl Phys 43: 032002.

Kar-Narayan S, Crossley S, Moya X, Kovacova V, Abergel J, Bontempi A, Baier N, Defay E & Mathur ND (2013) Direct electrocaloric measurements of a multilayer capacitor using scanning thermal microscopy and infra-red imaging. Appl Phys Lett 102: 032903.

Katayama K, Abe M, Akiba T & Yanagida H (1989) Sintering and dielectric properties of single phase $Pb(Mg_{1/3}Nb_{2/3})O_3$-$PbTiO_3$. J Eur Ceram Soc 5: 183.

Kelly J, Leonard M, Tantigate C & Safari A (1997) Effect of composition on the electromechanical properties of $(1-x)Pb(Mg_{1/3}Nb_{2/3})O_3$-$xPbTiO_3$ ceramics. J Am Ceram Soc 80: 957.

Khachaturyan AG, Shapiro SM & Semenovskaya S (1991) Adaptive phase formation in martensitic-transformation. Phys Rev B 43: 832.

Kiat J-M, Uesu Y, Dkhil B, Matsuda M, Malibert C & Calvarin G (2002) Monoclinic structure of unpoled morphotropic high piezoelectric PMN-PT and PZN-PT compounds. Phys Rev B 65: 064106.

Kiat J-M & Dkhil B (2008) From the structure of relaxors to the structure of MPB systems. In: Ye Z-G (ed.) Handbook of Advanced Dielectric Piezoelectric and Ferroelectric Materials – Synthesis, Properties and Applications. Cambridge, Woodhead: 391–446.

Kim B-H, Sakurai O, Wakiya N & Mizutani N (1997) Effect of atmosphere on stability of $Pb(Mg_{1/3}Nb_{2/3})O_3$ (PMN) ceramics. Mater Res Bull 32: 451.

Kisi EH & Forrester JS (2005) Crystal structure of the relaxor ferroelectric PZN: demise of the 'X-phase'. J Phys Condens Matter 17: L381.

Kobeco P & Kurtchatov IV (1930) Dielectric properties of Rochelle salt crystal. Z Phys 66: 192.

Krause HB, Cowley JM & Wheatley J (1979) Short-range ordering in $Pb(Mg_{1/3}Nb_{2/3})O_3$. Acta Cryst A 35: 1015.

Kutnjak Z, Petzelt J & Blinc R (2006) The giant electromechanical response in ferroelectric relaxors as a critical phenomenon. Nature 441: 956.

Kutnjak Z, Blinc R & Ishibashi Y (2007) Electric field induced critical points and polarization rotations in relaxor ferroelectrics. Phys Rev B 76: 104102.

Kutnjak Z, Vodopivec B & Blinc R (2008) Anisotropy of electric field freezing of the relaxor ferroelectric $Pb(Mg_{1/3}Nb_{2/3})O_3$. Phys Rev B 77: 054102.

Kutnjak Z (2008) Heat capacity response of relaxor ferroelectrics near the morphotropic phase boundary. Ferroelectrics 369: 198.

Kuwata J, Uchino K & Nomura S (1981) Phase-transitions in the $Pb(Zn_{1/3}Nb_{2/3})O_3$-$PbTiO_3$ system. Ferroelectrics 37: 579.

Kuwata J, Uchino K & Nomura S (1982) Dielectric and piezoelectric properties of $0.91Pb(Zn_{1/3}Nb_{2/3})O_3$-$0.09PbTiO_3$ single-crystals. Jpn J Appl Phys 21: 1298.

Laguta VV, Glinchuk MD, Bykov IP, Blinc R & Zalar B (2004) NMR study of ionic shifts and polar ordering in the relaxor ferroelectric PSN. Phys Rev B 69: 054103.

Lang SB (2005) Pyroelectricity: from ancient curiosity to modern imaging tool. Phys Today 58: 31.

La-Orauttapong D, Noheda B, Ye Z-G, Gehring PM, Toulouse J, Cox DE & Shirane G (2002) Phase diagram of the relaxor ferroelectric $(1-x)Pb(Zn_{1/3}Nb_{2/3})O_3$-$xPbTiO_3$. Phys Rev B 65: 144101.

Lebon A, Dammak H, Calvarin G & Ahmedou IO (2002) The cubic-to-rhombohedral phase transition of $Pb(Zn_{1/3}Nb_{2/3})O_3$: a high resolution x-ray diffraction study on single crystals. J Phys Condens Matter 14: 7035.

Le Goupil F, Berenov A, Axelsson A-K, Valant M & Alford NM (2012) Direct and indirect electrocaloric measuremnts on <001>-$PbMg_{1/3}Nb_{2/3}O_3$-$30PbTiO_3$ single crystals. J Appl Phys 111: 124109.

Levstik A, Kutnjak Z, Filipič C & Pirc R (1998) Glassy freezing in relaxor ferroelectric lead magnesium niobate. Phys Rev B 57: 11204.

Li F, Zhang S, Xu Z, Wei X, Luo J & Shrout TR (2010) Composition and phase dependence of the intrinsic and extrinsic piezoelectric activity of domain-engineered $(1-x)Pb(Mg_{1/3}Nb_{2/3})O_3$-$xPbTiO_3$ crystals. J Appl Phys 108: 034106.

Lim LC, Kumar FJ & Amin A (2003) Trapped metastable phases in $Pb(Zn_{1/3}Nb_{2/3})O_3$-(8-9)%$PbTiO_3$ single-crystal wafers. J Appl Phys 93: 3671.

Lin D, Li Z, Zhang S, Xu Z & Yao X (2010) Electric-field and temperature induced phase transitions in $Pb(Mg_{1/3}Nb_{2/3})O_3$-$0.3PbTiO_3$ single crystals. J Appl Phys 108: 034112.

Lines ME & Glass AM (1977) Principles and Applications of Ferroelectrics and Related Materials. Oxford, Oxford University Press.

Liou Y-C (2003) Stoichiometric perovskite PMN-PT ceramics produced by reaction-sintering process. Mater Sci Eng B 103: 281.

Liu Y, Zhang Y, Chow M-J, Chen QN & Li J (2012) Biological ferroelectricity uncovered in aortic walls by piezoresponse force microscopy. Phys Rev Lett 108: 078103.

Long X, Bokov AA, Ye Z-G, Qu W & Tan X (2008) Enhanced ordered structure and relaxor behavior of $0.98Pb(Mg_{1/3}Nb_{2/3})O_3-0.02La(Mg_{2/3}Nb_{1/3})O_3$ single crystals. J Phys Condens Matter 20: 015210.

Lu C-H & Wen CY (1998) Thermal decomposition and kinetic analysis of relaxor ferroelectric lead magnesium niobate. J Eur Ceram Soc 18: 1599.

Lu Y, Jeong D-Y, Cheng Z-Y, Zhang QM, Luo H-S, Yin Z-W & Viehland D (2001) Phase transitional behavior and piezoelectric properties of the orthorhombic phase of $Pb(Mg_{1/3}Nb_{2/3})O_3-PbTiO_3$ single crystals. Appl Phys Lett 78: 3109.

Lu S-G & Zhang Q (2009) Electrocaloric materials for solid-state refrigeration. Adv Mat 21: 1.

Lu S-G, Rožič B, Zhang QM, Kutnjak Z, Li X, Furman E, Gorny LJ, Lin M, Malič B, Kosec M, Blinc R & Pirc R (2010) Organic and inorganic relaxor ferroelectrics with giant electrocaloric effect. Appl Phys Lett 97: 162904.

Luo L, Chen H, Zhu Y, Li W, Luo H & Zhang Y (2011) Pyroelectric and electrocaloric effect of ⟨111⟩-oriented 0.9PMN-0.1PT single crystal. J Alloys Comp 509: 8149.

Luo L, Dietze M, Solterbeck C-H, Es-Souni M & Luo H (2012) Orientation and phase transition dependence of the electrocaloric effect in $0.71Pb(Mg_{1/3}Nb_{2/3})O_3$-$0.29PbTiO_3$ single crystal. Appl Phys Lett 101: 062907.

Merz WJ (1953) Double hysteresis loop of $BaTiO_3$ at the Curie point. Phys Rev 91:513.

Mischenko AS, Zhang Q, Scott JF, Whatmore RW & Mathur ND (2006) Giant electrocaloric effect in thin-film $PbZr_{0.95}Ti_{0.05}O_3$. Science 311: 1270.

Mischenko AS, Zhang Q, Whatmore RW, Scott JF & Mathur ND (2006) Giant electrocaloric effect in the thin-film relaxor ferroelectric $0.9Pb(Mg_{1/3}Nb_{2/3})O_3$-$0.1PbTiO_3$ near room temperature. Appl Phys Lett 95: 182904.

Moriya Y, Kawaji H, Tojo T & Atake T (2003) Specific-heat anomaly caused by ferroelectric nanoregions in $Pb(Mg_{1/3}Nb_{2/3})O_3$ and $Pb(Mg_{1/3}Ta_{2/3})O_3$ relaxors. Phys Rev Lett 90: 205901.

Moulson AJ & Herbert JM (2003) Electroceramics: Materials, Properties, Applications. 2nd edition, Chichester, John Wiley & Sons Ltd.

Moya X, Stern-Taulats E, Crossley S, González-Alonso D, Kar-Narayan S, Planes A, Mañosa J & Mathur ND (2013) Giant electrocaloric strength in single-crystal $BaTiO_3$. Adv Mater 25: 1360.

Neese B, Chu B, Lu S-G, Wang Y, Furman E & Zhang QM (2008) Large electrocaloric effect in ferroelectric polymers near room temperature. Science 321: 821.

Newnham RE (1998) Phase transformations in smart materials. Acta Cryst A54: 729.

Newnham RE (2005) Properties of Materials – Anisotropy, Symmetry, Structure. New York, Oxford University Press Inc.

Noheda B, Cox DE, Shirane G, Gonzalo JA, Cross LE & Park S-E (1999) A monoclinic ferroelectric phase in the $Pb(Zr_{1-x}Ti_x)O_3$ solid solution. Appl Phys Lett 74: 2059.

Noheda B, Cox DE, Shirane G, Guo R, Jones B & Cross LE (2000) Stability of the monoclinic phase in the ferroelectric perovskite $PbZr_{1-x}Ti_xO_3$. Phys Rev B 63: 014103.

Noheda B, Cox DE, Shirane G, Gao J & Ye Z-G (2002) Phase diagram of the ferroelectric relaxor $(1-x)PbMg_{1/3}Nb_{2/3}O_3$-$xPbTiO_3$. Phys Rev B 66: 054104.

Noheda B, Zhong Z, Cox DE, Shirane G, Park S-E & Rehrig P (2002) Electric-field-induced phase transitions in $Pb(Zn_{1/3}Nb_{2/3})_{1-x}Ti_xO_3$. Phys Rev B 65: 224101.

Noheda B (2002) Structure and high-piezoelectricity in lead oxide solid solutions. Curr Opin Solid State Mater Sci 6: 27.

Noheda B & Cox DE (2006) Bridging phases at the morphotropic boundaries of lead oxide solid solutions. Phase Transit 79: 5.

Novak N, Pirc R, Wencka M & Kutnjak Z (2012) High-resolution calorimetric study of $Pb(Mg_{1/3}Nb_{2/3})O_3$ single crystal. Phys Rev Lett 109: 037601.

Novak N, Kutnjak Z & Pirc R (2013) High-resolution electrocaloric and heat capacity measurements in barium titanate. EPL 103: 47001.

Nye JF (1980) Physical Properties of Crystals: their Representation by Tensors and Matrices. Oxford, Oxford University Press.

Ohwada K, Hirota K, Rehrig PW, Fujii Y & Shirane G (2003) Neutron diffraction study of field-cooling effects on the relaxor ferroelectric $Pb[(Zn_{1/3}Nb_{2/3})_{0.92}Ti_{0.08}]O_3$. Phys Rev B 67: 094111.

Park S-E & Shrout TR (1997) Ultrahigh strain and piezoelectric behavior in relaxor based ferroelectric single crystals. J Appl Phys 82: 1804.

Park S-E & Hackenberger W (2002) High performance single crystal piezoelectrics: applications and issues. Curr Opin Solid State Mater Sci 6: 11.

Pecharsky VK & Gschneidner KA Jr (1997) Giant magnetocaloric effect in $Gd_5(Si_2Ge_2)$. Phys Rev Lett 78: 4494.

Peräntie J, Correia T, Hagberg J & Uusimäki A (2014) Electrocaloric effect in relaxor ferroelectric -based materials. In: Correia T & Zhang Q (eds.) Electrocaloric Materials – New generation of coolers, Springer Series in Engineering Materials 34, New York, Springer Science.

Pirc R & Blinc R (1999) Spherical random-bond−random-field model of relaxor ferroelectrics. Phys Rev B 60: 13470.

Pirc R, Kutnjak Z, Blinc R & Zhang QM (2011) Upper bounds on the electrocaloric effect in polar solids. Appl Phys Lett 98: 021909.

Pirc R, Kutnjak Z, Blinc R & Zhang QM (2011) Electrocaloric effect in relaxors. J Appl Phys 110: 074113.

Ponomareva I & Lisenkov S (2012) Bridging the macroscopic and atomistic descriptions of the electrocaloric effect. Phys Rev Lett 108: 167604.

Pramanick A, Damjanovic D, Daniels JE, Nino JC & Jones JL (2011) Origins of the electro-mechanical coupling in polycrystalline ferroelectrics during subcoercive electrical loading. J Am Ceram Soc 94: 293.

Priya S & Uchino K (2003) Estimation of polarocaloric contribution to dielectric loss in oriented $0.92Pb(Zn_{1/3}Nb_{2/3})O_3{-}0.08PbTiO_3$ single crystals. Jpn J Appl Phys 42: 5158.

Qiu JH & Jian Q (2008) Film thickness dependence of electrocaloric effect in epitaxial $Ba_{0.6}Sr_{0.4}TiO_3$ thin films. J Appl Phys 103: 034119.

Qiu JH & Jian Q (2009) Orientation dependence of the electrocaloric effect of ferroelectric bilayer thin film. Sol State Commun 149: 1549.

Raevski IP, Prosandreev SA, Emelyanov AS, Raevskaya SI, Colla EV, Viehland D, Kleemann W, Vakhrushev SB, Dellis J-L & El Marssi M (2005) Bias-field effect on the temperature anomalies of dielectric permittivity in $PbMg_{1/3}Nb_{2/3}O_3$-$PbTiO_3$ single crystals. Phys Rev B 72: 184104.

Rajan KK & Lim LC (2003) Particle size dependent x-ray linewidth of rhombohedral phase in $Pb(Zn_{1/3}Nb_{2/3})O_3$-(6,7)%$PbTiO_3$. Appl Phys Lett 83: 5277.

Randall CA & Bhalla AS (1990) Nanostructural-property relations in complex lead perovskites. Jpn J Appl Phys 29: 327.

Ren W, Liu S-F & Mukherjee BK (2002) Piezoelectric properties and phase transitions of <001>-oriented $Pb(Zn_{1/3}Nb_{2/3})O_3$-$PbTiO_3$ single crystals. Appl Phys Lett 80: 3174.

Rose MC & Cohen RE (2012) Giant electrocaloric effect around T_c. Phys Rev Lett 109: 187604.

Rožič B, Malič B, Uršič H, Holc J, Kosec M & Kutnjak Z (2011) Direct measurements of the electrocaloric effect in bulk $PbMg_{1/3}Nb_{2/3}O_3$ (PMN) ceramics. Ferroelectrics 421: 103.

Rožič B, Kosec M, Uršič H, Holc J, Malič B, Zhang QM, Blinc R, Pirc R & Kutnjak Z (2011) Influence of the critical point on the electrocaloric response of relaxor ferroelectrics. J Appl Phys 110: 064118.

Samara GA (2003) The relaxational properties of compositionally disordered ABO_3 perovskites. J Phys Condens Matter 15: R367.

Saranya D, Chaudhuri AR, Parui J & Krupanidhi SB (2009) Electrocaloric effect of PMN-PT thin films near morphotropic phase boundary. Bull Mater Sci 32: 259.

Scott JF (2008) Ferroelectrics go bananas. J Phys Condens Matter 20: 021001.

Scott JF (2011) Electrocaloric materials. Annu Rev Mater Res 41: 1.

Sebald G, Seveyrat L, Guyomar D, Lebrun L, Guiffard B & Pruvost S (2006) Electrocaloric and pyroelectric properties of $0.75Pb(Mg_{1/3}Nb_{2/3})O_3$-$0.25PbTiO_3$ single crystals. J Appl Phys 100: 124112.

Sebald G, Pruvost S & Guyomar D (2008) Energy harvesting based on Ericsson pyroelectric cycles in a relaxor ferroelectric ceramic. Smart Mater Struct 17: 015012.

Sebald G, Guyomar D & Agbossou A (2009) On thermoelectric and pyroelectric energy harvesting. Smart Mater Struct 18: 125006.

Setter N & Cross LE (1980) The role of B-site cation disorder in diffuse phase transition behavior of perovskite ferroelectrics. J Appl Phys 51: 4356.

Shanthi M & Lim LC (2009) Electric-field- and stress-induced R-O phase transformation in [011]-poled $Pb(Mg_{1/3}Nb_{2/3})O_3$-(28-32)%$PbTiO_3$ single crystals of [100]-length cut. J Appl Phys 106: 114116.

Shaobo L & Yanqiu L (2004) Research on the electrocaloric effect of PMN/PT solid solution for ferroelectrics MEMS microcoolers. Mater Sci Eng B 113: 46.

Shebanov LA, Kapostin'sh PP, Birks EH & Zvirgzds YA (1986) Some peculiarities in the rearrangement of the crystal structure and electrocaloric effect in single crystal of lead magnoniobate in the region of the diffuse phase transition. Kristallografiya 31: 317.

Shebanov LA & Borman K (1992) On lead-scandium tantalite solid solutions with high electrocaloric effect. Ferroelectrics 127: 143-148.

Shebanovs L, Borman K, Lawless WN & Kalvane A (2002) Electrocaloric effect in some perovskite ferroelectric ceramics and multilayer capacitors. Ferroelectrics 273: 137.

Shi YP & Soh AK (2011) Modeling of enhanced electrocaloric effect above the Curie temperature in relaxor ferroelectrics. Acta Mater 59: 5574.

Shrout TR & Halliyal A (1987) Preparation of lead-based ferroelectric relaxors for capacitors. Am Ceram Soc Bull 66: 704.

Shrout TR, Chang ZP, Kim N & Markgraf S (1990) Dielectric behavior of single-crystals near the $(1-x)Pb(Mg_{1/3}Nb_{2/3})O_3$-$xPbTiO_3$ morphotropic phase-boundary. Ferroelectrics Lett 12: 63.

Shvartsman VV & Kholkin AL (2004) Domain structure of $0.8Pb(Mg_{1/3}Nb_{2/3})O_3$-$0.2PbTiO_3$ studied by piezoresponse force microscopy. Phys Rev B 69: 014102.

Singh AK & Pandey D (2003) Evidence for M_B and M_C phases in the morphotropic phase boundary region of $(1-x)Pb(Mg_{1/3}Nb_{2/3})O_3-xPbTiO_3$: A Rietveld study. Phys Rev B 67: 064102.

Singh AK, Pandey D & Zaharko O (2006) Powder neutron diffraction study of phase transitions in and a phase diagram of $(1-x)[Pb(Mg_{1/3}Nb_{2/3})O_3]$-$xPbTiO_3$. Phys Rev B 74: 024101.

Sinyavskii YV, Pashkov ND, Gorovoy YM, Lugansky GE & Shebanov L (1989) The optical ferroelectric ceramic as working body for electrocaloric refrigeration. Ferroelectrics 90: 213.

Sinyavsky YV & Brodyansky VM (1992) Experimental testing of electrocaloric cooling with transparent ferroelectric ceramic as a working body. Ferroelectrics 131: 321.

Sinyavskii YV (1995) Electrocaloric refrigerators: a promising alternative to current low-temperature apparatus. Chem Petrol Eng 31: 295.

Slodczyk A, Colomban Ph & Pham-Thi M (2008) Role of the TiO6 octahedra on the ferrolectric and piezoelectric behavior of the poled $PbMg_{1/3}Nb_{2/3}O_3$-$x$$PbTiO_3$ (PMN-PT) single crystal and textured ceramics. J Phys Chem Solids 69: 2503.

Smolenskii GA & Agranovskaya AI (1959) Dielectric polarization of a number of complex compounds. Sov Phys Solid State 1: 1429.

Smolenskii GA, Isupov VA, Agranovskaya AI & Popov SN (1961) Ferroelectrics with diffuse phase transitions. Sov Phys Solid State 2: 2584.

Slater JC (1950) The Lorentz correction in barium titanate. Phys Rev 78: 748.

Starkov AS & Pakhomov OV (2010) Influence of the dynamic polarization of a ferroelectric material on the magnitude of its electrocaloric response. Tech Phys Lett 36: 1.

Stenger CGF & Burggraaf AJ (1980) Order-disorder reactions in the ferroelectric perovskites $Pb(Sc_{1/2}Nb_{1/2})O_3$ and $Pb(Sc_{1/2}Ta_{1/2})O_3$. I. Kinetics of the ordering process. Phys Stat Sol (a) 61: 275.

Stock C, Ellis D, Swainson IP, Xu G, Hiraka H, Zhong Z, Luo H, Zhao X, Viehland D, Birgeneau RJ & Shirane G (2006) Damped soft phonons and diffuse scattering in $40\%Pb(Mg_{1/3}Nb_{2/3})O_3{-}60\%PbTiO_3$. Phys Rev B 73: 064107.

Stock C, Van Eijck L, Fouquet P, Maccarini M, Gehring PM, Xu G, Luo H, Zhao X, Li JF & Viehland D (2010) Interplay between static and dynamic polar correlations in relaxor $Pb(Mg_{1/3}Nb_{2/3})O_3$. Phys Rev B 81: 144127.

Swartz SL & Shrout TR (1982) Fabrication of perovskite lead magnesium niobate. Mater Res Bull 17: 1245.

Tagantsev AK, Cross LE & Fousek J (2010) Domains in Ferroic Crystals and Thin Films. New York, Springer Science.

Tailor HN & Ye Z-G (2010) Enhanced piezoelectricity and high temperature poling effect in (1-x)$Pb(Mg_{1/3}Nb_{2/3})O_3$-$x$$PbTiO_3$ ceramics via an ethylene glycol route. J Appl Phys 107: 104101.

Takesue N, Fujii Y & You H (2001) X-ray diffuse scattering study on ionic-pair displacement correlations in relaxor lead magnesium niobate. Phys Rev B 64: 184112.

Tang Y, Zhao X, Feng X, Jin W & Luo H (2005) Pyroelectric properties of [111]-oriented $Pb(Mg_{1/3}Nb_{2/3})O_3{-}PbTiO_3$ crystals. Appl Phys Lett 86: 082901.

Toulouse J (2008) The three characteristic temperatures of relaxor dynamics and their meaning. Ferroelectrics 369: 203.

Tu C-S, Schmidt VH & Siny IG (1995) Hypersound anomalies and elastic constants in single crystal $PbMg_{1/3}Nb_{2/3}O_3$ by Brillouin scattering. J Appl Phys 78: 5665.

Tu C-S, Chien RR, Wang FT, Schmidt VH & Han P (2004) Phase stability after an electric-field poling in $Pb(Mg_{1/3}Nb_{2/3})_{1-x}Ti_xO_3$ crystals. Phys Rev B 70: 220103.

Tu C-S, Schmidt VH, Chien RR, Tsai S-H, Lee S-C & Luo H (2008) Field-induced intermediate orthorhombic phase in (110)-cut $Pb(Mg_{1/3}Nb_{2/3})_{0.70}Ti_{0.30}O_3$ single crystal. J Appl Phys 104: 094105.

Tuttle BA (1981) Polarization reversal and electrocaloric measurements for field-enforced transitions in the system lead-zirconate - lead-titanate - lead-oxide : tin-oxide. PhD Thesis. University of Illinois at Urbana-Champaign.

Uchino K (1994) Relaxor ferroelectric devices. Ferroelectrics 151: 321.

Uchino K (2000) Ferroelectric Devices. New York, Marcel Dekker, Inc.

Uchino K & Hirose S (2001) Loss mechanisms in piezoelectrics: how to measure different losses separately. IEEE Trans Ultrason Ferroelectr Freq Control 48: 307.

Uchino K (2010) Relaxor ferroelectric-based ceramics. In: Uchino K (ed.) Advanced piezoelectric materials – Science and technology. Cambridge, Woodhead: 111–129.

Uesu Y, Tazawa H, Fujishiro K & Yamada Y (1996) Neutron scattering and nonlinear optical studies on the phase transition of ferroelectric relaxor $Pb(Mg_{1/3}Nb_{2/3})O_3$. J Korean Phys Soc 29: 703.

Vakhrushev SB, Kvyatkovsky BE, Naberezhnov AA, Okuneva NM & Toperverg BP (1989) Glassy phenomena in disordered perovskite-like crystals. Ferroelectrics 90: 173.

Vakhrushev S, Zhukov S, Fetisov G & Chernyshov V (1994) The high temperature structure of lead magnoniobate. J Phys Condens Matter 6: 4021

Vakhrushev SB, Naberezhnov AA, Okuneva NM & Savenko BN (1995) Determination of polarization vectors in lead magnoniobate. Phys Sol Stat 37: 1993.

Vakhrushev SB, Naberezhnov AA, Sinha SK, Feng YP & Egami T (1996) Synchrotron X-ray scattering study of lead magnoniobate relaxor ferroelectric crystals. J Phys Chem Solids 57: 1517.

Vakhrushev SB, Kiat J-M & Dkhil B (1997) X-ray study of the kinetics of field induced transition from the glass-like to the ferroelectric phase in lead magnoniobate. Solid State Commun 103: 477.

Vakhrushev S, Ivanov A & Kulda J (2005) Diffuse neutron scattering in relaxor ferroelectric $PbMg_{1/3}Nb_{2/3}O_3$. Phys Chem Chem Phys 7: 2340.

Valant M (2012) Electrocaloric materials for future solid-state refrigeration technologies. Prog Mater Sci 57: 980.

Valant M, Axelsson A-K, Le Goupil F & Alford NM (2012) Electrocaloric temperature change constrained by the dielectric strength. Mat Chem Phys 136: 277.

Vanderbilt D & Cohen MH (2001) Monoclinic and triclinic phases in higher-order Devonshire theory. Phys Rev B 63: 094108.

Viehland D, Jang SJ, Cross LE & Wuttig M (1990) Freezing of the polarization fluctuations in lead magnesium niobate relaxors. J Appl Phys 68: 2916.

Viehland D, Li JF, Jang SJ, Cross LE & Wuttig M (1991) Dipolar-glass model for lead magnesium niobate. Phys Rev B 43: 8316.

Viehland D, Jang SJ, Cross LE & Wuttig M (1992) Deviation from Curie-Weiss behavior in relaxor ferroelectrics. Phys Rev B 46: 8003.

Viehland D (2000) Symmetry-adaptive ferroelectric mesostates in oriented $Pb(B^{I}_{1/3}B^{II}_{2/3})O_3$-$PbTiO_3$ crystals. J Appl Phys 88: 4794.

Wakimoto S, Stock C, Birgeneau RJ, Ye Z-G, Chen W, Buyers WJL, Gehring PM & Shirane G (2002) Ferroelectric ordering in the relaxor $Pb(Mg_{1/3}Nb_{2/3})O_3$ as evidenced by low-temperature phonon anomalies. Phys Rev B 65: 172105.

Wan X, Luo H, Zhao X, Wang DY, Chan HLW & Choy CL (2004) Refractive indices and linear electro-optic properties of (1-*x*)$Pb(Mg_{1/3}Nb_{2/3})O_3$-*x*$PbTiO_3$ single crystals. Appl Phys Lett 85: 5233.

Wang H, Xu H, Luo H, Yin Z, Bokov AA & Ye Z-G (2005) Dielectric anomalies of the relaxor-based 0.9$Pb(Mg_{1/3}Nb_{2/3})O_3$-0.1$PbTiO_3$ single crystals. Appl Phys Lett 87: 012904.

Wang YU (2006) Three intrinsic relationships of lattice parameters between intermediate monoclinic M_C and tetragonal phases in ferroelectric $Pb[(Mg_{1/3}Nb_{2/3})_{1-x}Ti_x]O_3$ and $Pb[(Zn_{1/3}Nb_{2/3})_{1-x}Ti_x]O_3$ near morphotropic phase boundaries. Phys Rev B 73: 014113.

Westphal V, Kleemann W & Glinchuk MD (1992) Diffuse phase transitions and random-field-induced domain states of the "relaxor" ferroelectric $PbMg_{1/3}Nb_{2/3}O_3$. Phys Rev Lett 68: 847.

Wood ME & Potter WH (1985) General analysis of magnetic refrigeration and its optimization using a new concept: maximization of refrigerant capacity. Cryogenics 25: 667.

Wu H, Xue D, Lv D, Gao J, Guo S, Zhou Y, Ding X, Zhou C, Yang S, Yang Y & Ren X (2012) Microstructure at morphotropic phase boundary in $Pb(Mg_{1/3}Nb_{2/3})O_3$-$PbTiO_3$ ceramic: coexistence of nano-scaled {110}-type rhombohedral twin and {110}-type tetragonal twin. J Appl Phys 112: 052004.

Xiao DQ, Wang YC, Zhang RL, Peng SQ, Zhu JG & Yang B (1998) Electrocaloric properties of (1-*x*) $Pb(Mg_{1/3}Nb_{2/3})O_3$-*x*$PbTiO_3$ ferroelectric ceramics near room temperature. Mater Chem Phys 57: 182.

Xu G, Zhong Z, Bing Y, Ye Z-G, Stock C & Shirane G (2003) Ground state of the relaxor ferroelectric $Pb(Zn_{1/3}Nb_{2/3})O_3$. Phys Rev B 67: 104102.

Xu G, Viehland D, Li JF, Gehring PM & Shirane G (2003) Evidence of decoupled lattice distortion and ferroelectric polarization in the relaxor system PMN-*x*PT. Phys Rev B 68: 212410.

Xu G, Shirane G, Copley JRD & Gehring P (2004) Neutron elastic diffuse scattering study of $Pb(Mg_{1/3}Nb_{2/3})O_3$. Phys Rev B 69: 064112.

Xu G, Zhong Z, Bing Y, Ye Z-G, Stock C & Shirane G (2004) Anomalous phase in the relaxor ferroelectric $Pb(Zn_{1/3}Nb_{2/3})O_3$. Phys Rev B 70: 064107.

Xu G, Hiraka H, Shirane G & Ohwada K (2004) Dual structures in (1-*x*)$Pb(Zn_{1/3}Nb_{2/3})O_3$-*x*$PbTiO_3$ ferroelectric relaxors. Appl Phys Lett 84: 3975.

Xu G, Gehring PM, Stock C & Conlon K (2006) The anomalous skin effect in single crystal relaxor ferroelectric PZN-*x*PT and PMN-*x*PT. Phase Transitions 79: 135.

Xu G (2010) Competing orders in PZN-*x*PT and PMN-*x*PT relaxor ferroelectrics. J Phys Soc Jpn 79: 011011.

Yamashita Y & Ichinose N (1996) Can relaxor piezoelectric materials outperform PZT? Proc 10th IEEE International Symposium on Applications of Ferroelectrics. East Brunswick, USA 1: 71.

Yamashita Y, Hosono Y, Harada K & Yasuda N (2002) Present and future of piezoelectric single crystals and the importance of B-site cations for high piezoelectric response. IEEE Trans Ultrason Ferroelectr Freq Control 49: 184.

Yan H, Inam F, Viola G, Ning H, Zhang H, Jiang Q, Zeng T, Gao Z & Reece MJ (2011) The contribution of electrical conductivity, dielectric permittivity and domain switching in ferroelectric hysteresis loops. J Adv Dielect 1: 107.

Ye Z-G & Schmid H (1993) Optical, dielectric and polarization studies of the electric field-induced phase transition in $Pb(Mg_{1/3}Nb_{2/3})O_3$ [PMN]. Ferroelectrics 145: 83–108.

Ye Z-G (1998) Relaxor ferroelectric complex perovskites: structure, properties and phase transitions. Key Eng Mater 155–156: 81.

Ye Z-G & Dong M (2000) Morphotropic domain structures and phase transitions in relaxor-based piezo-/ferroelectric $(1-x)Pb(Mg_{1/3}Nb_{2/3})O_3$-$xPbTiO_3$ single crystals. J Appl Phys 87: 2312.

Ye Z-G, Bing Y, Gao J, Bokov AA, Stephens P, Noheda B & Shirane G (2003) Development of ferroelectric order in relaxor $(1-x)Pb(Mg_{1/3}Nb_{2/3})O_3$-$xPbTiO_3$ ($0 \le x \le 0.15$). Phys Rev B 67: 104104.

Ye Z-G (2009) High-performance piezoelectric single crystals of complex perovskite solid solutions. MRS Bulletin 34: 277.

Yoshida M, Mori S, Yamamoto N, Uesu Y & Kiat JM (1998) Tem observation of polar domains in relaxor ferroelectric $Pb(Mg_{1/3}Nb_{2/3})O_3$. Ferroelectrics 217: 327.

Zhang R, Jiang B & Cao W (2001) Elastic, piezoelectric, and dielectric properties of multidomain $0.67Pb(Mg_{1/3}Nb_{2/3})O_3$-$0.33PbTiO_3$ single crystals. J Appl Phys 90: 3471.

Zhang R, Jiang B & Cao W (2003) Single-domain properties of $0.67Pb(Mg_{1/3}Nb_{2/3})O_3$-$0.33PbTiO_3$ single crystals under electric field bias. Appl Phys Lett 82: 787.

Zhang SJ, Luo J, Snyder DW & Shrout TR (2008) High-performance, high-T_C piezoelectric crystals. In: Ye Z-G (ed.) Handbook of Advanced Dielectric Piezoelectric and Ferroelectric Materials – Synthesis, Properties and Applications. Cambridge, Woodhead: 130.

Zhang S & Li F (2012) High performance ferroelectric relaxor-$PbTiO_3$ single crystals: status and perspective. J Appl Phys 111: 031301.

Zhao X, Qu W, Tan X, Bokov AA & Ye Z-G (2009) Influence of long-range cation order on relaxor properties of doped $Pb(Mg_{1/3}Nb_{2/3})O_3$ ceramics. Phys Rev B 79: 144101.

Original papers

I Peräntie J, Hagberg J, Uusimäki A & Jantunen H (2008) Temperature characteristics and development of field-induced phase transition in relaxor ferroelectric $Pb(Mg_{1/3}Nb_{2/3})_{0.87}Ti_{0.13}O_3$ ceramics. Applied Physics Letters 93(13): 132905.

II Peräntie J, Hagberg J, Uusimäki A & Jantunen H (2009) Field-induced thermal response and irreversible phase transition enthalpy change in $Pb(Mg_{1/3}Nb_{2/3})O_3$–$PbTiO_3$. Applied Physics Letters 94(10): 102903.

III Peräntie J, Hagberg J, Uusimäki A & Jantunen H (2010) Electric-field-induced dielectric and temperature changes in a <011>-oriented $Pb(Mg_{1/3}Nb_{2/3})O_3$–$PbTiO_3$ single crystal. Physical Review B 82(13): 134119.

IV Peräntie J, Hagberg J, Uusimäki A, Tian J & Han P (2012) Characteristics of electric-field-induced polarization rotation in <001>-poled $Pb(Mg_{1/3}Nb_{2/3})O_3$–$PbTiO_3$ single crystals close to the morphotropic phase boundary. Journal of Applied Physics 112(3): 034117.

V Valant M, Dunne LJ, Axelsson A-K, Alford NM, Manos G, Peräntie J, Hagberg J, Jantunen H & Dabkowski A (2010) Electrocaloric effect in a ferroelectric $Pb(Zn_{1/3}Nb_{2/3})O_3$-$PbTiO_3$ single crystal. Physical Review B 81(21): 214110.

VI Peräntie J, Tailor H, Hagberg J, Jantunen H & Ye Z-G (2013) Electrocaloric properties in relaxor ferroelectric $(1-x)Pb(Mg_{1/3}Nb_{2/3})O_3$-$xPbTiO_3$ system. Journal of Applied Physics 114(17): 174105.

Book orders:
Granum: Virtual book store
http://granum.uta.fi/granum/

UNIVERSITY OF OULU P.O. Box 8000 FI-90014 UNIVERSITY OF OULU FINLAND

ACTA UNIVERSITATIS OULUENSIS

ISBN 978-952-62-0438-3 (Paperback)
ISBN 978-952-62-0440-6 (PDF)
ISSN 0355-3213 (Print)
ISSN 1796-2226 (Online)

UNIVERSITY of OULU
OULUN YLIOPISTO